

ABSTRACT

Title of Document: DESIGN AND TESTING OF A MICROBIAL FUEL CELL FOR THE GENERATION OF ENERGY FROM LIGNOCELLULOSIC BIOMASS

Kyla Gregoire, Master of Science, 2010
Civil & Environmental Engineering

Directed By: Associate Professor, Jennifer Becker
Environmental Science & Technology

Previous research has demonstrated that microbial fuel cells (MFCs) have the ability to degrade soluble substrates such as wastewater; however, very few studies have attempted the conversion particulate biomass to electricity in an MFC. A single-chamber, air cathode MFC was developed using a solid, lignocellulosic substrate (corn cob pellets) as the electron donor. The first trial, using a prototype reactor with a graphite rod anode, ran for 415 hours, and generated a maximum open circuit voltage and current of 0.67 V and 0.25 mA, respectively. The second trial employed graphite brush anodes and multiple microbial inocula. A pasteurized soil inoculum resulted in negligible power ($P_{max} = 0.144 \text{ mW/m}^3$). The addition of rumen fluid, which naturally contains cellulose-degrading microorganisms, and *Geobacter metallireducens*, resulted in P_{max} values of 77 mW/m^3 and 159 mW/m^3 , respectively. Analysis of hydrogen, methane, organic acids, and the mass of substrate consumed provided insight into the relationship between cellulose oxidation, methanogenesis, and power production.

DESIGN AND TESTING OF A MICROBIAL FUEL CELL FOR THE
CONVERSION OF LIGNOCELLULOSIC BIOMASS INTO ELECTRICITY

By

Kyla Gregoire

Thesis submitted to the Faculty of the Graduate School of the
University of Maryland, College Park, in partial fulfillment
of the requirements for the degree of
Master of Science
2010

Advisory Committee:
Dr. Jennifer Becker, Chair
Dr. Eric Seagren
Dr. Kaye Brubaker
Dr. Stephanie Lansing

© Copyright by
Kyla Gregoire
2010

Acknowledgements

I would like to first thank my advisor, Dr. Jennifer Becker, for the opportunity to work on this project. Her guidance and expertise over the last two years has allowed me to grow into a new field and expand my research skills so that I might be a better engineer and scientist in the future. I would also like to thank my committee members: Dr. Eric Seagren for his help with reactor design and for my introduction to the field of microbiology; Dr. Stephanie Lansing for her expertise in all things related to bioenergy and for the opportunity to be involved with the Haiti project; and Dr. Kaye Brubaker for a great introduction to the world of environmental modeling and for her genuine enthusiasm for learning and teaching. I am also greatly appreciative of Dr. Rick Kohn's research group in the Animal Sciences department for supplying rumen fluid and for performing organic acid analysis at the end of the experiment.

Funding for this project was provided by the Maryland Experiment Station and General Research Board, as well as a fellowship from the A. James Clark School of Engineering. The support from both organizations is greatly appreciated.

To my lab mates, Sean Lai & Preston Postl—thank you both for assistance in the lab, for the many microbiology lessons, and for your amazing sense of humor! Thanks to all of the graduate students of the ENST department—I will miss all of your wonderful personalities. Also, many thanks to Gary Seibel and Ali Djamshidi of the ENST Project Development Center for your patience and for your help during the design and construction of the reactors.

To my friends and family—this would not have happened without your encouragement, love, and support over the last 26 years.

Table of Contents

Acknowledgements.....	ii
Table of Contents.....	iv
CHAPTER 1.....	vii
INTRODUCTION.....	1
1.1 Need for Renewable Energy Technologies.....	1
1.2 Need for Solid-Substrate MFCs.....	3
1.3 Hypothesis & Objectives.....	4
1.4 Implications.....	5
CHAPTER 2.....	7
LITERATURE REVIEW.....	7
2.1 Literature Overview.....	7
2.2 Electricity Generation and Performance in Fuel Cells.....	7
2.3 Microbial Ecology of MFCs and Cellulose-Degrading Bacteria.....	12
2.3.1 Anode Respiration and EAB.....	12
2.3.2 Cellulolytic Bacteria & Cellulose-Fed MFCs.....	15
2.4 Fuel Cell Performance Measures.....	17
2.5 MFC Design Considerations.....	22
CHAPTER 3.....	24
MATERIALS & METHODS.....	24
3.1 Materials.....	24
3.1.2. Anode Materials.....	26
3.1.3 Cathode Materials.....	28
3.1.4 Plastic Matrix Material.....	29
3.1.5 Microbial Inoculum and Media.....	30
3.2 MFC Reactor Design.....	33
3.3 Reactor Start-Up Procedures.....	36
3.4 Electrochemical Measurements.....	37
3.5 Analytical Measurements.....	39
3.6 Reactor Tear-Down Procedures.....	42
CHAPTER 4.....	44
RESULTS & DISCUSSION.....	44
4.1 Trial 1—Prototype MFC.....	44
4.1.1 Results Overview.....	44
4.1.2 Electricity Generation from Prototype MFC.....	44
4.1.3 Methane and Hydrogen Generation.....	48
4.1.4 pH and Temperature.....	52
4.2 Trial 1 Implications.....	53
4.2.1 Microbial Limitations.....	53
4.2.2 Anode Limitations.....	55
4.2.3 Electron Scavengers.....	55
4.2.4 Internal Resistance.....	56
4.2.5 Voltage-Drop Off.....	56

4.3 Trial 2 Results Overview	57
4.4 Trial 2 Condition 1—Soil Inoculum	57
4.4.1 Electrochemical Performance Summary	57
4.4.2 Polarization Results (Reactor B Only)	58
4.5 Trial 2 Condition 2—Rumen Fluid Co-Inoculum	61
4.5.1 Electrochemical Performance Summary	61
4.5.2 Polarization Results	62
4.5 Trial 2 Condition 3— <i>G. metallireducens</i> Co-Inoculum	64
4.5.1 Electrochemical Performance Summary	64
4.5.2 Polarization Results	66
4.6 Trial 2 Analytical Measurements	67
4.6.1 Methane and Hydrogen Generation	67
4.6.2 Dissolved Oxygen, pH, and Temperature	69
4.6.3 Organic Acid Production	71
4.7 Comparison of Duplicate Reactor Performance	73
4.8 Comparison of Results from Cellulose-Fed MFCs	76
4.7 SEM Analysis of Substrate and Anodic Biofilms	80
CHAPTER 5	84
CONCLUSIONS	84
5.1 Implications and Future Work	84
APPENDICES	86
Appendix A Information on Reactor Set-Up	86
Appendix B Data from Trial 1	87
Appendix C Data from Trial 2	88
Appendix D SEM Images	92
REFERENCES	94

List of Tables

Table 2-1. Exogenous Electron Acceptors and Reduction Potential Values.....	12
Table 4-1. Trial 2 Summary of OCV & Steady-State Electrical Performance in Duplicate Reactors A and B Inoculated with Pasteurized Soil (Trial 2, Condition 1).....	57
Table 4-2. Trial 2, Summary of Steady-State Electrical Performance in Duplicate Reactors A and B Inoculated with Rumen Fluid (Trial 2, Condition 2).....	61
Table 4-3. Trial 2 summary of steady-State Electrical Performance in duplicate reactors A and B inoculated with <i>G. metallireducens</i> (Trial 2, Condition 3).....	65
Table 4-4. Performance of cellulose-fed MFCs to date.....	76
Table 4-5. Trial 2 Reactor A performance summary from the current study.....	77
Table 4-6. Trial 2 Reactor B performance summary from the current study.....	77

List of Figures

Figure 1-1. Corn stover remaining on fields post-harvest (<i>Sokhansanj et al. 2002</i>).....	2
Figure 2-1. Hydrogen Fuel Cell Schematic displaying the flow of electrons, protons, and oxygen molecules across a cation-specific boundary (<i>USDOE 2004</i>).....	8
Figure 2-2. Two-chambered H-type MFC where bubbling oxygen provides the electron acceptor and a cation-specific membrane separates the anode from the cathode (from: www.engr.psu.edu/ce/ENVE/logan).....	10
Figure 2-3. Single Chamber, Air Cathode MFC with Passive Diffusion of Oxygen (<i>Zielke 2005</i>).....	10
Figures 2-4. Single Chamber, Air-Cathode Configurations (A) Carbon cloth cathode is held in the side-arm of the bottle & Anode is submerged in liquid (<i>Logan et al. 2007</i>); (B) Graphite rod anodes are in a concentric circle around a carbon cloth cathode (<i>Liu et al. 2004</i>)	11
Figure 2-5. Chemoorganotrophic Metabolism (<i>Madigan & Martino 2006</i>)	13
Figure 2-6. Scanning electron micrograph of <i>Clostridium sp. EG3</i> (<i>Park et al. 2001</i>)	16
Figure 2-7. Ideal polarization curves displaying the relationship between maximum power (P_{max}), short-circuit current (i_{sc}), and internal resistance (R_{int}). The asymmetric shape of the power curve implies that ohmic losses do not dominate.....	19
Figure 2-8. Fuel cell polarization curves displaying three regions of overpotential. (<i>USDOE 2004</i>).. ..	20
Figure 2-9. Fuel cell polarization curves displaying the voltage-power relationship (<i>USDOE 2004</i>)	20
Figure 3-1. MFC Substrate Material—Corncob Pellets.....	25
Figure 3-2. Gradient Ratio Test with Constant Head Permeameter.....	26
Figure 3-3. Hydraulic Conductivity Set-Up for the Spent Material (http://geotech.uta.edu/lab/Main/Soil%20Lab/08_Permeability)	26
Figure 3-4. Graphite Granules (A) and Carbon Fiber Brush (B) Anode Materials.....	28
Figure 3-5. Plastic Filter Media added to the Anode Chamber.....	30
Figure 3-6. Schematic (A) and Picture (B) of Solid Substrate MFC.....	35

Figure 3-7. Parallel MFC Reactor Set-Up for Trial 2.....	35
Figure 3-8. MFC External Circuit.....	37
Figure 4-1. Trial 1 Voltage/Potential Readings (from Reactor A)	44
Figure 4-2. Trial 1 Polarization curves obtained by measuring the MFC potential at R_{ext} ranging from 1 to 300 k Ω . (A) Potential as a function of resistance; (B) potential as a function of current; and (C) power as a function of current. Power and current densities were calculated using the wet anode volume (0.00477 m ³).....	46
Figure 4-3. Trial 1 Methane Concentrations in a Single MFC Reactor determined from analysis of either headspace or liquid samples. Analysis of headspace samples did not start until hour 960.....	48
Figure 4-4. Trial 1 Hydrogen Concentrations in a single MFC reactor determined from analysis of either headspace or liquid samples. Analysis of headspace samples did not start until hour 960	49
Figure 4-5. Landfill gas production pattern (<i>Rovers et al. 1973</i>)	51
Figure 4-6. Trial 1 Methane Concentrations and pH after BES Addition. Methane was determined from analysis of either headspace of liquid samples.....	52
Figure 4-7. Open Circuit Voltage (OCV) in Duplicate Reactors A and B Inoculated with Pasteurized Soil (Trial 2, Condition 1).....	57
Figure 4-8. Soil inoculum polarization curves from reactor B obtained by measuring the MFC potential at R_{ext} ranging from 1 k Ω to 1 M Ω . (A) potential as a function of resistance; (B) potential as a function of current; and (C) power as a function of current. Power and current densities were calculated using the anode wet volume (0.00477 m ³).	60
Figure 4-9. Current for 77 hours after rumen fluid inoculation at hour 656 in the duplicate Reactors A and B (Trial 2, Condition 2).....	61
Figure 4-10. Rumen fluid polarization Curves obtained by measuring the MFC potential at R_{ext} ranging from 1 k Ω to 1 M Ω . (A) potential as a function of resistance; (B) potential as a function of current; and (C) power as a function of current. Power and current were normalized to the anode wet volume (0.00477 m ³).....	64
Figure 4-11. Current during the first 48 hours after <i>G. metallireducens</i> inoculation at hour 1506 in the duplicate reactors A and B (Trial 2, Condition 3)	65
Figure 4-12. <i>G. metallireducens</i> polarization curves obtained by measuring the MFC potential at R_{ext} ranging from 1 to 10 k Ω . (A) potential as a function	

of resistance; (B) potential as a function of current; and (C) power as a function of current. Power and current densities were normalized to the anode wet volume (0.00477 m ³).	67
Figure 4-13. Trial 2 methane concentrations in duplicate reactors determined from analysis of headspace samples.	69
Figure 4-14. Trial 2 methane concentrations in duplicate reactors determined from analysis of liquid samples.	69
Figure 4-15. Dissolved oxygen levels in the duplicate reactors during all conditions of Trial 2.	70
Figure 4-16. pH Levels in the duplicate reactors during all conditions of Trial 2.	71
Figure 4-17. Trial 2 relative organic acid production in duplicate reactors determined from analysis of liquid samples.	72
Figure 4-18. Trial 2 organic acid production in Reactor A determined from analysis of liquid samples.	73
Figure 4-19. Trial 2 organic acid production in Reactor B determined from analysis of liquid samples	73
Figure 4-20. Comparison of Power Density Curves from Conditions 2 and 3 (Reactor A)	74
Figure 4-21. Comparison of Power Density Curves from Conditions 2 and 3 (Reactor B)	75
Figure 4-22. (A) Sample molecule of lignin displaying the structural complexity; (B) Model of lignin, cellulose, and hemicelluloses structures within lignocellulose.	79
Figure 4-23. Micrograph of anodic fiber taken from the bottom half of Reactor B. Example of a filamentous bacteria surrounded by cocci.	82
Figure 4-24. Micrograph of anodic fiber taken from the middle section of Reactor A. Figure illustrates the patchy appearance of biofilm on the anode.	82
Figure 4-25. Micrograph of corncob taken from the top half of Reactor A. Figure illustrates the pili-like appendages attaching bacteria to the substrate surface.	83
Figure 4-26. Micrograph of anodic fiber taken from the bottom half of Reactor B. Figure displays bacterial attachment to the anode surface.	84
Figure 4-27. Micrograph of anodic fiber taken from the middle section of Reactor A. Figure displays the pili-like appendages attaching bacteria to one another.	84

CHAPTER 1

INTRODUCTION

1.1 Need for Renewable Energy Technologies

Motivation for this research is based on the worldwide need for energy from renewable resources, including the large quantities of waste biomass generated by agricultural sectors (*Fischer & Newell 2004; Searchinger et al. 2008; USDA/USDOE 2005*). Microbial fuel cells (MFCs) are devices that utilize bacteria as the catalyst to oxidize organic and inorganic materials via energy-producing respiratory processes. They have emerged as a potentially viable technology for the direct generation of electricity from soluble wastes like wastewater (*Logan et al. 2002*). However, the potential for converting solid, rather than soluble, substrates in MFCs is largely untested, which limits the applicability of this technology for major waste-producing sectors, including agriculture and solid waste management. This research focuses on evaluating the potential for electricity production from solid, cellulosic wastes in an MFC.

A number of technologies can be used for extracting energy from energy-rich biomass. For example, anaerobic digesters can be used to produce biogas from biomass; however, the conversions can be inefficient, and applicability is dependent on a number of factors, including wastewater strength, temperature and buffering capacity (*Mes et al. 2003; Rittmann 2008; Kaspar et al. 1978*). Abiotic, hydrogen fuel cells can utilize

readily available substrates like hydrogen or metal to generate energy, but most require highly purified fuels and expensive catalysts, making the technology less feasible for scale-up or commercial production (*Barbir 2005; Logan et al. 2002*). Hydrogen can also be produced via fermentation of organic waste; however, the gas must be collected continuously to prevent hydrogen consumption by methanogenic organisms (*Logan et al. 2002*). Thus, there is a need for complementary technologies that can be used to recover energy from wastes with a wide variety of characteristics.

In particular, the sustainability of worldwide agricultural operations could be improved, in part, by reducing net energy consumption through recovery of the energy available in the large quantities of plant residues that remain after crops are harvested. In the US, where corn is the most widely planted crop, approximately 254 million tons of corn grain is harvested each year (*USDA/NASS 2001*). Corn stalks, husks, leaves, and cob—collectively referred to as "stover"—are removed from the fields at a rate of roughly 6% (*Sokhansanj et al. 2002; USDA/NASS 2001*). Figure 1-1 illustrates the stover that typically remains on the fields post-harvest.



Figure 1-1. Corn stover remaining on fields post-harvest (*Sokhansanj et al. 2002*)

A portion of the corn stover must remain on the field to reduce erosion and maintain soil organic carbon levels; however, it is estimated that 20-60% of the stover can be harvested sustainably, amounting to roughly 75-100 million dry tons of usable material left on the fields each year (*Glassner et al. 1999; Kadam & McMillan 2003; USDA/USDOE 2005*). The fraction of stover made up of cobs, roughly 15%, is less essential to protecting soil quality than the leaves, stalks, and husks. Currently, most of the harvested stover is converted to silage for use as animal feed; however, this practice does not make use of the large quantities of biochemical energy available in unharvested stover (*USDA/USDOE 2005*).

1.2 Need for Solid-Substrate MFCs

To date, MFC research has focused on the oxidation of soluble organic substrates (e.g. wastewater primary effluent or landfill leachate) for the production of usable electricity (*Feng et al. 2008; Ren et al. 2007*). In the current study, a solid cellulosic waste was provided as the oxidizable organic material. Chopped corncob was chosen as the substrate for the MFC because the cob fraction of corn stover can be collected even on no-till farms (*Shinners & Benversie 2007*). Further, the cellulose content of cobs is as high or higher compared with the cellulose content of other stover fractions (*Montross & Crofcheck 2004*), and it is anticipated that power density will correlate with cellulose concentration in the fuel cell.

Anaerobic degradation of a solid waste in a MFC presents a number of challenges. Before the start of this study, it was not known if it is possible to generate electricity directly from cellulosic feedstock without significant methane production or

the development of acidic conditions. Further, the microbial hydrolysis of the cellulose in untreated biomass is hindered by its association with other plant polymers such as hemicellulose and lignin, and there is a general lack of knowledge about the capacity of different microbial communities to efficiently break down these biopolymers. Several aspects of a solid substrate MFC made the design of such a system challenging: (1) the cellulosic material must serve as both a bacterial support media and growth substrate; (2) substrate mass, volume, chemical and physical characteristics (particle size, porosity, mechanical resistance, etc.) change over time; and (3) the development of concentration gradients could lead to high levels of internal electrical resistance.

1.3 Hypothesis & Objectives

It was hypothesized that the biochemical energy available in waste biomass can be converted directly into electricity in simple MFCs. The specific objectives of the research were as follows:

- (1) To design and construct a prototype solid substrate MFC reactor;
- (2) To demonstrate that the prototype MFC can be used to convert a complex cellulosic solid substrate directly to electricity;
- (3) To characterize the electrochemical performance of the prototype MFC under steady-state conditions;
- (4) To evaluate the effects of different microbial inocula on MFC performance based on steady-state operation at a constant external resistance (R_{ext}) and during polarization of the anode and cathode.

- (5) To quantify and understand environmental conditions within the anode chamber during operation, including pH and dissolved oxygen, as well as hydrogen, methane, and organic acid concentrations;
- (6) To analyze for degradation intermediates (e.g. volatile fatty acids) and end products (e.g. methane, hydrogen) in order to identify system limitations and inefficiencies; and
- (7) To quantify the total mass of solid corncob consumed during one batch cycle of MFC operation.

1.4 Implications

This research focused on MFCs, which have broad application potential for recovery of energy from waste biomass generated by a number of energy-intensive industries. A new generation of MFCs with the ability to oxidize cellulosic substrates could make use of a variety of residuals for the production of decentralized and sustainable electricity.

The development of a MFC capable of direct lignocellulose degradation would have a number of positive, environmental impacts. Making better use of the 75-100 million tons of usable biomass left on agricultural fields each year through bioenergy production would improve the sustainability of worldwide agricultural operations (*Glassner et al. 1999; Montross & Crofcheck 2004*). If MFCs that utilize waste biomass, rather than food crops, as the energy source could be developed, they would be considered a carbon neutral technology, and their use by farmers would likely reduce

greenhouse gas emissions (*Searchinger et al. 2008*). Additionally, because MFCs are relatively simple in design and operation, they are a feasible technology for scale-up and commercial operation at a farm-level, though the cost of electrode materials is still quite high. From a scientific perspective, the results of this study could help advance the understanding of MFC process design and operation for solid substrate conversion to electricity.

CHAPTER 2

LITERATURE REVIEW

2.1 Literature Overview

The aim of this study was to develop a sustainable, low-cost MFC capable of hydrolyzing lignocellulosic biomass with and without rumen bacteria. In writing the literature review, special focus was therefore placed on: **(1)** the fundamentals of electricity generation in MFCs, **(2)** the microbial ecology of electrochemically active bacteria (EAB) and cellulose-degrading bacteria, **(3)** electrochemical measures of fuel cell performance, and **(4)** MFC design considerations.

2.2 Electricity Generation and Performance in Fuel Cells

Fuel cells are commonly described as devices that directly and continuously convert chemical energy into electricity, via the oxidation of a substrate (*Barbir 2005; Williams 1966*). They operate without combustion steps and do not require recharging, unlike voltaic batteries (*Barbir 2005; Hoogers 2003*). They do however, require a continuous supply of fuel and oxidant to maintain current. A reduced fuel (e.g. hydrogen or methanol) is oxidized at the anode, yielding electrons, which are captured by an external circuit and transferred to the cathode, where they are again captured by an

oxidant, such as O₂ (Figure 2-1). Abiotic fuel cells typically require non-renewable catalysts like platinum to catalyze the oxidation of electrochemically active fuels like hydrogen or solid oxides (Lovely 2006). The oxidation-reduction half reactions that take place at the anode and cathode of a gaseous, hydrogen fuel cell are as follows:

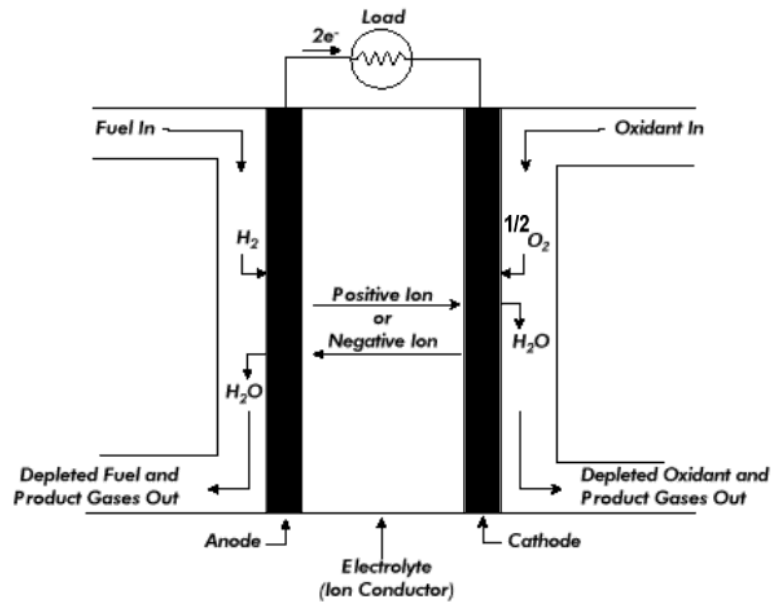
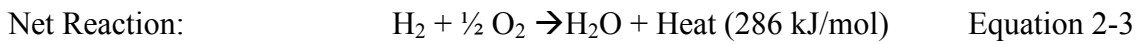
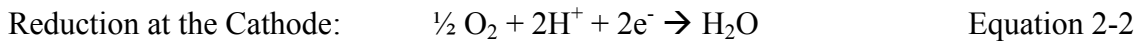


Figure 2-1. Hydrogen fuel cell schematic displaying the flow of electrons, protons, and oxygen molecules across a cation-specific boundary (from: USDOE 2004)

MFCs operate on similar principles. They convert the biochemical energy present in organic or inorganic material into electricity using bacteria, rather than platinum, as the catalyst to oxidize fuels (Bennetto et al. 1983; Logan et al. 2006). Oxidation of glucose,

or a similar substrate, by bacteria is accompanied by the release of CO₂, protons, and electrons, according to:



Early MFCs relied on chemical mediators (e.g. methylene blue or thionine) to shuttle the released electrons to the anode (*Logan 2006*). The more recent generation of mediator-less MFCs relies on the formation of an anaerobic biofilm by EAB to transfer the electrons released during oxidation of the substrate to the anode, typically a carbon or graphite material (*Watanabe 2008*). A current is subsequently generated when electrons flow from the anode to a cathode via a conductive wire and resistor (or load). The total amount of energy that can be captured is proportional to the potential difference between the electron carrier that donates the electrons to the respiratory chain (e.g., nicotinamide adenine dinucleotide, NADH) and the terminal electron acceptor (e.g., oxygen) (*Logan and Regan 2006*). A portion of this energy is captured by the EAB, and the remainder is used to create electrical current in the MFC. To maintain electrical current, protons must be continuously removed. Typically, protons and electrons react with oxygen at the cathode, (according to Equation 2-2) although an alternative electron acceptor like ferricyanide may also be used. The cathode and anode may be separated by a cation exchange membrane (CEM) into different compartments (two-chambered MFCs), wherein the CEM allows released protons and other cations to migrate to the cathode. If oxygen is the electron acceptor, it is provided by aerating the cathode chamber (Figure 2-2). Alternatively, the anode and cathode may be closely spaced, with or without a CEM, in a single-chamber or air cathode MFC.



Figure 2-2. Two-chambered H-type MFC in which the cathode chamber is aerated and a cation-specific membrane separates the anode from the cathode
 (from: www.engr.psu.edu/ce/ENVE/logan)

In air cathode systems—the configuration of interest in the current study—the cathode is not submerged in an aerated solution. Instead, oxygen is provided by exposing the cathode to air. This configuration relies on a semi-permeable cathode (e.g. Teflon-coated, carbon cloth) to separate the anode chamber from the oxygen. Figures 2-3 and 2-4 illustrate the electron transport process and some of the potential configurations of air cathode MFCs.

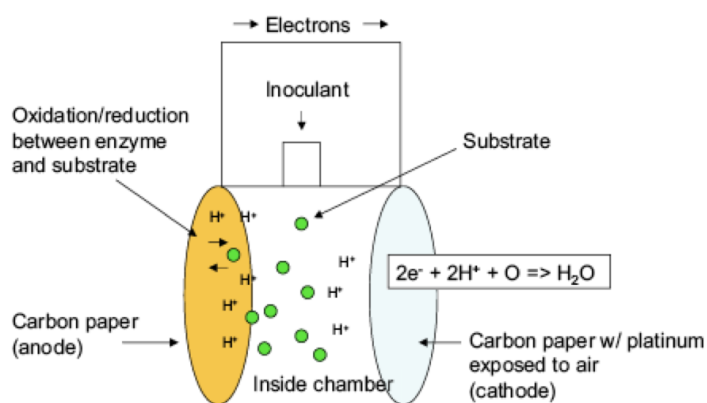
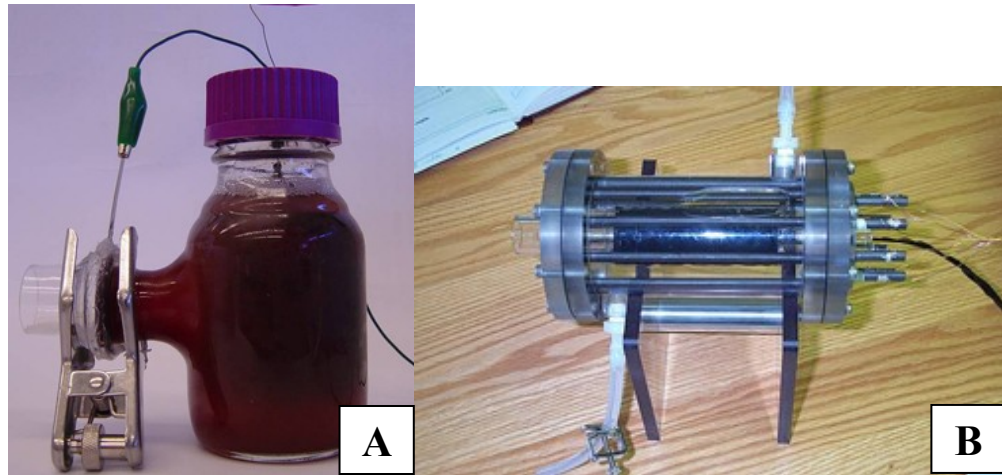


Figure 2-3. Single Chamber, Air Cathode MFC with Passive Diffusion of Oxygen (Zielke 2005)



Figures 2-4. Single Chamber, Air-Cathode Configurations
 (A) Carbon cloth cathode is held in the side-arm of the bottle & Anode is submerged in liquid (*Logan et al. 2007*); (B) Graphite rod anodes are in a concentric circle around a carbon cloth cathode (*Liu et al. 2004*)

To ensure the efficient conversion of the substrate to electrical current, dissolved electron acceptors such as oxygen, nitrate, and sulfate should be excluded to the extent possible, thereby forcing respiration using the anode as the terminal electron acceptor (*Liu et al. 2004; Logan & Regan 2006; Parameswaran 2009a*). In air cathode systems, an aerobic biofilm forms on the inside of the cathode to consume oxygen diffusing into the anode chamber, and reduces the amount of substrate lost to oxygen reduction, rather than anode reduction (*Liu & Logan 2004; Liu et al. 2004; 2005*). The addition of a CEM or diffusion layers can significantly reduce oxygen diffusion and minimize electron loss (*Liu & Logan 2005; Watanabe 2008*). It is unclear as yet if there is significant advantage to using standard anaerobic microbiological techniques to establish mixed-culture MFCs, as the reactors seem to quickly be quickly reduced by facultative bacteria. In fact, the majority of EAB identified thus far are facultative anaerobes. Prolonged exposure to

dissolved oxygen (DO) does not seem to impede long-term performance, and anaerobic conditions and cell voltage tend to recover quickly (*Oh et al. 2009*).

2.3 Microbial Ecology of MFCs and Cellulose-Degrading Bacteria

2.3.1 Anode Respiration and EAB

As bacteria oxidize organic matter, electrons are released. In aerobic environments, the electrons are transferred to and descend a respiratory chain of enzymes to oxygen, the terminal electron acceptor (TEA), in a process termed aerobic respiration (*Madigan & Martinko 2006*). In the absence of free molecular oxygen, either anaerobic respiration or fermentation serves as the mechanism for substrate catabolism. Respiration, both aerobic and anaerobic, relies on terminal electron acceptors, which theoretically are preferentially reduced by bacteria in the order of their reduction potential (E_0') (Table 2-1; *Maier et al. 2000*). Figure 2-5 illustrates the metabolic processes undertaken during cellular respiration.

Table 2-1. Exogenous Electron Acceptors and Reduction Potential Values (*Maier et al. 2000*)

TEA	→ Reduced Product	E_0' (V)
O ₂	H ₂ O	+ 0.815
Fe ³⁺	Fe ²⁺	+ 0.77
NO ₃ ⁻	N ₂	+ 0.75
Mn ⁴⁺	Mn ²⁺	+ 0.55
SO ₄ ²⁻	HS ⁻ → H ₂ S	- 0.22
CO ₂	CH ₄	- 0.25

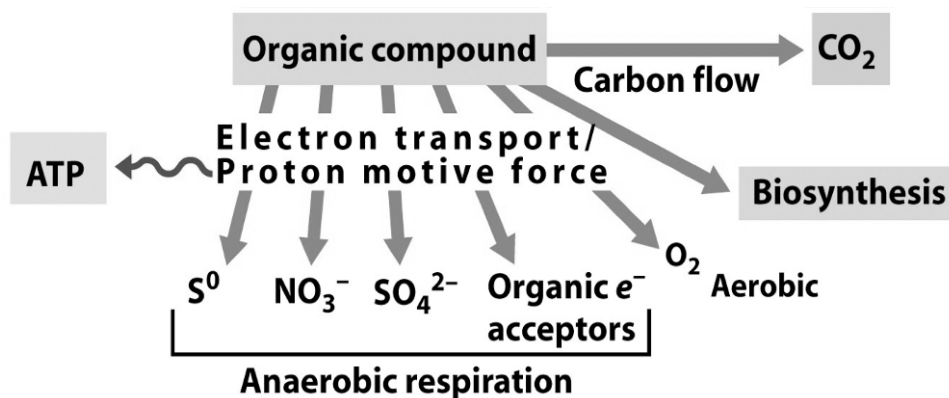


Figure 2-5. Chemoorganotrophic Metabolism
(Madigan & Martino 2006)

Fermentative metabolism, on the other hand, reduces some atoms of the electron donor and oxidizes others, and thus an external electron acceptor is not used (Madigan & Martinko 2006). Air-cathode MFCs rely on all three mechanisms for the conversion of complex substrates and extracellular electron transfer to an anode. The EAB, which are ultimately responsible for electricity generation, perform anaerobic respiration using an insoluble electron acceptor.

EAB have proven capable of electron transfer via three different mechanisms—direct transfer via outer-membrane cytochromes; microbially-produced mediators like pyocyanin (e.g. in *Pseudomonas* and *Shewanella* strains); and transfer via conductive pili, also known as ‘nanowires’ (e.g. in *Geobacter* species and *Aeromonas hydrophila*) (Bond et al. 2003; Lovely 2006; Rabaey et al. 2004; Torres et al. 2009). A number of MFC studies have examined the relative contributions of suspended versus attached populations, and while it appears that anode-attached bacteria are primarily responsible for direct electron transfer, it is unclear how the two mechanisms interact in the suspended anode solution (Kim et al. 2005; Liu & Logan 2004; Rabaey et al. 2004).

It has been demonstrated that a number of the EAB populations found in MFCs are phylogenetically related to metal-reducing bacteria (e.g. *Geobacter* and *Shewanella*), which are capable of reducing an insoluble terminal electron acceptor (e.g. Fe(III) or Mn(IV) oxides) (Lovely 2006). As such, a significant number of MFC studies to date used inocula that typically include *Geobacter* and/or *Shewanella* species—e.g. soil slurries, wastewater, and activated sludge (Zuo *et al.* 2006; Logan *et al.* 2002). *Shewanella (putrefaciens)* strains, *Geobacter (sulfurreducens* and *metallireducens)* strains, *Pseudomonas* strains, *Clostridium butyricum*, *Rhodoferax ferrireducens*, and *Aeromonas hydrophobia* have been commonly identified within anode biofilms (Bond & Lovely 2003; Gorby *et al.* 2006; Liu *et al.* 2005; Lovely 2006; Logan & Regan 2006). Suspended bacterial populations appear to be more phylogenetically diverse, compared with attached organisms, owing to their dual role in fuel oxidation and electron transfer. In any case, enrichment for EABs in both suspended and attached communities has been successfully accomplished (Rabaey *et al.* 2004).

Within one two-chambered MFC that achieved low internal resistance and high power density (4.31 W/m²), facultative anaerobic bacteria capable of hydrogen production were predominant (e.g. *Alcaligenes faecalis* and *Enterococcus gallinarum*) (Rabaey *et al.* 2004). These hydrogen- and electron-producing pathways were further explored by Parameswaran *et al.* (2009b), who found that three-way syntrophic interactions take place between fermenters, hydrogen consumers, and acetate-consuming bacteria that can reduce the insoluble anode. In this system, methanogenesis had to be suppressed so that the electron equivalents derived from hydrogen could be transferred to the anode. One caveat to these findings is that mixed cultures have been shown to

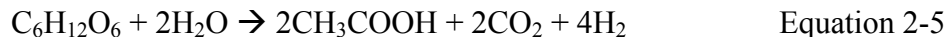
achieve greater power densities than pure cultures, likely owing to the fact that complex substrates require a consortium of microorganisms, capable of fermentation, H₂ consumption, and anode respiration (Logan *et al.* 2006; Lovely 2006; Parameswaran *et al.* 2009a, 2009b).

2.3.2 Cellulolytic Bacteria & Cellulose-Fed MFCs

The first step in the biodegradation of lignocellulosic biomass like corncobs—the substrate of interest in the current study—requires bacterial species capable of initially hydrolyzing the complex polymeric compounds into sugars and other fermentable substrates (Madigan & Martinko 2006; Tengerdy & Szakacs 2003). Pre-treatment measures, like steam explosion or crushing, can be used in order to make the polysaccharides available to most microorganisms during solid state fermentation and other biodegradation processes. However, the symbiotic anaerobic bacteria found in the gut wall of ruminants—collectively referred to as the "rumen bacteria"—naturally function as consortia to hydrolyze and ferment lignocellulosic biomass (Hu & Yu 2005; O'Sullivan *et al.* 2006). Common cellulolytic rumen bacteria include *Fibrobacter succinogenes*, *Ruminococcus albus*, and *Clostridium lochheadii* (Madigan & Martinko 2006; Rismani-Yazdi 2008). Other than *Clostridia*, rumen bacteria have been relatively unstudied to date with respect to their potential anode-reducing abilities.

In addition, fermentative bacteria are needed to convert the products of cellulose hydrolysis to organic acids (e.g. acetate and butyrate) and other small molecules that can be utilized directly as the electron donor by EAB for electricity generation (Parameswaran *et al.* 2009a; 2009b). For example, glucose can be fermented to H₂ and

acetate (Equation 2-5), which can be used as an electron donor by electrochemically active *Geobacter* strains.



Park et al. (2001) was the first to identify bacteria from the *Clostridium* sub-phylum as being capable of direct anode reduction. *Clostridium* sp. EG3 (Figure 2-6) was identified in Fe (III)-reducing colonies of a MFC utilizing glucose as the electron donor, and was found to have 98% 16S rRNA gene similarity to *Clostridium butyricum*.



Figure 2-6. Scanning electron micrograph of *Clostridium* sp. EG3 (Park et al. 2001)

These findings are consistent with the work of Rismani-Yazdi et al. (2009), who added microcrystalline cellulose and rumen fluid to a two-chambered MFC. Through denaturing gradient gel electrophoresis (DGGE) analysis, they found that bacteria within the *Firmicutes* division (specifically members of the *Clostridium* and *Sedimentibacter* genera) and *Deferribacteres* dominated the anode-attached populations, while *Comamonas* spp. (Gram negative, facultative anaerobes) dominated the suspended microbial populations. Despite these findings, Ren et al. (2007) concluded that a pure

culture of *Clostridium cellulolyticum* was incapable of current production, despite fermenting 42% of cellulose-derived sugars into hydrogen, acetate, and ethanol. Conversely, the pure culture of *Geobacter sulfurreducens* was incapable of cellulose-degradation, but, when combined with *C. cellulolyticum* in a co-culture, was capable of 64% cellulose degradation.

Similarly, Wang et al. (2009) developed a mixed, soil-based co-culture (consisting of a beta-proteobacterium and *Clostridium* strain) to have high cellulose saccharification abilities. By combining it with a secondary inocula of domestic wastewater in which *Rhodopseudomonas palustris*, Fe(III)-reducing, *Clostridium* and other strains were identified, the authors were able to produce electricity from powdered corn stover in a single-chamber, air cathode configuration. Community analysis of the DNA suggested that the composition of the microbial communities associated with the corn stover and the anode shifted and became more similar over time. These results suggest that the wastewater inocula may also be capable of cellulose hydrolysis, or alternatively, may be utilizing the intermediates of hydrolysis for electricity production; however, it is unclear whether the anode-attached *Clostridium*—a Gram positive bacteria with known cellulose hydrolysis capabilities—is also capable of exoelectron transfer. Outside of *Clostridium*, it is also unclear which, if any, bacterial populations in the rumen are capable of anode respiration.

2.4 Fuel Cell Performance Measures

The theoretical efficiency of a fuel cell (η) is defined as

$$\eta = \frac{\Delta G}{\Delta H}$$

Equation 2-6

where ΔG is the Gibb's free energy of the reaction (kJ/mol) (energy available for useful work), and ΔH is the reaction enthalpy (kJ/mol). Thus, η is limited only by the loss of ΔH to entropy/heat ($T\Delta S$) (Barbir 2005; Rosenbaum 2007), according to

$$\Delta G = \Delta H - T\Delta S \quad \text{Equation 2-7}$$

Using this approach, η for the oxidation of hydrogen by oxygen at standard temperature and pressure (at 25°C, 1 atm) is 83%.

Using the principle of electrical work, the theoretical potential (E_0) of the reaction can also be used to calculate efficiency as a ratio of two potentials:

$$W_e = -\Delta G = nFE \text{ [kJ/mol]} \quad \text{Equation 2-8}$$

where W_e = electrical work (kJ/mol), n = the number of electrons per mole fuel, and F = the Faraday's constant (96,485 C/mol)

$$\eta = E_0 / \left(\frac{\Delta H}{nF} \right) \quad \text{Equation 2-9}$$

This definition of efficiency does not account for irreversible losses within the fuel cell. Open circuit voltage (OCV), which is the measured voltage across the anode and cathode with no current flowing, is theoretically equivalent to the theoretical cell potential, or electromotive force (EMF). However, such losses result in OCV readings that are significantly below the EMF. As an example, the EMF of a 5 mM acetate-fed MFC with an oxygenated cathode ($P = 1 \text{ atm}$; $T = 25^\circ\text{C}$; $\text{pH } 7$) is 1.1 V (Logan *et al.* 2006). Losses in voltage are the result of (1) activation polarization (i.e. the energy lost to initiating the redox reactions at the electrode surface); (2) diffusion (mass-transport) polarization, where the concentration of substrate or oxidant becomes limiting, and (3) ohmic resistance (electronic, ionic, and contact resistance) (Barbir 2005; Chang *et al.*

2006; USDOE 2004). The cumulative effect of these overpotentials is to increase the anode potential and decrease the cathode potential—reducing cell voltage (Equation 2-9) (USDOE 2004). These losses can be quantified (and minimized) experimentally by controlling the potential of the electrode with a potentiostat or electrochemical impedance spectroscopy (EIS) techniques or by adjusting current flow from anode to cathode (via a variable resistor).

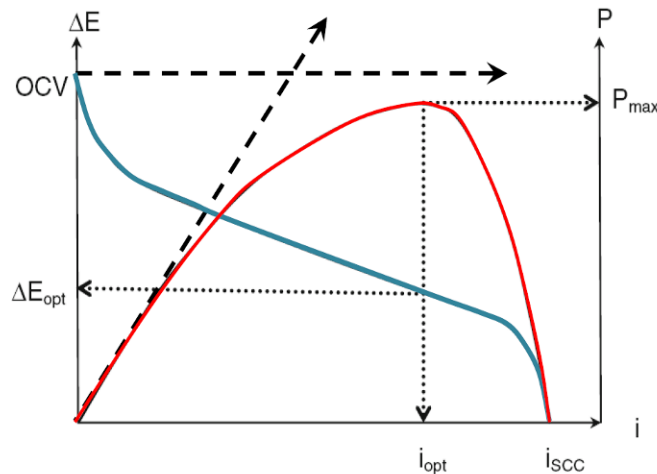


Figure 2-7. Ideal polarization curves displaying the relationship between maximum power (P_{max}), short-circuit current (I_{scc}), and internal resistance (R_{int}). The asymmetric shape of the power curve implies that ohmic losses do not dominate.

This allows the potential difference between the redox potential of the substrate and the anode potential to be increased—making the insoluble electrode preferential for bacterial reduction relative to alternative processes like fermentation, while still maximizing MFC voltage (Logan *et al.* 2006). Collectively, the activation, ohmic, and mass-transport losses are displayed graphically as a cell's polarization curve (Figures 2-7 and 2-8), which is widely used to assess performance (Borole *et al.* 2009; Logan *et al.* 2006; USDOE 2004). The polarization curve also describes the trade-off between cell potential/efficiency and power density (Figure 2-9). From these curves, cells can be

sized for maximum power density, maximum efficiency, or a target value that balances certain design parameters (*Barbir 2005; USDOE 2004*).

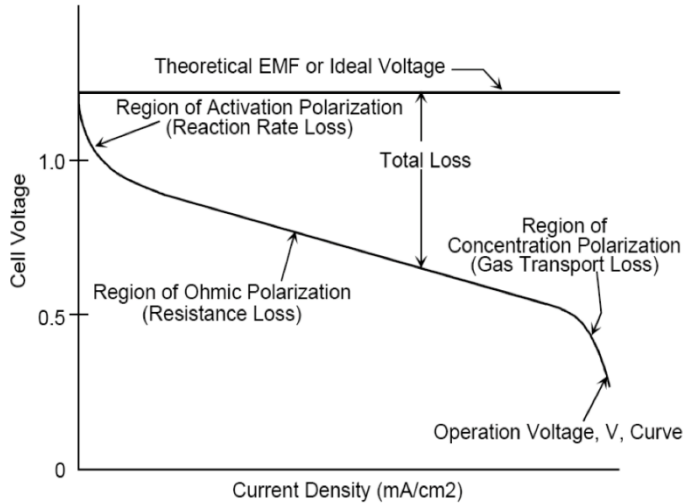


Figure 2-8. Fuel cell polarization curves displaying three regions of overpotential. (*USDOE 2004*)

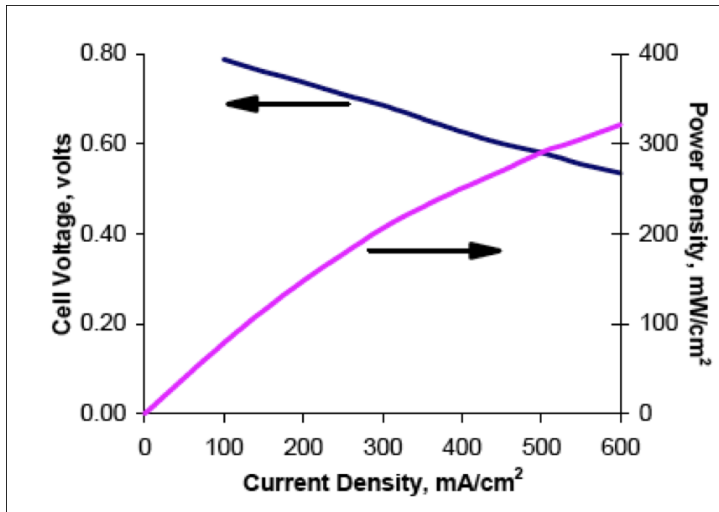


Figure 2-9. Fuel cell polarization curves displaying the voltage-power relationship. (*USDOE 2004*)

For MFCs, internal losses are primarily the result of ohmic losses—owing to electron transport limitations through organic matter—and can be minimized through reduced electrode spacing, increased solution conductivity, and decreased resistance through the CEM, electrode coatings, and electrical connections (*Logan 2006*). If the region of ohmic losses on a voltage-current plot is linear (as is the case in most MFCs),

then Ohm's law can be applied, and the slope of the linear portion corresponds to the cell's internal resistance:

$$R_{\text{int}} = \frac{\Delta E}{\Delta I} \quad \text{Equation 2-10}$$

Key performance measures for MFCs include current and power (density), Coulombic efficiency, and polarization losses. Because the performance of MFCs is largely dependent on the anode reaction (see discussion above regarding polarization losses), the current (and power) measurements are typically normalized by the projected surface area of the anode, or volume of the anode chamber when surface area is difficult to assess (*Logan et al. 2006; Logan 2008*). Alternatively, the cathode reaction can be the limiting factor in power generation when (1) the rate of oxygen reduction (typically sluggish) is not increased with a catalyst (e.g. platinum); (2) when oxygen diffusion into the anode chamber significantly reduces the amount of substrate utilized by anode respiration; and (3) when a small cathode area limits the oxygen available for reduction (*Chen et al. 2006*).

Coulombic efficiency—another key performance measure—represents the fraction of electrons (Coulombs) released during substrate oxidation that are successfully transferred to the external circuit. Coulombic efficiency (ϵ_{Cb}) can be calculated according to

$$\epsilon_{Cb} = \frac{M \int_0^{t_h} I \, dt}{FbV_{An} \Delta \text{ 'OD}} \quad \text{Equation 2-11}$$

where ΔCOD is the Coulomb-equivalent of the change in chemical oxygen demand (COD) over time, M is the molecular weight of oxygen, F = the Faraday's constant (96,485 C/e-mol), b is the number of electrons exchanged per mole oxygen ($b = 4$), and V_{An} is the liquid volume of the anode (*Cheng et al. 2006; Liu et al. 2004; Logan et al. 2006*).

Coulombic efficiency is reduced when electrons are diverted to various sinks, including terminal electron acceptors in respiration processes (e.g. oxygen, nitrate, and sulfate), as well as to fermentation and methanogenesis (*Cheng et al. 2006; Parameswaran et al. 2009a*). As mentioned in section 2.3, the potential of the anode can play a large role in the efficiency of electron transfer, and poisoning the anode such that its potential is as low (negative) as possible without encouraging fermentation as an alternative electron acceptor creates optimal conditions for voltage generation (*Logan et al. 2006*).

2.5 MFC Design Considerations

It is relatively well established that the primary factors affecting MFC performance are (1) internal resistance; (2) the rate of proton diffusion from anode to cathode (increased by reducing electrode spacing); and (3) reducing the fraction of electrons lost to fermentation/methane production (*Fan et al. 2007; Kim et al. 2005; Liu et al. 2005; Parameswaran 2009a,b; Watanabe 2008*). Additionally, single-chamber, air cathode systems seem to represent the configuration that best balances power production with scale-up feasibility, as they tend to minimize internal resistance (via close electrode

spacing), thereby improving power density without requiring multiple saturated chambers or unregenerable oxidants like ferricyanide (*Watanabe 2008*).

Designs for soluble-substrate MFCs do not take into account the potential short-circuiting and dead zones that more readily develop in solid-substrate bioreactors (*Reinhart & Townsend 1997; Wang et al. 2009*). For this reason, the present study reviewed literature on solid substrate fermentation (SSF) reactors and landfill bioreactors for known design strategies, hydrolysis kinetics, and recirculation rates. Significant decreases in porosity and hydraulic conductivity were consistently reported in SSF literature (*Durand 2003; Haydar 2007; Richard et al. 2004*). Rotation and mixing have been explored as methods to improve SSF performance, and agitation of the substrate seems to improve oxygen, water, and heat transfer throughout the reactor (*Durand 2003; Haydar 2007*). Additionally, Durand (2003) found that minimizing substrate depth with the use of trays (e.g. Koji-type processes) improves performance by minimizing compaction of the material. Finally, Klotz & Moser (1974) determined that a minimum ratio of 25:1 for reactor diameter to particle diameter is needed to minimize short-circuiting and improve contact between bacteria and the substrate. In the present study, it was anticipated that all of these factors would contribute to the internal resistance of the MFC, and minimizing their effects would have a beneficial impact on current and power density.

CHAPTER 3

MATERIALS & METHODS

3.1 Materials

3.1.1 Cellulosic Substrate

Corn cob pellets, which are commonly sold as bedding material for caged rodents, were used as the cellulosic substrate in the MFC (Figure 3-1). The use of a commercially available product ensured that a consistent material—in terms of particle size and aging—would be available for all experiments. Though there is a significant amount of storage time and processing that takes place between harvest and commercial production of corn stover, previous research has demonstrated that storage and processing methods of stover have little impact on cellulose conversion to glucose (*Montross & Crofcheck 2004*). It was therefore not anticipated that any reduction in cellulose content that might occur during storage of the corn cob pellets will significantly impact MFC performance.

The pellets were manually sieved for 5 minutes. Particles within the 2.36 mm to 4.76 mm size range were retained for use in this study. Average effective porosity, based on this particle diameter and hydraulic conductivity testing, was 0.3. The corn cob pellets were pasteurized at 60°C for 24 hr and stored in sealed plastic bags at room temperature

prior to use. The corncob pellets are highly absorbent and swell when wet. Therefore, before being placed in the bioreactors, the pellets were saturated with water for 1-2 hrs.



Figure 3-1. MFC Substrate Material—Corncob Pellets

A previous study demonstrated that the porosity, and hence the permeability, of straw were related to moisture content (*Richard et al. 2004*). For this reason, the hydraulic conductivity of the saturated corncob was measured over time. Initial values of hydraulic conductivity (K , [L/T]) and specific discharge (q , [L/T]) were obtained using the gradient ratio test with a constant head permeameter (diameter = 4 in., hydraulic head = 1 cm/cm) (Figure 3-2). Corncob material was layered loosely by hand in one shift to a total depth of roughly 24 inches. The material was saturated with water. Flowrate and hydraulic conductivity were measured three times, twice immediately after saturation and after two hours, to gauge the effects of prolonged swelling on permeability. At the end of the second trial, the reactors were modified to serve as constant head permeameters (Figure 3-3), such that hydraulic conductivity of the oxidized material could be re-tested, in situ.



Figure 3-2. Gradient Ratio Test with Constant Head Permeameter

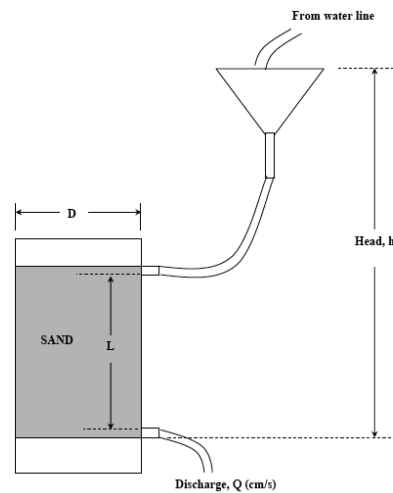


Figure 3-3. Hydraulic Conductivity Set-Up for the Spent Material (from: http://geotech.uta.edu/lab/Main/Soil%20Lab/08_Permeability)

3.1.2. Anode Materials

Two different anode materials were employed in the MFC trials, which are displayed below in Figure 3-4. In Trial 1, graphite granules (100 x 325 Grade 4012; Asbury Graphite) conducted electrons from the anode bed to two graphite rods (1/4 in. x

12 in.; Asbury Graphite), which served as the anode material. While the granules were responsible for electron conduction and were potentially reduced by the bacteria, they were not wired to the external circuit, and thus are not considered as part of the anode surface area. The graphite granules were manually sieved to obtain an average particle diameter of 3/8 in (0.953 cm). According to the manufacturer, the specific surface area of the granules was 16,000 cm²/g, and the surface area of each graphite rod was 60.8 cm². The graphite rods were first placed within the MFC, and then the granules were layered in alternating shifts, of approximately two inches, with the corncobs. Two graphite rods were used in the reactor, resulting in a total anode surface area of 121.6 cm², and a specific anode surface area of 0.1216 cm² per cm³ of anode wet volume (4.77 L; defined as the total volume between the top and bottom perforated plates). The graphite granules also provided void space and facilitated leaching through the substrate. The graphite rods were wired in series with a multimeter (Keithley 2700) and/or a resistor substitution box (RS-500, Elenco) to monitor open circuit voltage, potential, and current.

For Trial 2, carbon-fiber brushes with titanium stems (d= 5.5 in; 13 in brush; 16 in stem; Mill Rose Co.) were utilized as the sole anode material in each reactor. The brushes were pre-treated at 450°C for 30 min in a muffle furnace to decrease the relative oxygen-to-carbon ratio and increase the electrochemically active surface area (*Feng et al. 2009; Wang et al. 2009*). According to the manufacturer, there were approximately 500,000 fibers per inch of brush length, and the diameter of each fiber was 7.5 μm, resulting in a surface area of 3.292 mm² per fiber. The total anode surface area was 21.40 m² (213,980 cm²) and the specific anode surface area was 44.86 cm² per cm³ of anode

wet volume, providing more than 350 times greater surface area than Trial 1 for anode reduction.

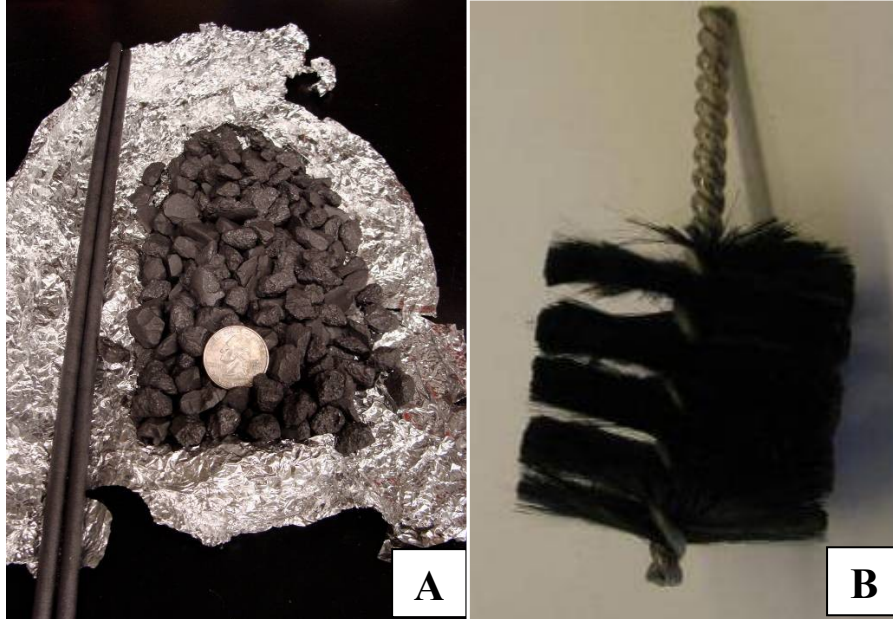


Figure 3-4. Graphite Granules (A) and Carbon Fiber Brush (B) Anode Materials

3.1.3 Cathode Materials

Rough strips of carbon cloth (8 in. x 13 in.) (AvCarb 2002HD; Ballard Industries Inc.) were used as the raw cathode material, providing an area of 2168 cm² for oxygen reduction. The holes drilled into the MFC body allowed for fluid transfer. Therefore, it was necessary to waterproof the carbon cloth, which was bound around the outside of the reactor. This involved submerging the cloth in a solution of 30% polytetrafluoroethylene (PTFE) in deionized water, allowing it to dry for 12 hours, and curing it at 370°C for 30 min. A base carbon layer and four additional PTFE layers (60%) were then applied to the air-side of the cathode as diffusion layers to reduce oxygen flow to the anode chamber,

following the method of Middaugh et al. (2006). The base layer consisted of carbon black (Vulcan XC-72R) suspended in 40% PTFE and was applied with a small brush at a rate of 1.56 mg carbon black per cm^2 cathode surface area. The four diffusion layers (60% PTFE dispersions; Fisher Scientific) were painted on with a small brush, air-dried, and cured at 370°C for 10-15 min between applications. Previous research has demonstrated that four PTFE layers reduce the mass transfer coefficient (k_L) for oxygen from 0.0033 cm/s for untreated carbon cloth to 0.0023 cm/s and eliminate water loss through the cathode (Cheng et al. 2006). Finally, a platinum catalyst layer was added to promote oxygen reduction at the cathode. The layer was made by mixing a 20% Platinum in Carbon black powder (Vulcan XC-72) with 5% by wt. Liquion (Nafion; Ion Power Inc.) and pure iso-propanol (99.5%; Acros Organics). Mixing was accomplished by vortexing for 10-20 sec. The suspension was painted onto the solution side of the cathode and allowed to air dry for 24 hrs. This protocol yielded 0.45 mg Pt per cm^2 of cathode area. The cathode cloth was bonded to the outside of the reactor using a non-conductive epoxy sealant to reduce leakage and water loss. The seams between pieces of carbon cloth were sealed first with conductive graphite cement to maintain electric current, and then sealed with silicone to eliminate leaks. Seams between the carbon cloth and the polycarbonate column were also coated with silicone, where necessary, to eliminate water loss from the MFC.

3.1.4 Plastic Matrix Material

For the second trial, a plastic filter material was added to the anode bed; the filter material is displayed in Figure 3-5. This type of material is typically used in trickling

filter processes and rotating biological contactors to provide surface area for microbial attachment (*Parker & Douglas 1984*). In the MFC, the purpose of the material is to provide structure and to facilitate leaching through the substrate.

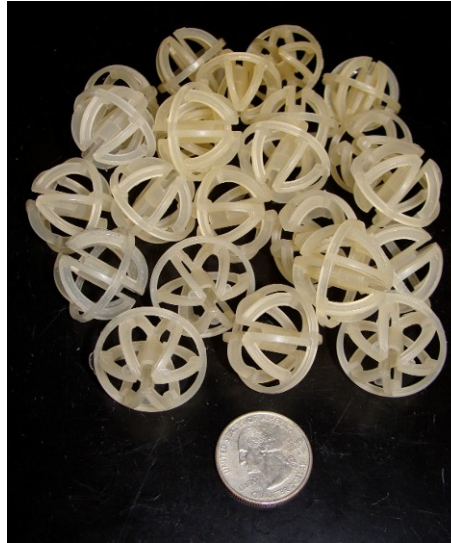


Figure 3-5. Plastic Filter Media added to the Anode Chamber

3.1.5 Microbial Inoculum and Media

Several different groups of bacteria are required to convert cellulose to electrical current in an MFC, including organisms that hydrolyze cellulose, those that ferment the products of hydrolysis, and EAB that oxidize the fermentation products and transfer the electrons to the anode. Different complex environmental samples were added to the MFCs in the experimental trials in an attempt to stimulate those key microbial activities.

In Trial 1, rumen fluid was added to the reactor at a ratio of 1:10 v/v (300 mL rumen fluid per reactor) to promote cellulose hydrolysis and fermentation. The inoculum was extracted from a fistulated cow that was fed a forage-based diet at the University of Maryland campus farm. The rumen fluid was stored in headspace-free vials, and

subsequently homogenized in a commercial blender (Waring Model 70125) under a 80% N₂/20%CO₂ gas mixture (ultra high purity; AirGas). The fluid was again stored in headspace free containers at room temperature for no more than three hours until inoculation. Rumen fluid was pumped into the MFC during the reactor start-up phase described below. During the addition of rumen fluid, the MFC was sparged with N₂ gas (ultra high purity; AirGas) to maintain anaerobic conditions.

Several inocula were added to the MFCs in trial 2. Initially, soil was added as the primary inoculum, at a dose of 26.7 g soil per liter anode volume (*Logan et al. 2002*; *Niessen et al. 2006*). The soil was taken from 8 in. below the ground surface of a pasture at the University of Maryland campus farm. It was subsequently transferred to aluminum pans, and heat-treated at 104°C for 90 min. The soil was then removed from the oven, cooled to room temperature, and packed into 60 mL plastic vials without headspace, and stored at 4°C until inoculation (*Logan et al. 2002*). Just before addition the soil to the MFCs, it was ground with a mortar and pestle to reduce particle size, mixed with the saturated corncob substrate (see below), and added to the reactor as described below.

After 658 hours, rumen fluid was added to the duplicate MFCs at a rate of 1:10 (v/v), following the procedures above to stimulate cellulose hydrolysis and fermentation. After 1409 hours, 0.6 g of 2-bromoethane sulfonate (BES) was added to each MFC to inhibit methanogenesis, thereby making conditions more favorable for growth of an anodophilic biofilm. *G. metallireducens* is a known EAB and was added to the MFCs at a dose of 300 mL per reactor after 1506 hours (transfer rate of 1 mL inocula per 100 mL media; transferred 5 days prior to inoculation).

The mineral media supplied to the MFCs is based on a complex media recipe used to enrich for cellulolytic bacteria and contained (per L): 300 mL clarified rumen fluid (described below); 0.5 g trypticase; 0.5 g yeast extract; 8 g NaHCO₃; 0.9 g KH₂PO₄; 0.09 g CaCl₂; 0.9 g NaCl; 0.9 g (NH₄)₂SO₄; 0.09 g MgSO₄·7H₂O; 2 mL trace element solution A (10 mL HCl (25% w/w), 1.5 g FeCl₂·4H₂O; 0.19 g CoCl₂·6H₂O; 0.1 g MnCl₂·4H₂O; 0.07 g ZnCl₂; 0.006 g H₃BO₃; 0.036 g Na₂MoO₄·2H₂O; 0.024 g NiCl₂·6H₂O; and 0.002 g CuCl₂·2H₂O in 1 L deionized water); 2 mL trace element solution B (0.006 g Na₂SeO₃; 0.008 g Na₂WO₄·2H₂O; 0.5 g NaOH in 1 L deionized water); 0.5 g Cysteine HCl·H₂O; and 1 mg resazurin (*Makkar & McSweeney 2005*). All biochemicals and growth factors, except trace elements, cysteine, and rumen fluid, were added to deionized water, boiled for 10 min to remove dissolved oxygen, then autoclaved for 40 min. Trace elements were added while cooling under the oxygen-free 80% N₂ / 20% CO₂ gase mixture (Ultrahigh purity; AirGas), and the flask was sealed with a rubber stopper, Neoprene tubing, and a two-way ball valve to prevent oxygen entry until the media was used (*Tanner 2007*). Cysteine and the clarified rumen fluid were added to the media immediately prior to MFC start-up.

Preparation of the clarified rumen fluid was performed by the Animal and Avian Sciences Department of the University of Maryland, according to the following procedure: Raw rumen fluid was obtained from a fistulated cow as described above. It was filtered through two layers of cheesecloth and centrifuged at 27,400 x g for 2 hr. The supernatant was then decanted and frozen at -20°C until use. Once thawed, the supernatant was centrifuged again at 27,400 x g for 2 hr, sparged with CO₂ for 2 hr, and then autoclaved at 121°C for 30 min. It was again frozen at -20°C (aseptically under

CO₂). Before use, it was again thawed and centrifuged at 27,400 x g for 2 hr.

Autoclaving sterilizes the rumen fluid so that only the growth factors needed for microbial growth remain.

G. metallireducens was maintained on acetate and ferric citrate as previously described and was added to the MFCs five days after transferring the culture to fresh media (Piwkhov 2007).

3.2 MFC Reactor Design

A new MFC reactor design was needed in this study because previous MFC designs are based on soluble, microcrystalline, or finely ground solid substrates and are not appropriate for complex solid substrates.

The MFC design used in this study functions as a packed bed biofilm reactor, in which the attachment media also serves as the growth substrate, somewhat similar to a leach-bed bioreactor (Mitchell *et al.* 2006). The MFC is typically operated in a batch mode, in which the solid substrate is not replaced until MFC performance declines. The leachate from the packed bed was continuously recycled in down flow mode to distribute soluble substrates generated by cellulose hydrolysis to EAB. The potential to add or drain off media if the liquid level fell below, or exceeded, saturation levels was also included in the reactor design. Flow was controlled by a peristaltic pump (Masterflex) at 8 mL/min—maintaining plug flow conditions. It was hypothesized that over time, biodegradation of the corncobs would cause them to agglomerate, leading to a reduction in porosity over the course of a trial. Therefore, bulking material (graphite granules

and/or plastic matrix media) (as described in Section 3.1.4) was packed into the MFC bed in each trial to provide structure and facilitate leaching through the substrate.

To minimize short-circuiting and improve contact between bacteria and the substrate, the ratio of reactor diameter to particle diameter was set at 25:1 (*Klotz & Moser 1974*). The corncob particle size ($2.36 \leq d_p < 4.76$ mm) dictated a minimum reactor diameter of 7.5 cm (3 in)—significantly larger than most lab-scale MFCs to date. Using a two-to-one ratio of reactor height-to-diameter further encouraged even distribution of flow and substrates throughout the column.

Initially, a single prototype MFC reactor was constructed from a polycarbonate cylinder (5.5 in I.D. x 14 in. height) (Figure 3-6). It was used in a preliminary experiment (Trial 1), described below. Subsequent experiments were conducted in duplicate using an additional reactor that was constructed to run in parallel with the first (Figure 3-7). Rows of ½ in. holes spaced at 1 in. center-to-center were drilled into each cylinder. The rows were vertically spaced at 2 in. on center. Plastic perforated plates were installed 3.76 in from the top and 1.25 in from the bottom of the reactor to contain the corncob pellets and other materials. As stated previously, the wet volume of the anode was 0.00477 m^3 . A 15 cm filter paper circle (Whatman, $>25\mu\text{m}$) was placed on top of the upper perforated plate to ensure even distribution of the water across the plate. The top of the reactor was sealed with a flat acrylic lid and secured with a rubber gasket and three screws. An influent port was drilled into the lid, and made gas-tight with a rubber septum. A recycle line was constructed using Norprene tubing (Masterflex; L/S 16, 3.1 mm I.D.) to minimize oxygen diffusion into the leachate, as it was recycled to the top of the MFC. The recycle line was drawn through a rubber stopper in the lid of the

MFC and was connected with a 1/8" threaded hose barb (Industrial Specialties Inc.) at the base of the reactor. A peristaltic pump (Masterflex) was used to control the recycle flow at 8 mL/min. The recycle rate was determined by extrapolating (on a volume basis) the flow rates used in similar MFC configurations that did not produce a decrease in power output (*He et al. 2006; Moon et al. 2005; You et al. 2007*). A tabular summary of the reactor's geometric properties can be found in Appendix A.

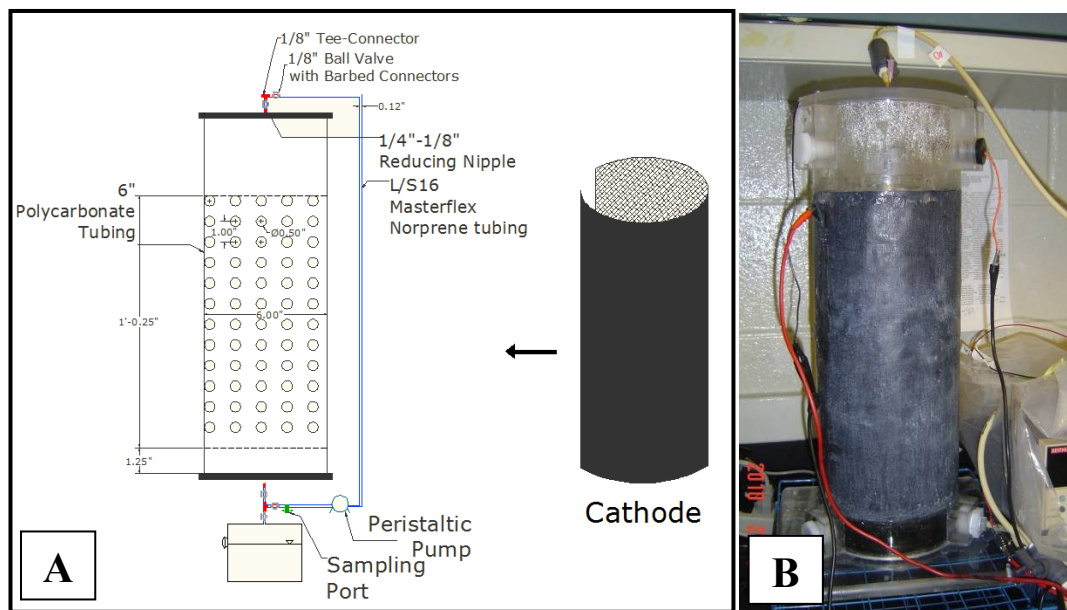


Figure 3-6. Schematic (not to scale) (A) and Picture (B) of Solid Substrate MFC

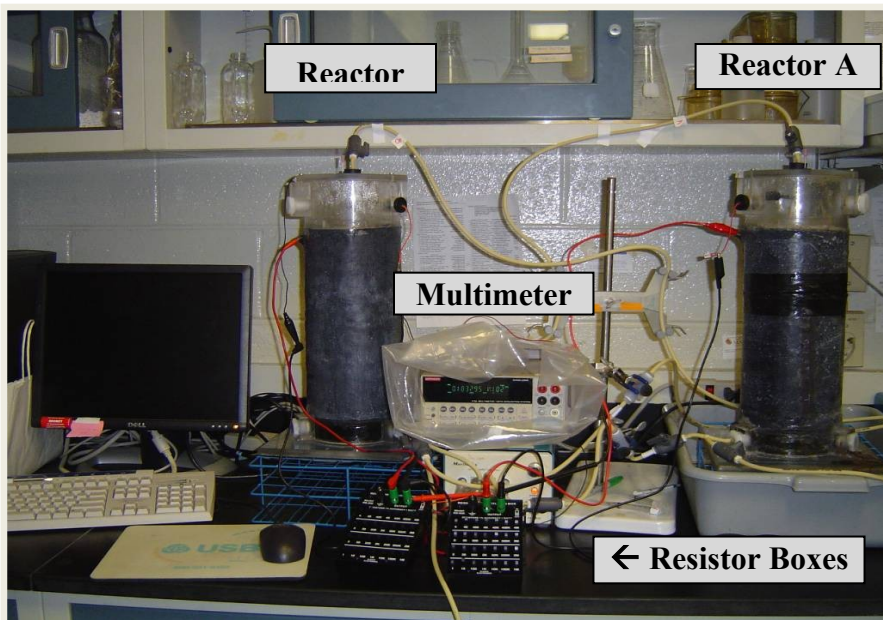


Figure 3-7. Parallel MFC Reactor Set-Up for Trial 2

3.3 Reactor Start-Up Procedures

The anode material (graphite rods or carbon fiber brushes) was inserted into the reactor body, and then equal parts (volume basis) of the corncob and sterile plastic matrix were filled in around it. In Trial 1, a total of 488 g of corncob and 3030 g deionized water were filled in around it. In Trial 1, a total of 488 g of corncob and 3030 g deionized water was added to the reactor—a loading rate of approximately 102 g/L/trial. In trial 2, 692 g of dry corncob and 1460 g (1.46 L) deionized water was added to each reactor—a loading rate of 145 g/L/trial. The saturated corncob was then mixed with the sterilized plastic matrix material at a 1:1 ratio. The anode was then connected to the external circuit using copper connectors and wire (#22 Cu in Trial 1; #10 in Trial 2). Dielectric grease (Standard; SL-4) was used at each electrical connection to minimize corrosion and maintain current flow over time. The reactor was then sealed and sparged with N₂ gas for 30 min. Media was pumped into each reactor using a peristaltic pump (Masterflex),

while simultaneously sparging with N₂ gas to maintain positive pressure and minimize oxygen intrusion. For Trial 1, a small amount of headspace was left in the reactor to allow addition of the rumen fluid inoculum. For all trials, the media plus microorganisms were recycled for the hydraulic residence time (HRT = 2 hr). The recycle flow was then turned off for 24 -32 hr to facilitate microbial attachment and biofilm development on the anode and/or corncob pellets. During the attachment period, potential (V) and current (i) was monitored every 20 min, and pH, temperature, and the concentrations of dissolved oxygen, methane, and hydrogen were analyzed once. The recycle stream was restarted after the 24-36 hr attachment period at a flow rate of 8 mL/min, and thereafter the leachate was recirculated continuously. Occasionally, water loss through the cathode resulted in water levels falling below saturation levels within the MFCs. When this occurred, additional media was pumped into the MFC until the pellets were saturated.

3.4 Electrochemical Measurements

OCV readings, where $R_{ext} \rightarrow \infty$, were taken during the first 24 hr of Trials 1 and 2 to gauge the cell's electromotive force (E_{emf}) and overpotential (see Section 2.4). Thereafter, current was allowed to discharge across a known resistance (500-1100 Ω), and potential readings were taken every 20-30 min using a multimeter and data acquisition system (Keithley 2700; ExceLINX software). The MFC circuit used in this study is shown in Figure 3-8 below. Current and power across a known R_{ext} were calculated via Equations 2-10 and 3-1.

$$P = V^2/R \quad \text{Equation 3-1}$$

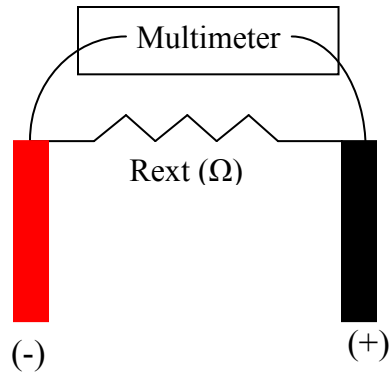


Figure 3-8. MFC External Circuit

At least once per trial, the R_{ext} was varied between 5Ω and $2,000,000 \Omega$ using a resistor substitution box (RS-500; Elenco) to measure the effects on cell potential and to develop polarization curves (see Section 2.4). After each change in resistance, the reactor was allowed to equilibrate before taking steady-state readings. During this period, potential was plotted in real time, using a time step of 1 min, and a plateau could be observed in the plot when the system had successfully equilibrated to the new external resistance. Changes in potential were recorded going from both low-to-high and high-to-low resistance values. The steady-state values for potential were then used to calculate i and P (Equations 2-10 and 3-1). Because the estimations of anode surface area were approximate, I and P measurements were normalized to the wet volume of the anode (0.00477 m^3) to determine current and power density. Power density was also plotted as a function of current density to gauge ohmic (internal) resistance, and the relative polarization losses of each system.

3.5 Analytical Measurements

Analytical measurements during each trial run included: ambient temperature, pH, dissolved oxygen (DO), leachate temperature, hydrogen and methane concentrations, organic acids, and the mass of substrate consumed.

Ambient temperature and humidity in the laboratory were continuously measured using a chart recorder (Dickson THDX). Every two days leachate pH, temperature, and DO measurements were made on the MFCs. The flow-through micro DO probe (OM-4; MI-730A; Microelectrodes Inc.) was calibrated prior to each analysis, using a saturated sodium sulfite solution (15 g Na₂SO₃ in 250 mL deionized water) as 0% DO and water-saturated air as 21% DO. DO was measured by withdrawing a 2 mL sample from the recycle line anaerobically and injecting it into the DO probe. The DO concentration (in mg/L) was calculated according to

$$DO(mg / L) = \frac{DO(\%)}{21\%} * DO_{sat}[mg / L] \quad \text{Equation 3-2}$$

An additional sample of 10 mL was withdrawn from each reactor to measure temperature and pH, using an Accumet 950 pH probe and meter and a glass thermometer (accuracy of 0.1 °C), respectively

Twice per week, the concentrations of methane, hydrogen, COD, and organic acids in the leachate were measured. Methane and hydrogen in the MFC headspace were quantified at the same time. Following the method of Freedman and Gosset (1989), methane was quantified using a gas chromatograph (Agilent HP5890 Series II GC) equipped with a flame ionization detector (FID), ChemStation software (Agilent; A.10.02), and a stainless steel column packed with 1% SP-1000 on 60/80 Carbopack-B

(2.4 m x 3.2 mm; Supelco). Ultra high purity carrier grade helium (Airgas) was used as the carrier gas, at a flow rate of 40 mL/min. Hydrogen and air (ultra high purity carrier grade; Airgas) were provided to the detector at flow rates of 60 mL/min and 260 mL/min, respectively. The injector and detector temperatures were set at 200°C and 250°C, respectively. Oven temperature was initially set at 60°C, subsequently increased at 20°C/min to 150°C, and then increased at 10°C/min to 200°C. The retention time for methane was 5.5 min. Hydrogen concentrations were determined using a Peak Performer 1 GC (Peak Labs, California) with a reducing compound photometer (RCP) detector and 2 columns—a 31 in. UNI 1S guard column and a 31 in molecular sieve 13X. Column temperature was set at 105°C; detector and temperature programs were set at 265°C. Nitrogen was used as the carrier gas (Airgas) at a flow rate of 20 mL/min. The retention time for hydrogen was 66 sec.

Calibration curves were obtained for both hydrogen and methane using known concentrations of the gases, ranging from 0.935 ppmv to 16.83 ppmv for hydrogen and from 0.077 mM to 0.129 mM for methane. Gas standards (18.7 ppm hydrogen and 99.0% methane; AirGas) were used to purge empty vials (10 mL to 160 mL), suspended upside down for 10-15 min to force out the gas with greater molecular weight (MW air = 28 g/mol; MW CH₄ = 16 g/mol). Gas aliquots were then used to serially dilute gas-tight vials that had been purged with N₂ (ultra high purity; AirGas) with known concentrations of each gas. For hydrogen only, the vial contents were analyzed to check for background H₂. For both gases, the standard bottle was re-sparged with pure gas for each 1 mL of gas removed. The injection volumes were 0.2 mL for hydrogen and 0.5 mL for methane.

Hydrogen and methane concentrations were measured in both the liquid (leachate) and gas phases of the MFC. For determination of aqueous concentrations, a 2 mL liquid sample was collected from the recycle line, transferred to a 10 mL gas tight sampling vial, and allowed to equilibrate for 3 min before injecting a headspace sample into the GC. The sample vials were flushed with N₂ and analyzed for background hydrogen concentrations, as described above, and 2 mL of gas was removed to avoid excess pressure when the aqueous samples were added. Gas-phase hydrogen and methane were analyzed by removing two separate 0.5 mL gas samples from the MFC headspace (above the packed bed) using a gas-tight syringe (Vici Corp.) and rubber septum (Geo-Microbial Technologies) installed in the reactor lid, and manually injecting the samples on to the appropriate GC. The amount of gas in each injection was reported as a peak area value by the GC, which was then converted to a concentration using the calibration curve.

Analysis for volatile fatty acids, using GC techniques, was performed by the Animal & Avian Sciences Department of the University of Maryland. The following organic acids were quantified: acetate, propionate, (iso)butyrate, and (iso)valerate. To prepare samples for analysis, 1 mL of solution was filtered (0.2 µm syringe filter) and stored at -20°C until analysis. Once thawed, samples were centrifuged at 7200xg for 21 min. Then 0.5 mL of each centrifuged sample was diluted with 0.5 mL deionized water and 0.4 mL H₃PO₄ (10% v/v) in 2 mL autosampler vials. An Agilent 7890 GC with 7683B autosampler, equipped with a 2 m x 4 mm glass column packed with GP15%SP-1220/1% H₃PO₄ on 100/120 Chromosorb WAWW (Supelco; Bellefonte, PA) and flame ionization detector was used for analysis. Helium was used as the carrier gas at 40

mL/min. Temperatures for the oven, injector, and FID were 120, 220, and 200°C, respectively.

At the end of the second trial, scanning electron microscopy (SEM) was performed with the assistance of Tim Maugel of the Center for Biological Ultrastructure (University of Maryland) to examine microorganisms attached to the carbon fiber anodes and the corncob pellets. The carbon fibers analyzed were from the section of brush furthest from the titanium stem and were taken from the top, middle, and bottom thirds of the anode chamber. The carbon fibers were cut to $< \frac{1}{2}$ " in length with a sterile straight-edge blade while still submerged in the anode chamber. SEM sample preparation involved: (1) Fixing the samples in a 2% solution of glutaraldehyde (diluted in phosphate buffered saline) for 60 min at room temp, followed by refrigerating the samples for two days; (2) Washing the samples in PBS buffer three times for 5 min each to remove excess glutaraldehyde; (3) Post-fixing the samples in 1% osmium tetroxide (diluted in PBS) for 60 min; (4) Washing the samples with double distilled water three times for 10 min each to remove osmium tetroxide; and (5) Serially dehydrating the samples using ethanol (75% 10 min, 95% 10 min, and 3 X 100% 5 min each). Critical point drying was performed, following the protocol of Cohen (1977). Samples were vapor deposited with 60% Au/40% Pd and analyzed with a Hitachi S-4700 scanning electron microscope at an accelerating voltage 15,000 V.

3.6 Reactor Tear-Down Procedures

As stated above, hydraulic conductivity was re-tested at the end of Trial 2. This was accomplished by modifying the reactor set-up to accommodate a hydraulic

conductivity test (see Figure 3-3) in order to gauge the effects of corncob oxidation on hydraulic conductivity and permeability through the anode bed.

Additionally, the saturated corncob material was removed from each reactor and weighed. The corncob was then dried at 70°C for 24 hours and re-weighed. This procedure was repeated every 24 hours thereafter until the dry weight of the corn could be determined.

CHAPTER 4

RESULTS & DISCUSSION

4.1 Trial 1 – Prototype MFC

4.1.1 Results Overview

The prototype MFC successfully utilized a raw, lignocellulosic substrate for the production of electricity. Four sets of data were collected to characterize MFC performance and interpret results: polarization curves, pH, methane, and hydrogen generation.

4.1.2 Electricity Generation from Prototype MFC

The ability of rumen microorganisms to generate electricity from a corncob substrate was demonstrated using the prototype, air-cathode reactor (Reactor 'A'). The batch system—initially loaded with 488 g (145 g per liter of anode chamber volume) untreated corn cob pellets—generated an OCV > 0.3 V for 428 hours, with a maximum OCV of 0.672 V (hrs 700-704) (Figure 4-1). In comparison, the average time to exhaustion in batch wastewater-fed MFCs seems to be around 200 hours (*Cheng et al. 2006; Feng et al. 2008; Liu et al. 2005*). Voltage persisted above 0.6 V during hours 400-

735 (14 days), but dropped off at hour 768, coinciding with the onset of clogging within the anode bed, and remained ≤ 0.2 V for the remainder of the trial.

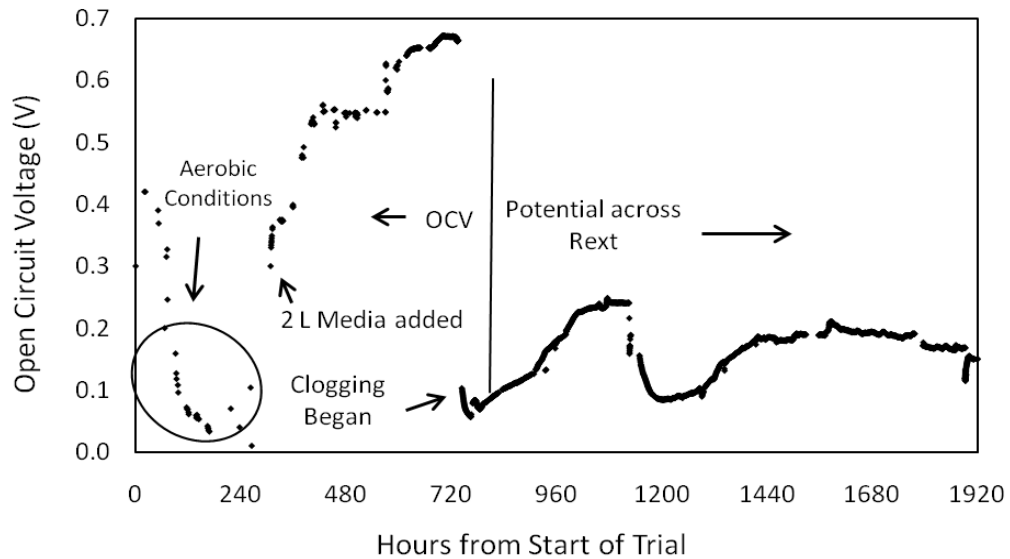


Figure 4-1. Trial 1 Voltage/Potential Readings (from Reactor A)

Dips in OCV (to less than 0.10 V) during the first 300 hours were due to evaporation and leakage, which were occurring at a higher rate than anticipated (45.7 mL/day), thereby reducing the water level and allowing oxygen diffusion into the anode chamber. Additional anaerobic media (2 L) was added at hour 307, and again at hour 570 (500 mL) to account for evaporation losses. These media additions resulted in immediate increases in OCV, followed by a gradual climb to the maximum OCV (0.672 V) achieved during the trial. The long-term increase in OCV was presumably due to the re-establishment of anoxic conditions after media addition. In addition, microbial activity was likely reduced and mass transfer inhibited in regions of the MFC that became dry due to leakage and evaporation of media. These effects would have been reversed when saturation conditions were reversed.

By hour 735, the water level in the MFC began increasing (above the perforated plate at the top of the reactor), indicating that the anode chamber had become clogged. After the reactor was manually unclogged and voltage readings resumed, the OCV had dropped to 0.10 V. The DO in the leachate was measured the following day (DO = 0.20 mg/L at hr 764) indicated that anoxic conditions had been re-established within the anode chamber; however, the OCV remained below 0.20 V for the remainder of the trial.

At hour 768, the external circuit was modified to evaluate potential difference between the anode and cathode, and polarization testing was performed (hrs 1319–1944), by varying R_{ext} (1 k Ω -300 k Ω) and allowing 24 hours to reach pseudo steady-state conditions before measuring the voltage at a particular R_{ext} (Figure 4-2A). The polarization (Figure 4-2B) and power (Figure 4-2C) curves from this trial are somewhat atypical for MFCs (Figure 2-7 illustrates the characteristics of a typical parabolic power curve). The polarization curve (Figure 4-2B) does display a relatively linear trend from 0-5 mA/m³ ($R^2 = 0.54$), which provides a measure of R_{int} (approximately 2.78 k Ω). The high R_{int} measured is corroborated by the fact that the solid substrate MFC was unable to reach short circuit conditions at external resistance of 1 k Ω , indicating that the cell itself was restricting the flow of electrons at high current. Maximum current and power density (29.3 mA/m³ and 0.65 mW/m³) were significantly lower than power data from single-chamber, membrane-less MFCs to date, which ranges from 10 – 21,200 mW/m³ (Chang *et al.* 2006). These values suggest a drastic underperformance of this configuration; however, these curves were developed after the voltage had dropped off in the system, and were therefore not indicative of normal operating conditions.

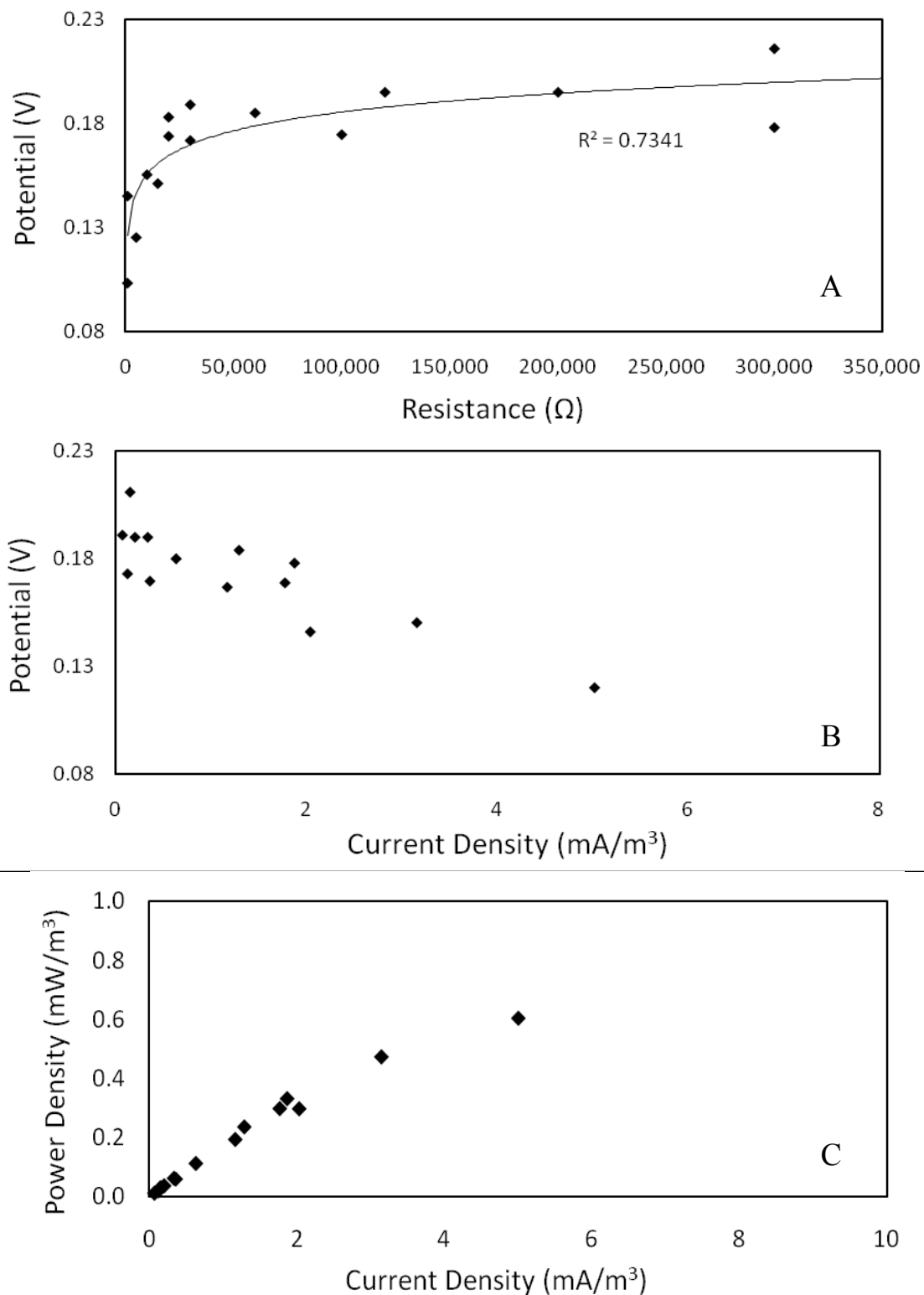


Figure 4-2. Trial 1 Polarization curves obtained by measuring the MFC potential at R_{ext} ranging from 1 to 300 k Ω . (A) Potential as a function of resistance; (B) potential as a function of current; and (C) power as a function of current. Power and current densities were calculated using the wet anode volume (0.00477 m^3).

4.1.3 Methane and Hydrogen Generation

Figures 4-3 and 4-4 below illustrate methane and hydrogen production during the first trial. Methane production was negligible for the first 620 hours of the trial, but then rose rapidly to 946 μM (hr 788). The onset of methane production coincided with a drop in OCV at hour 735 (Figure 4-3), suggesting that methanogenesis may have begun to dominate electron capture, or the production of a gas phase within the anode chamber was impeding mass transport of protons and electrons. Additionally, when the reactor was unclogged at hour 735, gas bubbles could be seen rising to the surface of the water column, again suggesting that methane production may have been significant enough to produce a gas phase within the saturated zone and to impede electrical performance. At hour 935, BES (0.2 g/L) was added to the MFC as a specific inhibitor of the coenzyme M found in methanogenic archaea, which resulted in a temporary cessation of methane production, as well as an increase in power density from 3.71 mW/m^3 to 12.22 mW/m^3 over the course of 6 days (data not shown). As compared with similar studies, the resulting power density was still low; however, this represents a > 200% increase in power after BES was added. The decline in methane levels also allowed the reactor to operate in recycle mode without further clogging for an additional 768 hours.

A significant increase in power production after BES addition indicates that methanogens were previously in competition with EAB for available substrate (*He et al. 2005*). A small (< 25%) increase in power production after BES addition, however, suggests that methanogens were only subsisting on excess substrate not utilized by EAB. It is difficult to determine, from these results, the extent to which methanogenesis affected power production in the current study. There was a clear excess in available

cellulosic substrate, as demonstrated by the presence of undegraded corn cob pellets in the MFC at the end of the trial. However, aqueous hydrogen, which can serve as a direct substrate for methanogens was generally quite low ($< 0.1 \mu\text{M}$), suggesting that methanogens and EAB may have been in competition for limiting amounts of hydrogen or other metabolites derived from the corn cobs.

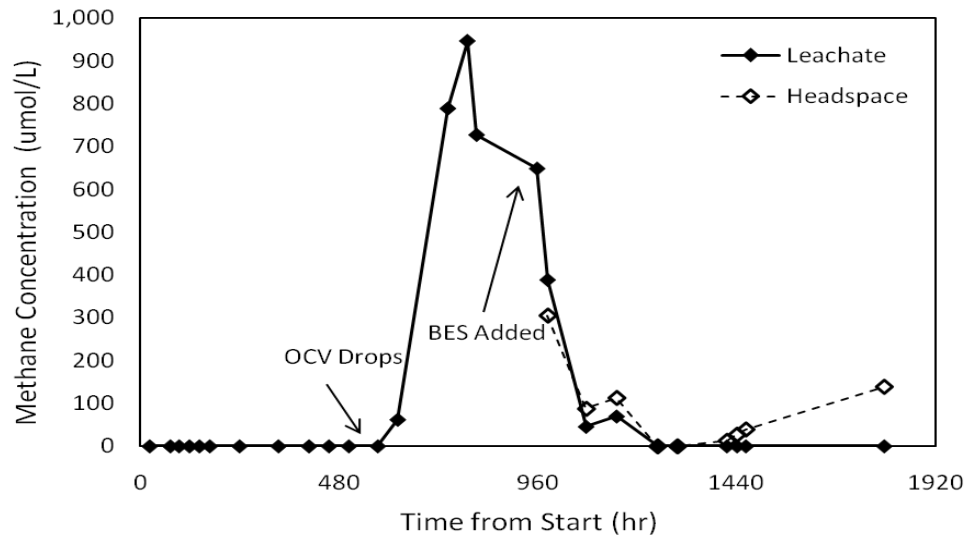


Figure 4-3. Trial 1 Methane Concentrations in a Single MFC Reactor determined from analysis of either headspace or liquid samples. Analysis of headspace samples started at hour 960

Hydrogen concentrations ($< 1 \mu\text{M}$) were significantly lower than methane levels (Figure 4-4), as expected, due to the high rate hydrogen turnover rate in many anaerobic environments. Following the addition of media at hour 332, leachate hydrogen levels spiked from 0.1 to $0.79 \mu\text{M}$. The gas-phase measurements suggested that the addition of BES also caused hydrogen to accumulate (to $0.85 \mu\text{M}$), presumably by inhibiting hydrogen-consuming methanogens.

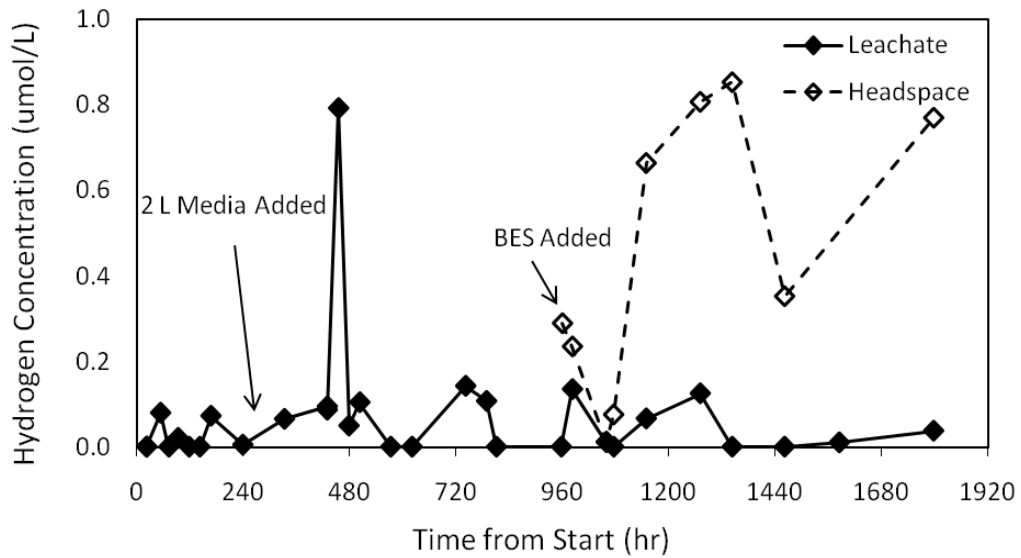


Figure 4-4. Trial 1 Hydrogen Concentrations in a single MFC reactor determined from analysis of either headspace or liquid samples. Analysis of headspace samples started at hour 960.

Headspace analyses of gas concentrations, which began at hour 960, allowed for an empirical check of the partitioning of hydrogen and methane between the aqueous and headspace phases of the reactor. Henry's Law describes the partitioning of volatile compounds between the gas and liquid phases at equilibrium according to

$$K_H = \frac{C_{air}}{C_{water}} \quad \text{Equation 4-1}$$

where K_H is the dimensionless Henry's constant ($K_{H,H_2}=29.2$; $K_{H,CH_4}=50.4$; *Loffler & Sanford 2005*); C_{air} is the concentration of hydrogen or methane in the MFC headspace; and C_{water} is the concentration of hydrogen or methane in the MFC leachate. The results indicate that the reactor was unable to establish equilibrium conditions between the liquid and gas phases, and thus the C_{water} could not be predicted by the C_{air} (*Loffler & Sanford 2005*; Equation 4-1). At approximately 1050 hours, the hydrogen and methane

concentrations from headspace analyses began to diverge from aqueous phase concentrations and began to more closely resemble the theoretical partitioning patterns.

One possible explanation for these results is that hydrogenotrophic methanogens were rapidly converting hydrogen to methane (Equation 4-2) in the leachate at a rate faster than the rates of mass transfer of hydrogen and methane across the liquid-gas interface, thereby creating non-equilibrium conditions. The addition of BES created conditions that more closely resembled equilibrium, again suggesting that methanogenic microorganisms were at least partially responsible for the non-equilibrium conditions.



A similar pattern of time-dependent hydrogen and methane concentrations has been found in other MFCs fed with fermentable substrates. Hydrogen initially accumulated in these systems, but declined over time as methanogens were able to out-compete EAB for available hydrogen and methane levels (*Parameswaran et al. 2009a; Ren et al. 2007*). Interestingly, long-term monitoring of landfill biogas has also revealed similar trends (Figure 4-5), where the stages of cellulose degradation can predict the relative concentrations of biogases.

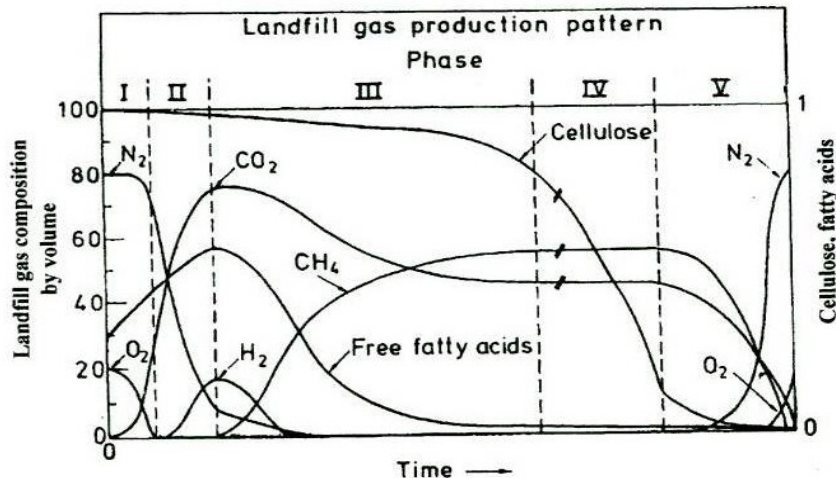


Figure 4-5. Landfill gas production pattern (Rovers et al. 1973)

4.1.4 pH and Temperature

It was initially thought that the formation of organic acids during fermentation could lead to a pH reduction and the creation of acidic conditions in the anode bed. The pH, however, remained between 6 and 8 during the first trial (data not shown) and did not require the addition of any alkalinity to maintain neutral conditions. These results suggest one of two things—(1) that the buffering capacity present in the microbial media was adequate for the amount of organic acids produced, and (2) the organic acid uptake by methanogens and EAB was sufficient to prevent acidification in the MFC.

The addition of BES coincided with a pH drop from 7.35 to 6.30, in addition to inhibiting methane production (Figure 4-6). Acetotrophic methanogens consume 1 mol of H^+ for every mol acetate that is converted to methane. Thus, it is possible that the inhibition of acetotrophic methanogens by BES contributed to the observed decrease in pH. The fact that pH and methane reached their minimum at the same time, and then began to rise again further suggests that the effectiveness of BES was temporary.

Reactor leachate temperature remained between 22.5°C and 25.0°C. Ambient temperature in the laboratory remained at 23.5°C throughout the course of the trial.

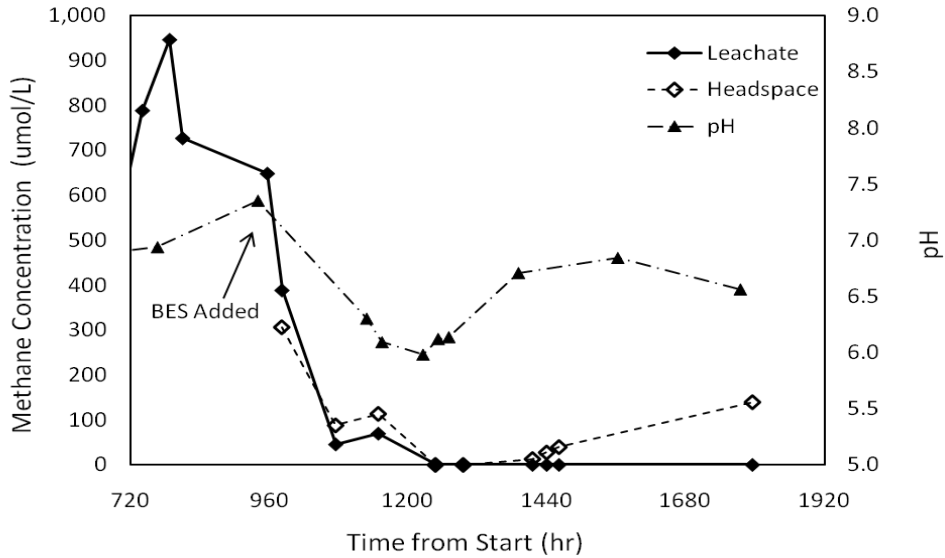


Figure 4-6. Trial 1 Methane Concentrations and pH after BES Addition. Methane was determined from analysis of either headspace of liquid samples.

4.2 Trial 1 Implications

The results of Trial 1 demonstrate the potential for long-term electricity production from lignocellulosic materials in MFC reactors; however, the maximum current and power density were lower than published values (Table 4-4). These results, combined with the analytic results of hydrogen, methane, and pH monitoring, suggest a number of potential factors that could have affected electrical performance of the MFC.

4.2.1 Microbial Limitations

One potential explanation for the low power production in Trial 1 is that there may have been an insufficient number of EAB in the inoculum to efficiently utilize the

organic acids and other fermentation products released during the breakdown of cellulose. For example, it is still unclear which, if any, of the *Clostridium* species are capable of extracellular electron transfer (Section 2.3.2; *Ren et al. 2007; Rismani-Yazdi 2008; Wang et al. 2009*). Additionally, it has been demonstrated that when crystalline cellulose is used as the MFC substrate and a undefined mixed-culture, rather than a defined co-culture of known cellulose degraders and EAB is used as the inoculum, not as much power is generated (*Ren et al. 2007*).

Alternatively, environmental conditions within the reactor (e.g., pH, temperature, and moisture and/or DO levels) may not have been optimal for EAB and/or rumen microorganisms and thus production of electrical current. Much of the MFC research published to date used temperature-controlled chambers—maintaining MFCs near 30°C, which is optimal for growth of mesophilic microorganisms as well as for the kinetics of oxygen reduction at the cathode (*Liu et al. 2005; Reimers et al. 2001; Zhao et al. 2006*). A 9% power reduction has been observed in wastewater-fed MFCs that were maintained at 20°C versus 32°C (*Liu et al. 2005*). Further, it has been documented that the optimal temperature for rumen microorganisms is near 39°C (*Hu et al. 2005*). Because this research aims to develop and characterize an MFC that is feasible for scale-up in agricultural operations, MFC operation at room temperature was considered desirable but may inherently limit power production. Similarly, it was noted in the literature review that a number of studies adjust to pH 6.0 prior to inoculation. Optimal pH for cellulose-degrading microorganisms is 6.8 (*Hu et al. 2005*). Our reactors maintained a slightly higher pH of 7.3, which may have also limited the rate of cellulose degradation. Finally, because of the high rate of evaporation and leakage from the reactor, moisture content

likely dropped below tolerable levels for the microbial community, and may have impeded long-term growth.

4.2.2 Anode Limitations

The small surface area of the anode (0.012 m²) may have been an additional factor that contributed to the low power production. Previous research has demonstrated that the surface area of the anode relative to the cathode affects power production, and using materials like carbon felt or foam can increase the area available for electron deposition (*Logan et al. 2006*). The spacing between anode and cathode also has detrimental effects on power generation (*Liu et al. 2005b*). If the anode reaction is limiting—typically the case in MFCs—these factors can significantly improve electricity production. Alternatively, there may have been fouling of the anode surface, which could have inhibited anode respiration (*Reimers et al. 2006*).

4.2.3 Electron Scavengers

The addition of BES was motivated by the hypothesis that a fraction of the electrons released during substrate oxidation were being diverted from anode reduction, by methanogenesis. Methane levels did decline with the addition of BES; however, current/power production remained low for the remainder of the trial, and it was unclear what caused the permanent drop in electrical performance. The minimal effect of BES implicates the microbial community, and suggests that the rumen inoculum was not capable of long-term anode respiration.

4.2.4 Internal Resistance

Finally, the internal (ohmic) resistance of the system—approximated as the slope of the polarization curve—was 2.78 k Ω , significantly larger than that of soluble MFCs to date. Because the oxidation of a lignocellulosic substrate is typically accompanied by a significant reduction in porosity, it is possible that a reduction in porosity may have increased internal resistance (*Durand 2003; Richard et al. 2004*). Also, because of the potential compaction of the substrate and the large distance between the anode and cathode (2.75 in; 6.99 cm), mass transfer losses undoubtedly affected power production, e.g., due to the development of a proton gradient near the substrate. To counter this, and to address long-term clogging issues, plastic matrix media were added to the anode bed in Trial 2 to provide void space for recirculation. Additionally, measurements for hydraulic conductivity were added at the beginning and end of Trial 2 to assess changes in porosity.

4.2.5 Voltage-Drop Off

Because the polarization test was performed after potential dropped off, the results may not be indicative of the system's performance prior to clogging began. That is, the low power production may have been the result, at least in part, of the reduced potential/current after clogging began.

4.3 Trial 2 Results Overview

Trial 2 examined the effects of different inocula on the performance of duplicate MFC reactors. Structural modifications to the reactors between Trials 1 and 2 included the addition of graphite brush anodes, which replaced the graphite rods used in Trial 1, and the addition of plastic matrix media as bulking material for the anode chamber. Both reactors were again batch loaded with corn cob substrate (692 g/reactor). Trial 2 also quantified hydrogen and methane production, pH, DO, organic acid production, and the amount of substrate consumed. These six data sets allowed for a better understanding of the limiting factors and losses associated with power production from lignocellulosic biomass.

4.4 Trial 2 Condition 1 – Soil Inoculum

4.4.1 Electrochemical Performance Summary

The duplicate reactors, initially inoculated with 26.7 g/L pasteurized soil, ran at OCV for > 400 hours, and achieved maximum OCV values of 0.594 V and 0.634 V for reactors A and B, respectively. Voltage production, as evidenced in Figure 4-7, was somewhat episodic for the first 90 hours, but subsequently leveled off around 0.54 V in both reactors, which falls within the typical range of working voltages (0.3 – 0.8 V) reported on in MFC studies (Logan 2008). The circuit was subsequently modified to analyze potential across a variable resistor, and a summary of the steady-state electrochemical performance is highlighted below in Table 4-1. No clogging, or the subsequent voltage drop off that was seen in Trial 1, was observed during the entire course of the second trial (1620 hrs).

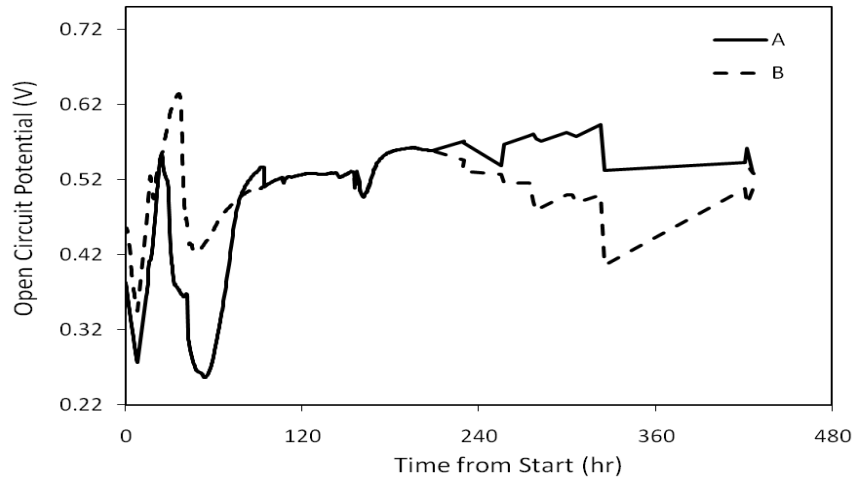


Figure 4-7. Open Circuit Voltage (OCV) in Duplicate Reactors A and B Inoculated with Pasteurized Soil (Trial 2, Condition 1).

Table 4-1. Trial 2, Summary of OCV^a in Duplicate Reactors A and B Inoculated with Pasteurized Soil (Trial 2, Condition 1).

	OCV	
	A	B
Max	0.594	0.634
Min	0.256	0.345
Mean ^b	0.465 (0.10)	0.512 (0.05)
No. measurements	485	181

^a OCV measured during hours 0-400

^b Mean (standard deviation)

4.4.2 Polarization Results (Reactor B Only)

After operation at an external resistance of 1 kΩ for 40 hours, polarization testing was performed (on Reactor B only) using a 1 hr equilibration period, and minimum and maximum R_{ext} values of 5 kΩ and 1 MΩ (Figure 4-8A). From the power curve (Figure 4-8C), the short-circuit current density and maximum power production were estimated as 1.15 mA/m³ and 0.144 mW/m³, respectively. The R_{int} estimated from the slope of Figure 4-8B was 92.75 kΩ. Maximum power production (MPP) occurs when $R_{ext} = R_{int}$

(Logan *et al.* 2006) and was observed at $R_{\text{ext}} = 100 \text{ k}\Omega$ (Figure 4-8C), verifying the R_{int} value estimated from the slope of the polarization curve. The linearity of the polarization curve and the symmetrical shape of the power curve also implicate ohmic losses as the primary source of overpotential within the reactor (Logan *et al.* 2006; USDOE 2004).

Power production using a soil-based inoculum was 3.5% that observed after inoculating with rumen fluid in Trial 1 (Trial 1 $P_{\text{max}} = 4.11 \text{ mW/m}^3$; $i_{\text{max}} = 29.34 \text{ mA/m}^3$). Further, the current MFC showed considerably less power, as compared with a similar study, which achieved 150 W/m^3 using paddy field soil microorganisms in the degradation of crystalline cellulose (Ishii *et al.* 2008a). Such results might be explained by the presence of native cellulose-degrading bacteria in paddy field soil (Weber *et al.* 2001). The absence of such microorganisms in our soil inoculum would have resulted in conditions where lignocellulose hydrolysis was the rate-limiting step. The observed power may have resulted from the microbial oxidation of small quantities of glucose and/or organic acids produced during abiotic dissolution of the corncob.

Inoculum type also affected internal resistance; as the internal resistance estimated after inoculation with rumen fluid during Trial 1 was significantly lower ($2.78 \text{ k}\Omega$). Such results were also demonstrated by Manohar & Mansfield (2009), who illustrated the inverse relationship between R_{int} and the maximum current density, and proved that the addition of a known EAB (*Shewanella oneidensis* MR-1) directly resulted in a reduction in anode potential and internal resistance of a MFC (Manohar *et al.* 2008; Manohar & Mansfeld 2009). An insufficient number of EAB and/or hydrolytic bacteria in the current MFC may have created sluggish anode kinetics—contributing to the low current and high internal resistance.

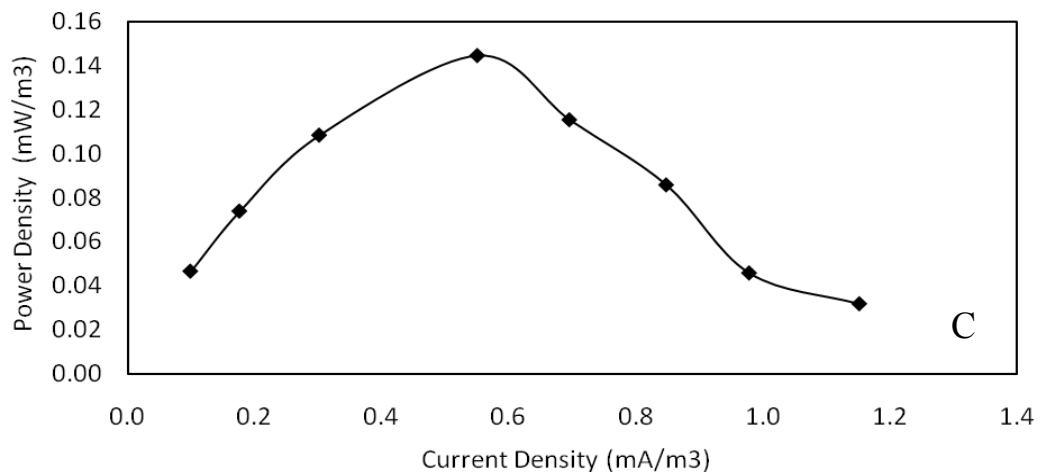
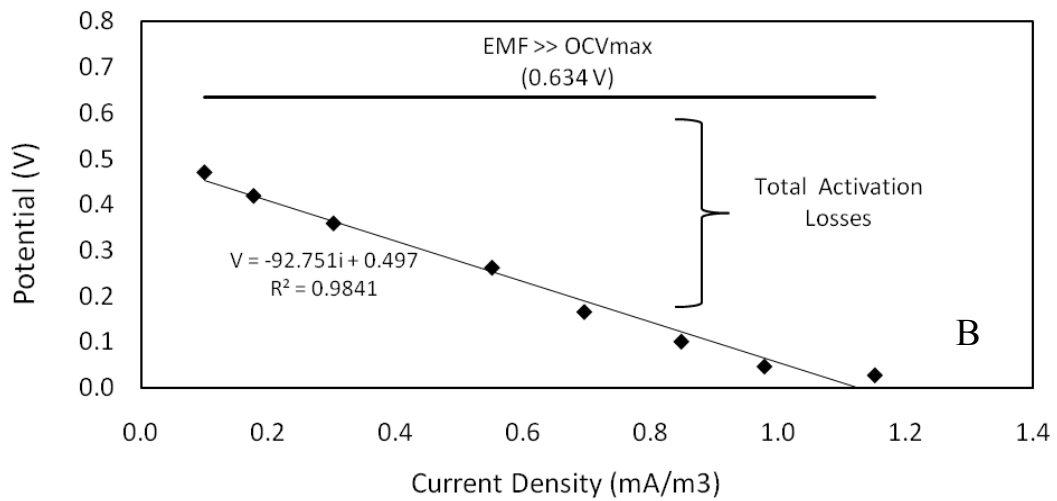
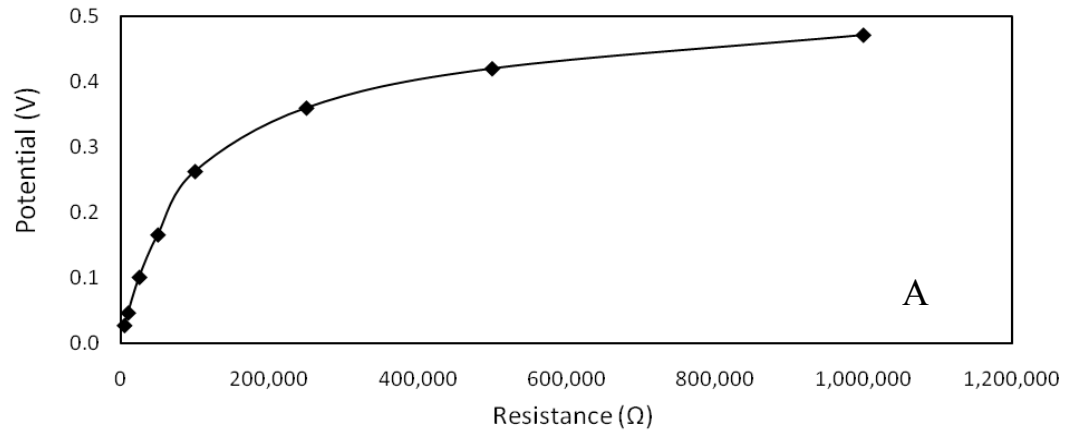


Figure 4-8. Soil inoculum polarization curves from reactor B obtained by measuring the MFC potential at R_{ext} ranging from 1 $\text{k}\Omega$ to 1 $\text{M}\Omega$. (A) potential as a function of resistance; (B) potential as a function of current; and (C) power as a function of current. Power and current densities were calculated using the anode wet volume (0.00477 m^3).

4.5 Trial 2 Condition 2 – Rumen Fluid Co-Inoculum

4.5.1 Electrochemical Performance Summary

To counter the high R_{int} and low power production observed with a pasteurized soil inoculum (see Table 4-4), rumen fluid was added in hour 658 to try to stimulate substrate oxidation in the anode chamber. The reactors were then operated at 1 k Ω for 77 hours (Figure 4-9). Potential dropped by 28 mV in Reactor A and 0.2 mV in Reactor B during this period, and power production immediately prior to polarization testing was 37.36 mW/m³ in Reactor A and 27.26 mW/m³ in Reactor B.

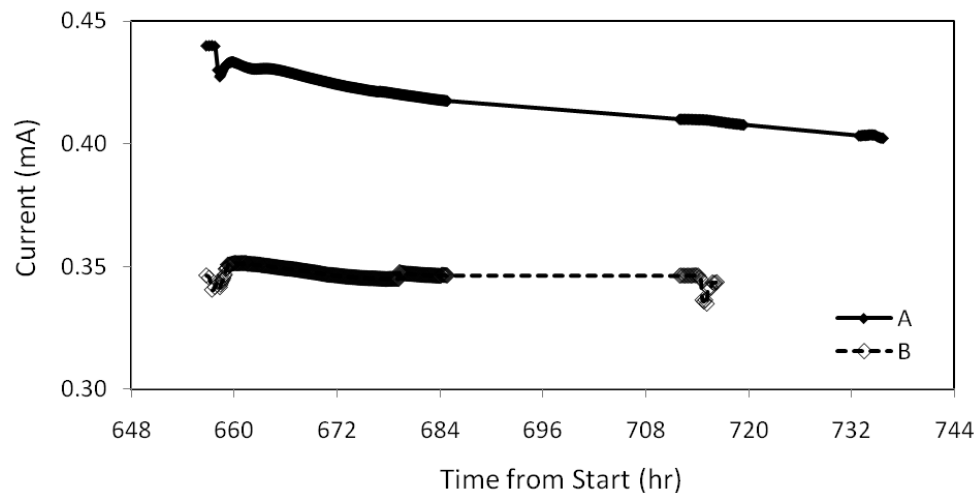


Figure 4-9. Current for 77 hours after rumen fluid inoculation at hour 656 in the duplicate Reactors A and B (Trial 2, Condition 2)

Table 4-2. Trial 2, Summary of Steady-State^a Electrical Performance in Duplicate Reactors A and B Inoculated with Rumen Fluid (Trial 2, Condition 2)

	Steady State Potential (V)		Steady-State Current Density (mA/m ³) ^b		Steady-State Power Density (mW/m ³) ^b	
	A	B	A	B	A	B
Max	0.440	0.351	101.58	81.2	44.7	28.5
Min	0.402	0.340	92.88	78.6	37.4	26.8
Mean ^c	0.422(0.08)	0.347(0.002)	97.5(1.87)	80.2(0.50)	41.2(1.57)	27.9(0.35)

^a Steady-state performance was measured during hours 656-735 at $R_{ext} = 1 \text{ k}\Omega$

^b Normalized to the wet volume of the anode (0.00477 m³).

^c Mean (standard deviation) based on 387 measurements.

4.5.2 Polarization Results

Polarization curves were developed three days after rumen fluid inoculation, using minimum and maximum external resistors of 5 Ω and 2.25 M Ω (Figure 4-10). The OCV and limiting (short circuit) current density were 0.52 V and 785 mA/m³ for Reactor A, and 0.51 V and 517 mA/m³ for Reactor B.

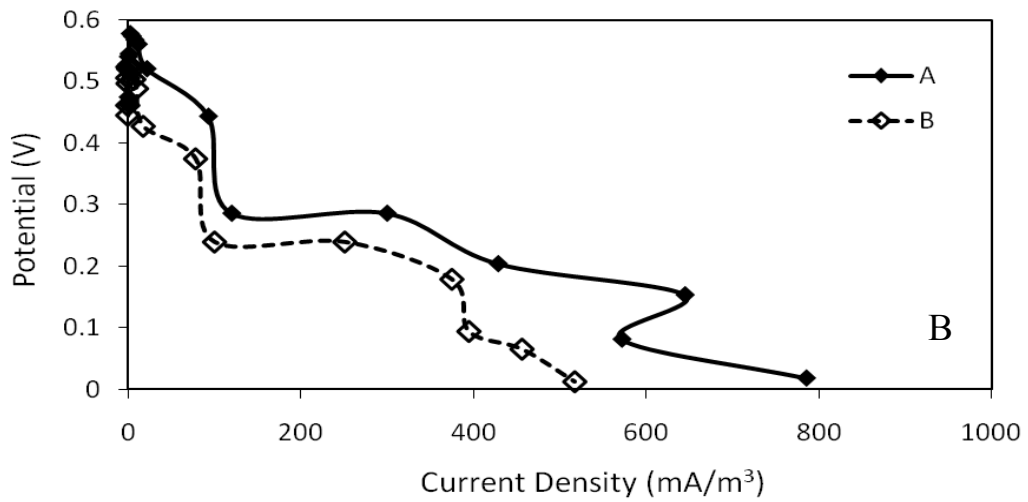
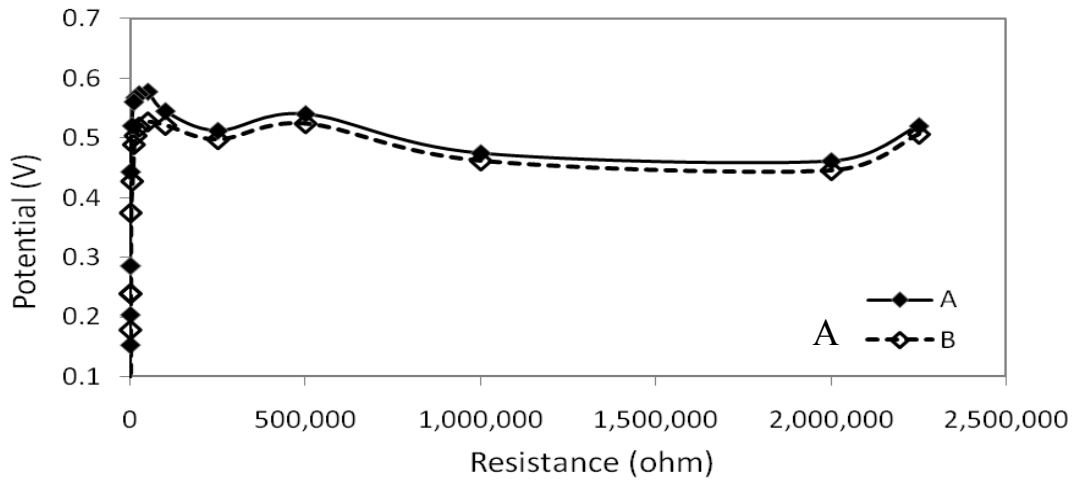
Further, there was a 500-fold increase in power production in Reactor B after the addition of rumen fluid. The MPP in Reactor B reached 77.3 mW/m³. The MPP in Reactor A reached 87.5 mW/m³.

The addition of rumen fluid also had a significant effect on the shape of the polarization curve (compare Figures 4-8B and 4-10B). The slope of the polarization curve is often used as an approximation of R_{int} in cells dominated by ohmic losses (described in Section 2.4); however, the fact that the addition of rumen microorganisms reduced the slope from 93 k Ω to 169 Ω (39% decrease in Reactor B) supports the hypothesis made in Section 3.4.2—that is that microbial activity and anode kinetics were previously limiting. The addition of rumen fluid acted to reduce the potential of the anode, increased current and power, and decreased anodic losses.

A minimum period of 2 hr was required to reach steady-state potential—defined as a potential flux no greater than 0.1 mV between data points (taken at 1 min intervals). Interestingly, it was also necessary to drop R_{ext} to 5 Ω in order to reach short-circuit (limiting current) conditions during this polarization test—indicative of an increase in the limiting current.

The power curve also experienced somewhat of a collapse at higher current values, possibly indicating conditions were not steady-state when the value was recorded.

Data points corresponding to 50 Ω and 500 Ω were re-tested with extended equilibration periods (4-6 hours); however, the new values did little to improve the overall shape of the curve. Such a collapse might be the result of anode fouling or of the large heterogeneity of the system, where the potential between the anode and cathode was in a constant state of flux, hindering our ability to reach steady-state conditions for the duration of polarization testing.



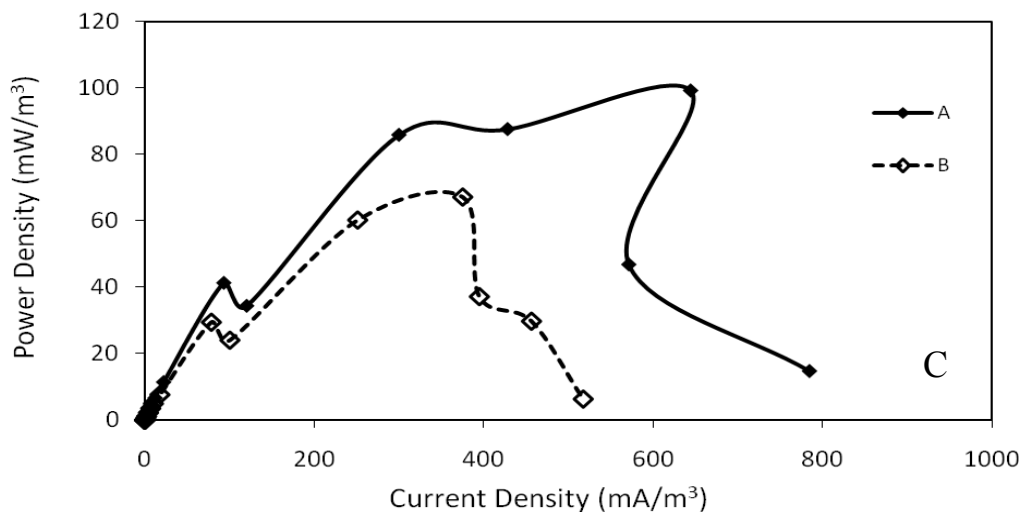


Figure 4-10. Rumen fluid polarization Curves obtained by measuring the MFC potential at R_{ext} ranging from 1 k Ω to 1 M Ω . (A) potential as a function of resistance; (B) potential as a function of current; and (C) power as a function of current. Power and current were normalized to the anode wet volume (0.00477 m³).

4.6 Trial 2 Condition 3 – *G. metallireducens* Co-Inoculum

4.6.1 Electrochemical Performance Summary

Because power production in the duplicate MFCs remained relatively low, even after adding the rumen inoculum, it was thought that methanogens might be competing with EAB in the anode chamber, thereby reducing the efficiency of conversion of cellulose to electrical current. As discussed below, methane began accumulating in Reactor B after the rumen inoculum was added. Therefore, BES, was added at hour 1410 to inhibit methanogenesis, and inoculation with the EAB *G. metallireducens* occurred at hour 1506 to promote anode reduction. This was followed by equilibration at 1 k Ω for 48 hours before polarization testing. Potential dropped by 32 mV in Reactor A and increased by 134 mV in Reactor B during this period (data not shown), and power density immediately prior to polarization testing was 31.92 mW/m³ in Reactor A and 41.74

mW/m³ in Reactor B, representing a 31% difference in power production between the two reactors (Figure 4-11). The rapid rise in power observed in reactor B was likely due to the temporary inhibition of methanogens after BES addition (see Figure 4-13). Because methanogenic activity in A was minimal, BES had little effect on power production. The same downward trend that was observed after rumen fluid addition (Figure 4-9) was again observed in the reactor after *G. metallireducens* was added. Compared to the conditions after rumen fluid inoculation, this represents a power increase of 5.44 mW/m³ in Reactor A and a decrease of 20.48 mW/m³ in Reactor B.

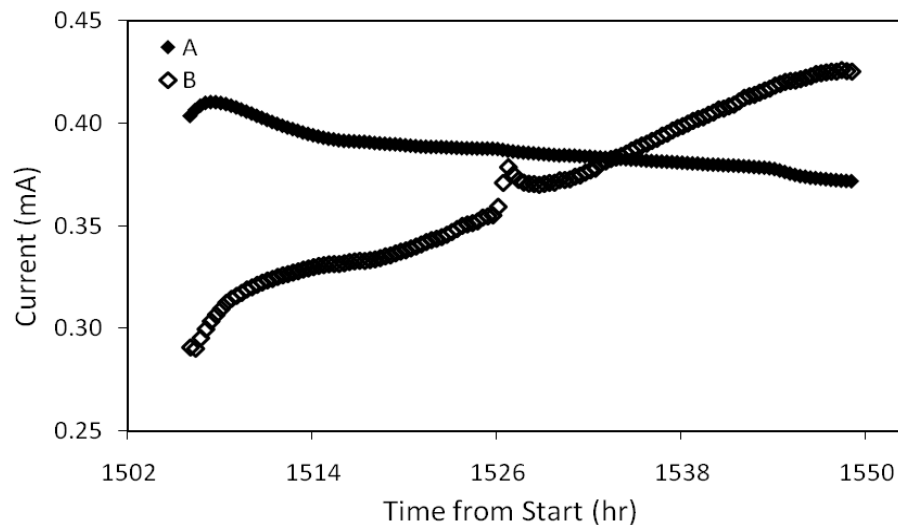


Figure 4-11. Current during the first 48 hours after *G. metallireducens* inoculation at hour 1506 in the duplicate reactors A and B (Trial 2, Condition 3)

Table 4-3. Trial 2 summary of steady-state electrical^a performance in duplicate reactors A and B inoculated with *G. metallireducens* (Trial 2, Condition 3)

	Steady State Potential (V)		Steady-State Current Density (mA/m ³) ^a		Steady-State Power Density (mW/m ³) ^a	
	A	B	A	B	A	B
Max	0.41	0.43	94.71	98.36	38.84	41.89
Min	0.37	0.29	85.86	67.04	31.92	19.46
Mean ^b	0.39 (0.01)	0.37 (0.04)	63.11 (2.22)	84.54 (8.73)	24.45 (1.74)	31.28 (6.41)

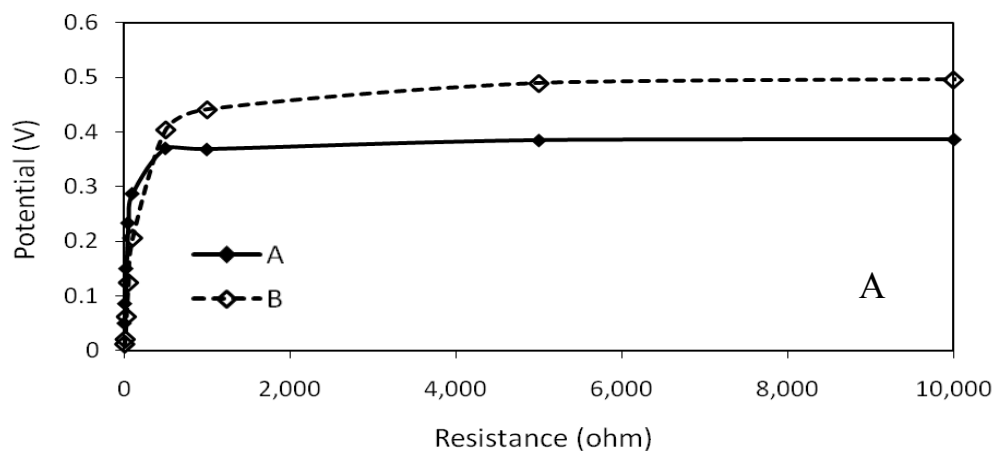
^a Steady-state measured during hours 1506-1550 at R_{ext} = 1 kΩ.

^b Normalized to the wet volume of the anode (0.00477 m³).

^b Mean (standard deviation) based on 129 measurements.

4.6.2 Polarization Results

Polarization and power curves were developed by measuring voltage across the MFC using minimum and maximum R_{ext} values of 5Ω and $100 \text{ k}\Omega$, and a minimum equilibration period of two hours (Figure 4-11). Longer equilibration periods (4-6 hr) were used when $R_{\text{ext}} \leq 1 \text{ k}\Omega$, and the data points corresponding to 500Ω , 100Ω , and 50Ω were re-done at the end of the polarization test to confirm results. Short-circuit current densities in Reactors A and B were 2117 mA/m^3 and 520 mA/m^3 , respectively. The addition of BES and *G. metallireducens* further increased power production 131% in Reactor A and 22% in Reactor B. The MPP in Reactor A was 229 mW/m^3 and occurred at 50Ω . The MPP in Reactor B was 89 mW/m^3 and occurred at 100Ω . Additionally, R_{int} decreased 75% in Reactor A (to 35Ω) and decreased 5% in Reactor B (to 187Ω). These findings suggest that the concentration of EAB was previously limiting anode kinetics, and their addition to the anode chamber increased the transfer of electrons derived from fermentation metabolites (e.g., acetate) to electricity production.



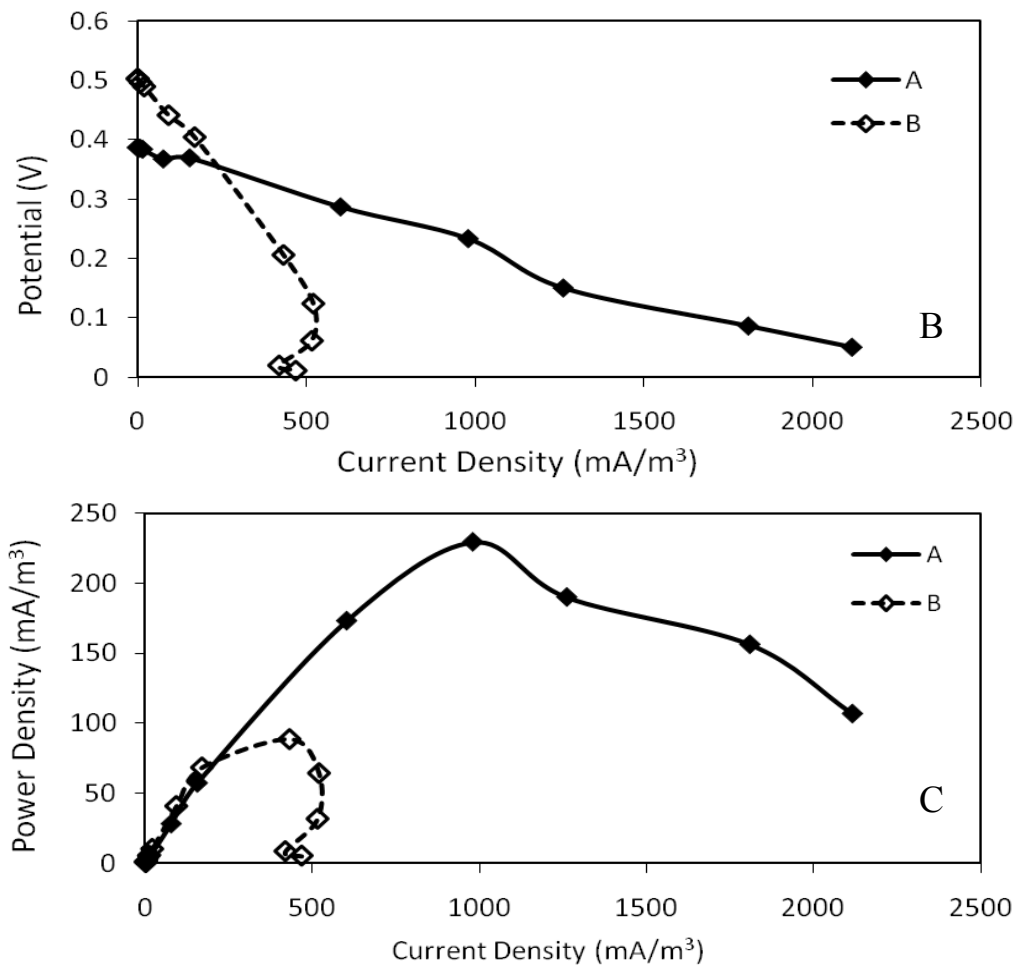


Figure 4-12. *G. metallireducens* polarization curves obtained by measuring the MFC potential at R_{ext} ranging from 1 to 10 k Ω . (A) potential as a function of resistance; (B) potential as a function of current; and (C) power as a function of current. Power and current densities were normalized to the anode wet volume.

4.7 Trial 2 Analytical Measurements

4.7.1 Methane and Hydrogen Generation

As compared with Trial 1, hydrogen production increased somewhat during the second trial, but no visible patterns could be seen with methane production or electricity generation, as described for Trial 1 in Section 4.1.3 (data in Appendix C).

Methane production was negligible in both reactors for the first 500 hours and remained low ($\leq 40 \mu\text{M}$) in Reactor A throughout the trial (Figure 4-13). Reactor B experienced greater increases in methane production, after rumen fluid was added at 658 hours. The addition of BES temporarily reduced methane levels in Reactor B, resulting in noticeable increases in power production before, and immediately after addition of *G. metallireducens* (Figure 4-11).

Comparison of the concentrations of methane (Figures 4-13 and 4-14) and hydrogen in the liquid and gas phases again revealed that equilibrium conditions with respect to these gases were not reached within either reactor during the second trial.

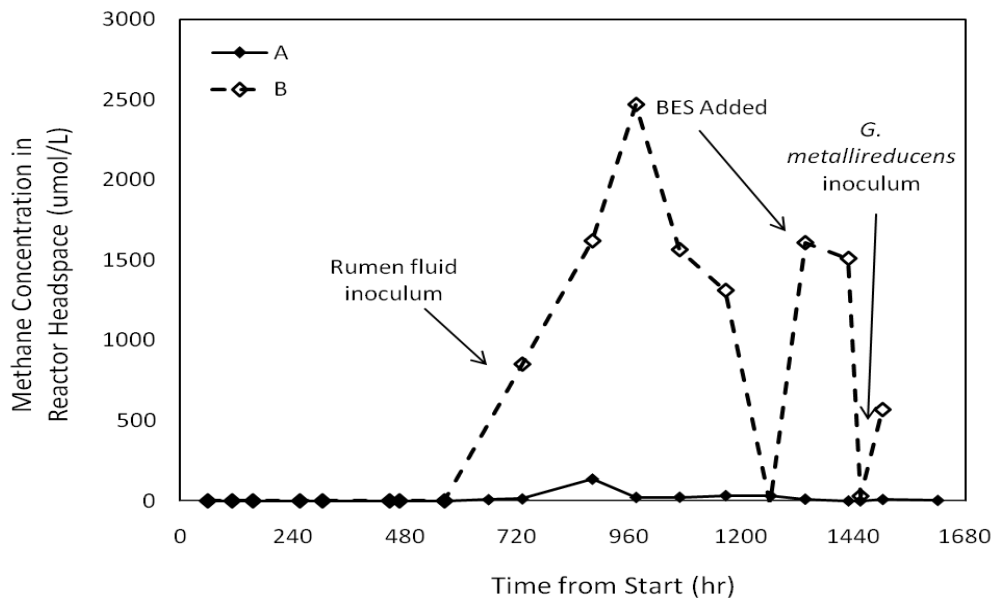


Figure 4-13. Trial 2 methane concentrations in duplicate reactors determined from analysis of headspace samples.

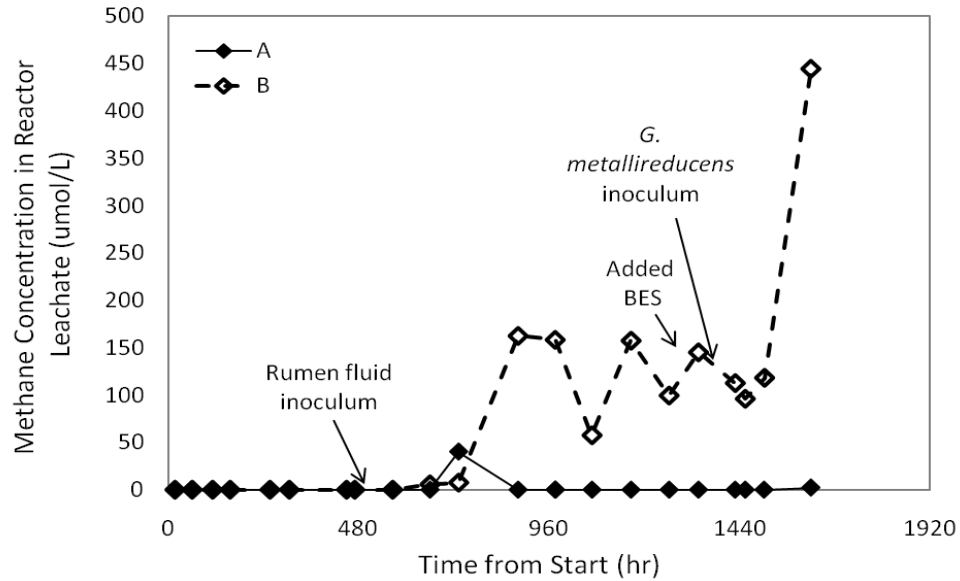


Figure 4-14. Trial 2 methane concentrations in duplicate reactors determined from analysis of liquid samples.

4.7.2 Dissolved Oxygen, pH, and Temperature

A summary of DO and pH levels during Trial 2 is presented in Figures 4-15 and 4-16, respectively. DO levels were relatively constant and remained below 2 mg/L throughout the trial. Average DO was above the threshold of 0.3 mg/L at which power generation is compromised by oxygen intrusion (*Oh et al. 2009*). The size of the holes drilled into the anode chamber ($\frac{1}{2}$ in.) may have permitted enough oxygen to diffuse into the anode chamber to reduce power output, even under saturated conditions,

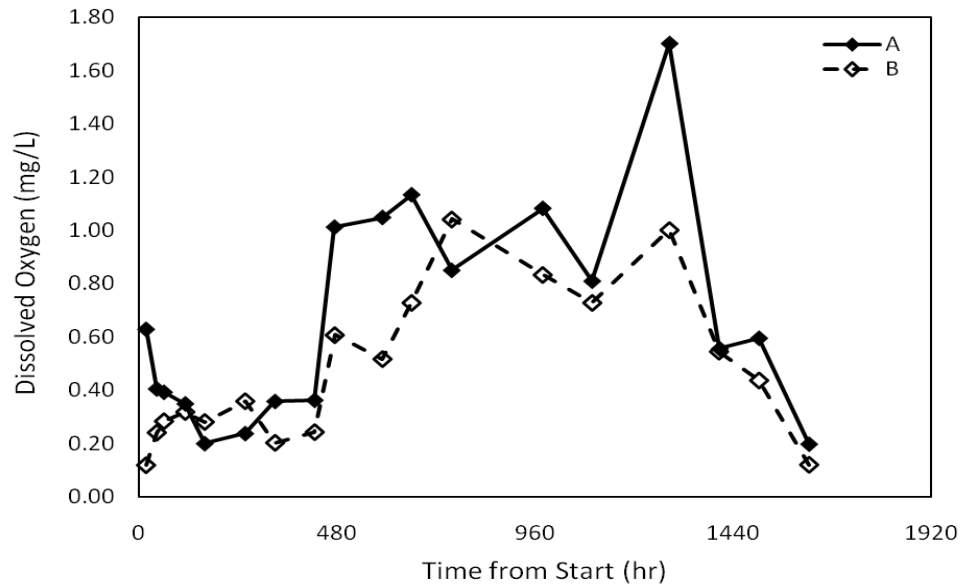


Figure 4-15. Dissolved oxygen levels in the duplicate reactors during all conditions of Trial 2

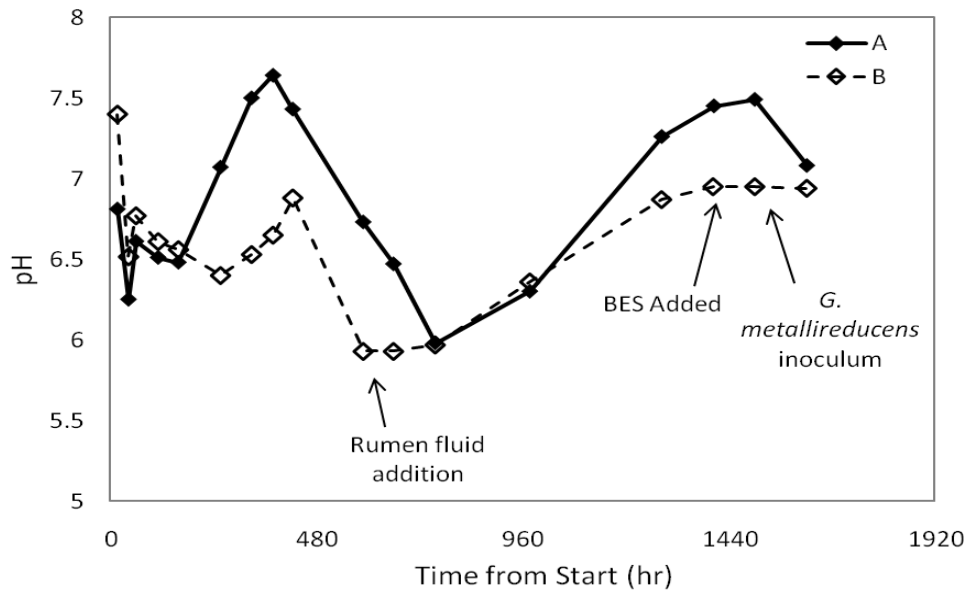


Figure 4-16. pH Levels in the duplicate reactors during all conditions of Trial 2

The pH oscillated somewhat more than during Trial 1. There was a decline in pH prior to rumen fluid inoculation, but the concurrent rise in methane that was observed in

Trial 1 did not occur. After rumen fluid addition, however, a similar increase could be observed in both the liquid-phase methane and pH of reactor B—presumably caused by the uptake of protons and CO₂ by methanogens.

Leachate temperature was again relatively constant (data not shown). This suggests that anaerobic activity within the anode bed was not generating excess heat.

4.7.3 Organic Acid Production

Degradation of the lignocellulosic biomass was accompanied by the production of high levels of acetic, propionic, and butyric acids, with acetic acid being the primary metabolite. Accumulation of the organic acids was somewhat episodic, and peaks occurred concomitantly with the introduction of additional microbial communities (Figures 4-18 and 4-19). The average concentration of organic acids in reactors A and B was 3578 mg/L and 5752 mg/L, respectively, and, in both reactors, 68% of the total composition was comprised of acetic acid. These findings are consistent with that of another cellulose-fed MFC, which found concentration ranges between 4423 and 7760 mg/L (*Rismani-Yazdi 2008*). Such high levels of acid production were interpreted by *Rismani-Yazdi* to mean that fermentative metabolism dominated over anaerobic respiration, which fits well with our observations of high methane production and low current generation. Based on this, the oxidation of organic acids by EAB was a rate-limiting step in the production of electricity from the lignocelluloses.

Reactor B experienced 60% higher organic acid concentrations than Reactor A, and concentrations did not fluctuate as greatly. This suggests that the rate of depletion for organic acids is much faster in A. The higher concentrations of organic acids in B

would suggest that the reactor was experiencing a higher rate of fermentation, which is supported by its elevated methane levels.

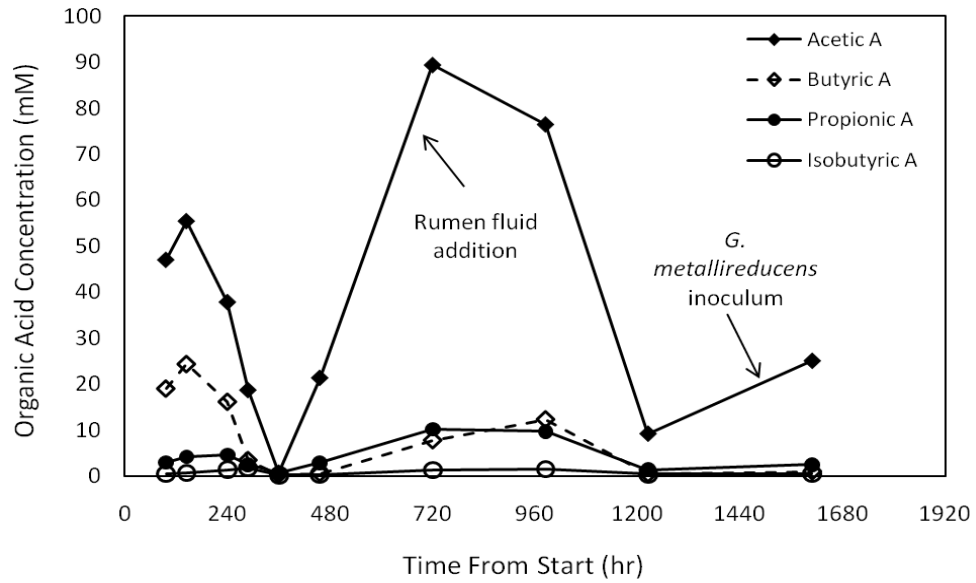


Figure 4-18. Trial 2 organic acid production in Reactor A determined from analysis of liquid samples.

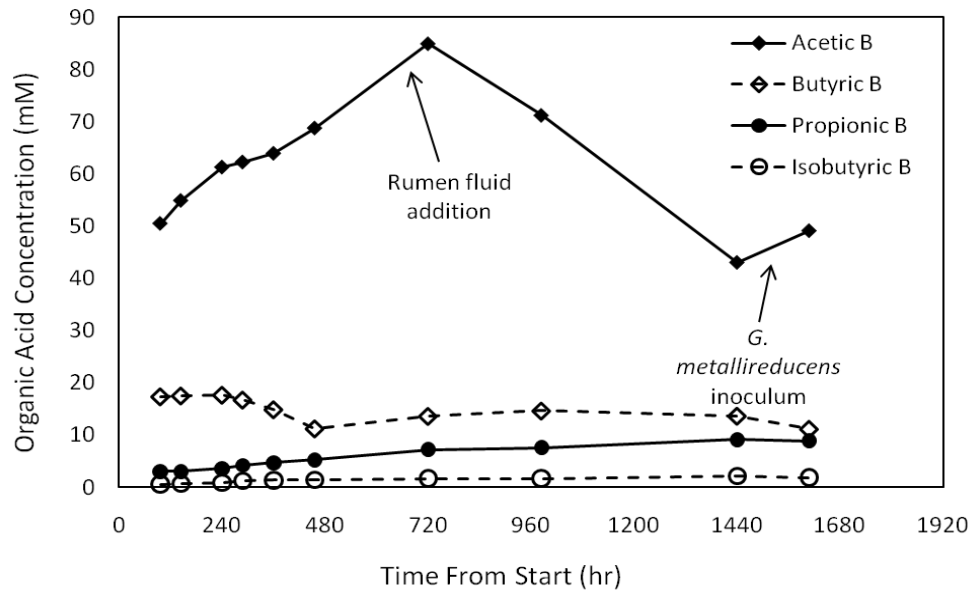


Figure 4-19. Trial 2 organic acid production in Reactor B determined from analysis of liquid samples.

4.8 Comparison of Duplicate Reactor Performance

There were significant differences in the performance of the duplicate reactors, with respect to maximum power, internal resistance, amount of substrate consumed, and organic acid production. As evidenced in Figures 4-20 and 4-21, Reactor A generated 157% more power than B during the final polarization test (229 mW/m^3 vs. 89 mW/m^3) and also had a much lower internal resistance (35Ω vs. 190Ω). Also of note, the final polarization curve of B experienced a collapse in power at higher current, but A did not. Despite its decreased power, Reactor B reactor degraded a larger fraction of corncob during the course of the second trial; it oxidized 24% of the original 692 g, as compared with the 10% oxidized by Reactor A (data not shown). Combined, these findings suggest that an unaccounted-for variable affected performance of the two duplicate reactors.

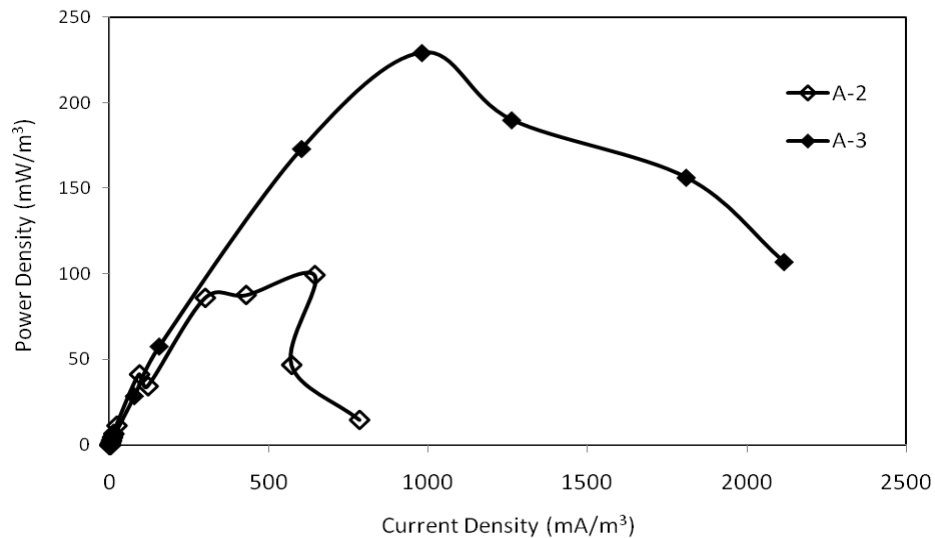


Figure 4-20. Comparison of Power Density Curves from Conditions 2 and 3 (Reactor A)

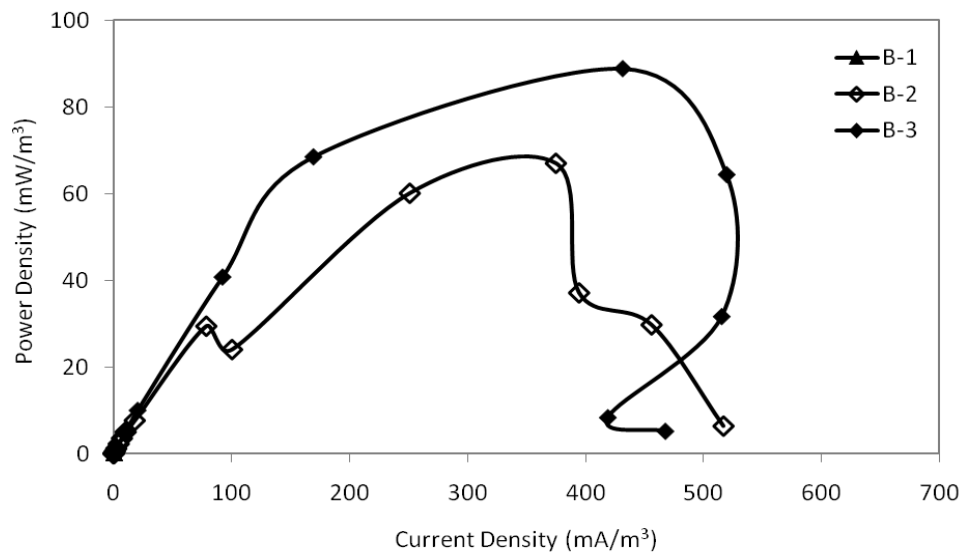


Figure 4-21. Comparison of Power Density Curves from Conditions 2 and 3 (Reactor B); the results from condition 1 (B-1) are not visible at the current scale.

There were a number of possible explanations for the dissimilar performance of the reactors. First, because reactor A was also used as the prototype reactor during Trial 1, there may have been carry-over of microorganisms attached to the cathode, which could have enhanced performance. The anode material was changed between trials however, and it is unlikely that any cathode-attached biofilm would enhance substrate oxidation. An alternative explanation is that leakage from the anode chamber of reactor A affected its power production in a positive way. A number of previous reports have demonstrated the importance of ionic conductivity to minimizing the internal resistance of MFCs (*He et al. 2007; Liu et al. 2005; Zuo et al. 2006*). The periodic addition of fresh media to reactor A likely increased, or at least maintained, solution conductivity over the length of the trial. This is in line with the significant decrease in R_{int} observed during each polarization test of A, whereas reactor B saw little decrease in internal resistance after the addition of *G. metallireducens*.

Further, a decrease in the water level of reactor A allowed for oxygen intrusion into the anode chamber. The work of He (2007) demonstrated that periodic aeration of the anode chamber can improve power production and Coulombic efficiency by inhibiting the strictly anaerobic methanogens. This mechanism could explain the finding of enhanced power production in A. The maintenance of strict anaerobic conditions in reactor B, on the other hand, allowed for greater rates of fermentation, as evidenced by the fact that methane concentrations increased significantly after the addition of rumen fluid (up to 2.5 mM in the headspace), but remained insignificant in Reactor A. This explanation is further supported by the heightened organic acid levels (Figure 4-19) and greater rate of corncob degradation in B, suggesting that the reactor was more efficient in the fermentation of corncob, even though it did not produce as much electricity. Conversely, the rapid increase and decline in organic acid levels in Reactor A (Figure 4-18) reveals that it was more efficient at the uptake of VFAs, resulting in its heightened power production. Consequently, Reactor B seems to have had greater *potential* for electricity generation from corncob fermentation, but would require augmentation with additional EAB, or modification of environmental conditions, to support metabolite uptake and to achieve greater power production.

4.9 Comparison of Results from Cellulose-Fed MFCs

The theoretical cell voltage (EMF) of an acetate-fed MFC with an oxygenated cathode is 1.1 V (Logan et al. 2006). Maximum OCV during Trial 1 of this study was 0.672 V, and during Trial 2 was 0.594 V (Reactor A) and 0.634 V (Reactor B). These values fall within the range of commonly reported OCVs to date—typically 0.3-0.7 V (Logan 2008; Ren et al. 2007; Wang et al. 2009). The observed current and power density values are, however, lower than most other cellulose-fed MFCs (Table 4-4). The most compelling reason for these results is that all cellulose-fed MFCs to date have utilized a (micro)crystalline substrate, which lacks a lignin shell and is thus, significantly easier to degrade via microbial processes. The few studies that have attempted the conversion of lignocellulose have utilized the residual products (e.g. hydrolysates or solids) remaining after steam-explosion of corn stover, or alternatively have crushed the stover to a powdered form prior to use—all of which are processes that make the compound more amenable to biodegradation, but which make the overall process less sustainable and impractical for scale-up. In the current study, the capacity of the bacteria to degrade untreated corncob within an MFC was unknown. The refractory lignin structure (Figure 4-22) may have inhibited hydrolysis and yielded a very slow rate of fermentable sugars. If this was the case, then the amount of substrate bioavailable to the electrogenic community was the limiting factor for growth, and consequently, for power production.

Table 4-4. Performance of cellulose-fed MFCs to date

Substrate	Microbes	Reactor Type	V_{max} (mV)	Power (mW/m ²)		Batch Cycle (d)	Reference
				steady-state	maximum		
Glucose + CSP	WW + H-C	SCAC	380	296	331 (at 800 Ω)	14	<i>Wang et al. 2009</i>
Glucose + CSRS	WW + H-C	SCAC	410	343	406 (600 Ω)	12.5	
CSP	H-C	SCAC	86	< 10	NG	NG	
CSH	WW	SCAC	~ 500	NG	952 (250 Ω)	1	<i>Zuo et al. 2006</i>
MC	RF (10%)	TCFeCN	475	27	55	5.2	<i>Rismani-Yazdi et al. 2007</i>
CMC	<i>C. cellulolyticum.</i> + <i>G.sulfurreducens</i>	TCFeCN	~800 (50k Ω)	NG	143 (770 Ω)	24	<i>Ren et al. 2007</i>
MN301 C.	<i>C. cellulolyticum.</i> + <i>G.sulfurreducens</i>	TCFeCN	~800 (50k Ω)	NG	59.2 (890 Ω)	24	
CMC	AS ^a	TCFeCN	NG	NG	15 (R _{ext} NG)	NG	

SCAC = single-chamber, air cathode

TCFeCN= two-chambered, ferricyanide reactor

CSP = corn stover, powdered

CSRS = corn stover residual solids (from steam-explosion)

CSH = corn stover hydrolysate (from steam-explosion)

MC = microcrystalline cellulose

CMC= soluble carboxymethyl cellulose

MN301 C. = amorphous + microcrystalline cellulose

AS^a = activated sludge; used aqueous oxygen as catholyte

Table 4-5. Trial 2 Reactor A performance summary from the current study

	R_{int} (Ω)	R_{ext} at MPP (Ω)	P_{max} (mW/m ³)	V_{max} (V)
Condition 1	NA	NA	NA	NA
Condition 2	141.5	100	87.48	0.577
Condition 3	34.6	50	229.2	0.388

Table 4-6. Trial 2 Reactor B performance summary from the current study

	R_{int} (Ω)	R_{ext} at MPP (Ω)	P_{max} (mW/m ³)	V_{max} (V)
Condition 1	92,751	100,000	0.144	0.471
Condition 2	196.2	100	67.1	0.527
Condition 3	186.9	100	88.8	0.503

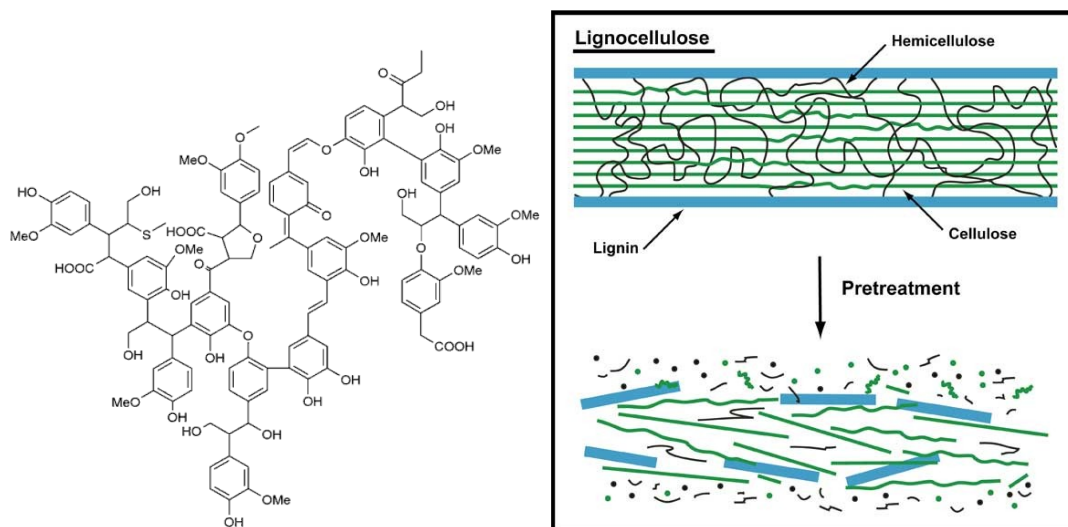


Figure 4-22. (A) Sample molecule of lignin displaying the structural complexity (Wool & Sun 2005); (B) Model of lignin, cellulose, and hemicelluloses structures within lignocellulose (Hector *et al.* 2008)

Additionally, the loading rates of corn into the reactor (102-105 g/L/trial) were significantly higher than the rate of 65 g/L that was found to be optimal for biogas production from corn stover (Pang *et al.* 2008). An excessive loading rate was likely the reason for the low degradation rate—only 9% of corncob was degraded in Reactor A and 23.9% in Reactor B. Further, oversupplying the microorganisms with substrate may have unintentionally created a niche substrate for methanogenic activity (observed in Reactor B; Figures 4-13 and 4-14).

An additional performance number that deviates from published literature and that may partially explain the atypical polarization curves is the internal resistance of the solid substrate MFCs. The R_{int} observed during Condition 1 (92.8 k Ω) was likely the result of extremely slow anode kinetics, which were caused by ineffective substrate degradation using the soil-based inoculum. After subsequent inoculations, the final, observed values of internal resistance in A and B were 190 Ω and 35 Ω . It is hypothesized that two separate processes were affecting the observed values of internal resistance, although

only the effects of the first were observed in the R_{int} data: (1) kinetics of the anodic reactions, and (2) characteristics and compaction of the substrate. Based on the fact that the addition of rumen fluid and *G. metallireducens* vastly improved R_{int} in both reactors, it is likely that anode kinetics were the best predictor of power performance. Despite these improvements, a collapse in power was observed at higher current densities in both reactors, and the external resistance required to reach short-circuit conditions decreased each time polarization was completed. It is hypothesized that the oxidation of substrate over the course of the trial may have created structural shifts within the anode chamber, leading to an increase in ohmic resistance and/or transient effects that were visible during polarization, which took place over fairly long periods (2-4 days). The ability to perform accurate polarization testing in solid substrate MFCs may require the use of more sensitive techniques (e.g. EIS or potentiodynamic testing) or testing potential at fewer external resistance values to reduce the visibility of such transient effects.

An additional factor that seems to have significant impact on power generation is the time period allowed for colonization of the anode by EAB. In the current experiment, there was a 24 hour attachment period where the external circuit remained disconnected, and the recycle flow was turned off to facilitate bacterial colonization of the anode. In contrast, a large number of MFC publications report inoculation periods up to 30 days to develop a biofilm of EAB before electrochemical characterization (*Biffinger et al. 2007*; *Gil et al. 2003*; *Rismani-Yazdi et al. 2005*; *Zuo et al. 2006*). Especially in the case of cellulose-fed MFCs, where no pure culture has proven capable of simultaneous cellulose degradation and anode respiration, it is common to operate for several batch cycles with a wastewater, or known electrogenic, inoculum in order to optimize the anode reaction and

establish stable power generation before switching to a cellulosic substrate (*Ren et al. 2007; Wang et al. 2009; Zuo et al. 2006*). Futher, Kim et al. (2005) report that the use of an anodic biofilm from an existing MFC to inoculate a new cell is a critical factor in acclimating the MFC for power production. Thus, the time for biofilm development, and the colonization of EABs on the anode—two variables that were not optimized for in the current study—seem to be critical to optimizing power generation.

Despite the performance limitations, it should be noted that the corncob substrate was not exhausted and the MFC in the current study was able to produce stable power for the duration of the second trial (1620 hours)—a significantly longer time frame than the batch cycles of other studies using (micro)crystalline cellulose or pre-treated corn stover (Table 4-4). Thus, the slow degradation of lignocellulose in an MFC could be feasible as a sustainable, long-term energy source, similar to that of biogas generation from a landfill, in that does not require frequent loading and could be maintained without extensive maintenance.

4.10 SEM Analysis of Substrate and Anodic Biofilms

Examination of the graphite fibers and the corncob substrate after Trial 2 revealed bacterial colonization on both materials. The biofilm developed on the anode fibers was heterogeneous, with approximately equal numbers of cocci and bacilli present, as well as sporadic examples of filamentous and spirochetes bacteria (Figure 4-23). However, the biofilm that developed was patchy (Figure 4-24), supporting the idea that the time allowed for enrichment of key bacteria (including EAB on the anode) may have been

inadequate. On the other hand, micrographs from a previous cellulose-fed MFC revealed comparable complexity in structure and a sparse biofilm development (*Ishii et al. 2008*).



Figure 4-23. Micrograph of anodic fiber taken from the bottom half of Reactor B. Example of a filamentous bacterium surrounded by cocci.

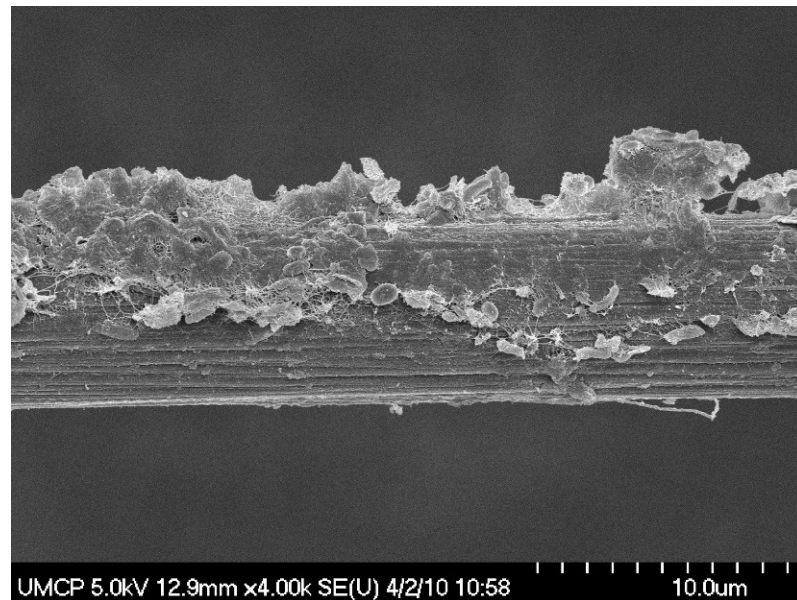


Figure 4-24. Micrograph of anodic fiber taken from the middle section of Reactor A. Figure illustrates the patchy appearance of biofilm on the anode.

One defining feature of the biofilm was the abundance of thin, pili-like appendages connecting cells to the substrate (Figure 4-25), to the electrode surface (Figure 4-26), and to other bacteria (Figure 4-27). The presence of such pili in previous reports has been used as evidence of electron transfer via conductive ‘nanowires’; however, these appendages have also been shown to be essential in the general formation of biofilms and in bacterial growth (*Reguera et al. 2005; 2006*).

There was no evidence of mineral deposits on any of the sample fibers as hypothesized in Section 4.2.2; however, there was evidence of the dense polymer-like material in certain areas on the fibers, but it is unclear if the agglomeration of cellulose metabolites could have impeded electron transport.

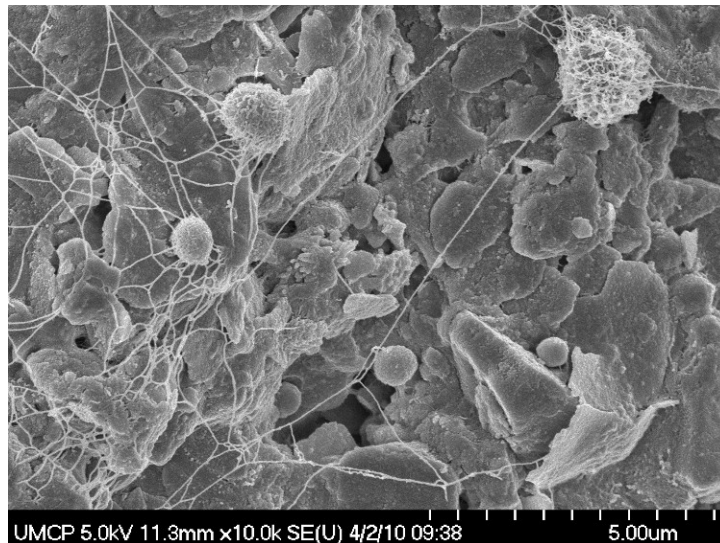


Figure 4-25. Micrograph of corn cob taken from the top half of Reactor A. Figure illustrates the pili-like appendages attaching bacteria to the substrate surface.

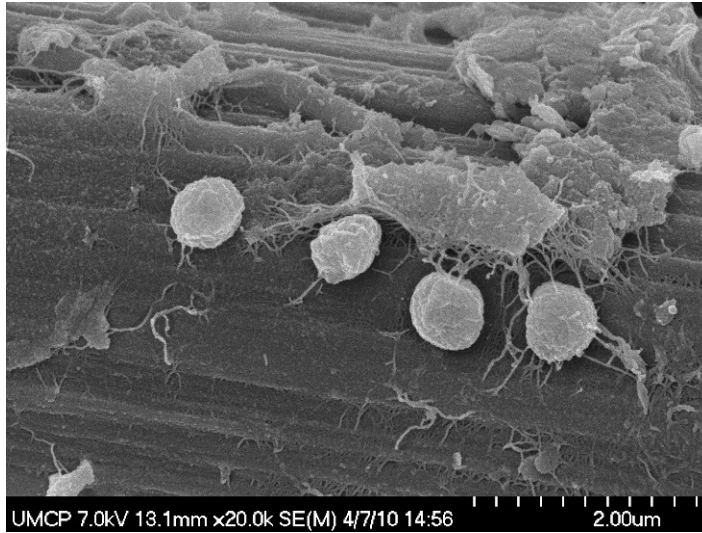


Figure 4-26. Micrograph of anodic fiber taken from the bottom half of Reactor B. Figure displays bacterial attachment to the anode surface.

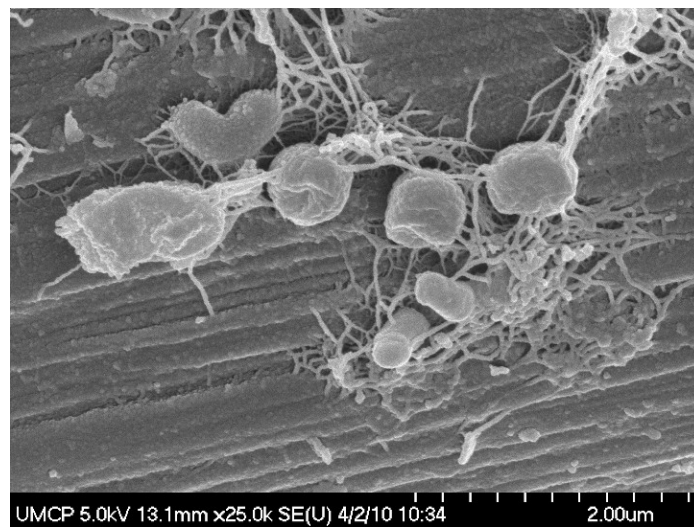


Figure 4-27. Micrograph of anodic fiber taken from the middle section of Reactor A. Figure displays the pili-like appendages attaching bacteria to one another.

CHAPTER 5

CONCLUSIONS

5.1 Conclusions

The development of a solid-substrate MFC could provide an alternative to anaerobic digestion in the production of electricity from waste biomass; however, such an MFC must produce power up to 160 W/m^3 to be competitive (*He et al. 2006; Rabaey et al. 2004*). The results of this study indicate that the conversion of untreated lignocellulosic biomass for long-term power production in an MFC is feasible, though the power density is not yet at a similar magnitude as that of soluble substrate MFCs or of anaerobic digesters. Based on comparisons in performance between the two reactors, oxidation of the fermentative metabolites (e.g. acetate), rather than lignocellulose hydrolysis, seems to be the rate-limiting step in the generation of electricity. Despite these limitations, scale-up of this prototype MFC could be feasible as a long-term power source for agricultural operations, as it does not require frequent loading, nor does it require extensive maintenance.

5.2 Recommendations

Based on lessons learned from these experiments, there are a number of structural modifications to the reactor design that may help to reduce internal resistance and the fraction of electrons lost to oxygen or methane reduction: (1) modification of the anode brush so that it maintains its shape within a solid-substrate reactor; (2) reduction of the area for proton transfer so as to reduce oxygen diffusion; and (3) modification of the design to allow for periodic aeration of the cathode.

These results also suggest that microbial species and their relative activity play a significant role in improving power production and reducing internal resistance (R_{int}). For future work to improve electricity generation from corncobs, it would be beneficial to elucidate the mechanism by which the microbial communities reduced R_{int} . Additionally, in both reactors, it was demonstrated that corncob was successfully fermented into organic acids; however, the conversion of such intermediates may have been a rate-limiting step. As little is known about the ability of rumen microorganisms to simultaneously degrade cellulose and reduce an electrode, it may be beneficial to quantify spatial and temporal shifts in the microbial communities over a cycle of cellulose degradation. To improve the practicality of the design, it would also be necessary to find or develop an inoculum capable of cellulose degradation that is more readily accessible than rumen fluid.

APPENDICES

Appendix A Information on Reactor Set-Up

Table A-1. MFC Reactor Geometric Properties

Reactor Feature	Dimension
Inner Diameter	13.97 cm (5.5 in)
Anode Wet Volume	4.77 L
Height of Water Column	31.12 cm (12.25 in)
Headspace Volume	1.463 L
Leachate Collection Volume	0.487 L
Cathode Surface Area	2168 cm ²
Anode Surface Area- Trial 1	121.6 cm ²
Anode Surface Area- Trial 2	213,980 cm ²

Table A-2. Structural modifications to MFC reactors between trials.

	Trial 1	Trial 2		
		Condition 1	Condition 2	Condition 3
Anode	Graphite granules (3/8 in)	Carbon-fiber bottle brush ^(a)		
Cathode	Carbon cloth with 0.35 mg Pt/cm ² ^(b)			
Substrate	Corncob (2.36 < dp ≤ 4.76 mm) ^(c)			
Inoculum	Rumen Fluid (10% v/v) ^(d)	Soil spores (26.7 g/L) ^(e)	Rumen fluid ^(d)	<i>G. Metallireducens</i>
Bulking Material	None	Plastic Matrix Media		

Appendix B Data from Trial 1

Table B-1 Trial 1 Polarization Test (11/10/09 – 12/08/09)

	Potential (mV)	Current (mA)	Current Density (mA/m ³) ^a	Current Density (mA/m ²) ^b	Power (mW)	Power Density (mW/m ³) ^a	Power Density (mA/m ²) ^b	R _{ext} at min/max Power (Ω)
Max	211	0.140	29.34	0.65	1.96E-02	4.11	9.04E-02	1000
Min	98	0.000	0.07	0.001	6.08E-05	0.013	2.80E-04	600,000

^a Normalized to the anode wet volume (0.00477 m³)

^b Normalized to the cathode surface area (0.2168 m²)

Table B-2 Trial 1 Hydrogen Levels in Liquid and Gas Fractions

	[H ₂] in Background (μM)	[H ₂] in Leachate (μM)	[H ₂] in Headspace (μM)
Max Value	0.555	0.792	0.853
Min Value	0.000	-0.126	0.012
Mean Value ^a	0.118 (0.15)	0.066 (0.19)	0.451(0.33)

^a Mean (Standard Deviation) based on 21 measurements.

Appendix C Data from Trial 2

Table C-1 Results of Polarization Test (01/28/2010)

External Resistance (Ω)	Potential (V)	Current (mA)	Current Density (mA/m^3) ^a	Current Density (mA/m^2) ^b	Power (mW)	Power Density (mW/m^3) ^a	Power Density (mW/m^2) ^b
5000	0.027	5.49E-03	1.152	0.025	1.51E-04	3.16E-02	6.96E-04
10000	0.047	4.67E-03	0.978	0.022	2.18E-04	4.56E-02	1.00E-03
25000	0.101	4.04E-03	0.848	0.019	4.09E-04	8.57E-02	1.89E-03
50000	0.166	3.32E-03	0.695	0.015	5.50E-04	1.15E-01	2.54E-03
100000	0.262	2.62E-03	0.550	0.012	6.89E-04	1.44E-01	3.18E-03
250000	0.359	1.44E-03	0.301	0.007	5.17E-04	1.08E-01	2.38E-03
500000	0.419	8.39E-04	0.176	0.004	3.52E-04	7.38E-02	1.62E-03
1000000	0.471	4.71E-04	0.099	0.002	2.22E-04	4.64E-02	1.02E-03
Min	0.027	4.71E-04	0.9987	2.17E-03	1.51E-04	0.0316	6.96E-04
Max	0.471	5.49E-03	1.15	2.53E-02	6.89E-04	0.144	3.18E-03

^a Normalized to the wet volume of the anode (0.00477 m³)

^b Normalized to the cathode area (0.2168 m²)

Table C-2 Trial 2, Condition 2 Results of Polarization Test (02/19/2010)

	Potential (V)	Current (mA)	Current Density (mA/m^3) ^a	Current Density (mA/m^2) ^b	Power (mW)	Power Density (mW/m^3) ^a	Power Density (mW/m^2) ^b
Min-A	0.019	2.31E-04	4.84E-02	1.06E-03	1.06E-04	2.23E-02	4.91E-04
Min-B	2.23E-04	4.67E-02	1.03E-03	9.93E-05	2.08E-02	4.58E-04	2.23E-04
Max-A	0.577	3.74	784.93	17.27	0.47	99.08	2.18
Max-B	0.527	2.47	517.21	11.381	0.320	67.10	1.48

^a Normalized to the wet volume of the anode (0.00477 m³)

^b Normalized to the cathode area (0.2168 m²)

Figure C-1. Trial 2 hydrogen concentrations in duplicate reactors determined from analysis of liquid samples.

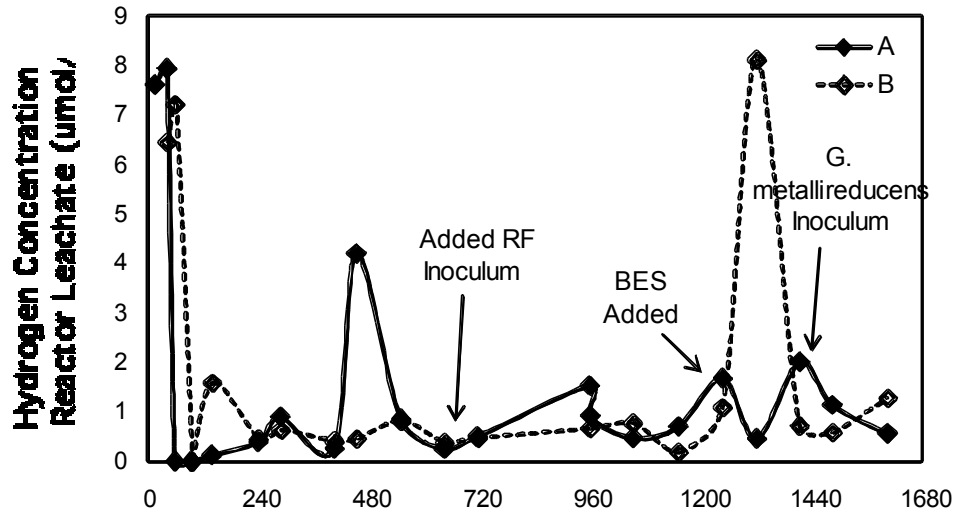


Table C-3. Trial 2 Hydrogen Levels in Liquid and Gas Fractions (Reactor A)

	[H ₂] in background (nM)	[H ₂] in Leachate (µM)	[H ₂] in Headspace (µM)
Max	0.246	7.944	2.025
Min	0.000	0.000	0.038
Mean	0.094 ± 0.06 ^a	1.517 ± 2.30 ^a	0.598 ± 0.59 ^a

^a Mean values are presented with respect to standard deviation.

Table C-4 Trial 2 Hydrogen Levels in Liquid and Gas Fractions (Reactor B)

	[H ₂] in background (nM)	[H ₂] in Leachate (µM)	[H ₂] in Headspace (µM)
Max	0.497	8.127	1.411
Min	0.012	0.000	0.131
Mean	0.151 ± 0.132 ^a	1.584 ± 2.504 ^a	0.582 ± 0.386 ^a

^a Mean values are presented with respect to standard deviation.

Table C-5 Trial 2 Methane Levels in Liquid and Gas Fractions (Reactor A)

	[CH ₄] in Leachate (µM)	[CH ₄] in Headspace (µM)
Max Value	40.08	137.23
Min Value	-81.59	-20.30
Mean Value	-63.38 ± 32.66	5.96 ± 36.26

^a Mean values are presented with respect to standard deviation.

Table C-6 Trial 2 Methane Levels in Liquid and Gas Fractions (Reactor B)

	[CH ₄] in Leachate (μM)	[CH ₄] in Headspace (μM)
Max Value	444.83	2469.62
Min Value	-81.61	-20.31
Mean Value	40.47 ± 135.49	630.99 ± 827.80

^a Mean values are presented with respect to standard deviation.

Table C-7 Trial 2 pH, T, and DO Summary (Reactor A)

	pH	Temp (°C)	DO (mg/L)
Max	7.64	25.10	1.70
Min	5.98	22.90	0.20
Mean	6.89 ± 0.52	23.59 ± 0.65	0.66 ± 0.41

^a Mean values are presented with respect to standard deviation.

Table C-8 Trial 2 pH, T, and DO Summary (Reactor B)

	pH	Temp (°C)	DO (mg/L)
Max	7.40	25.00	1.04
Min	5.93	23.00	0.12
Mean	6.60 ± 0.40	23.62 ± 0.55	0.48 ± 0.29

^a Mean values are presented with respect to standard deviation.

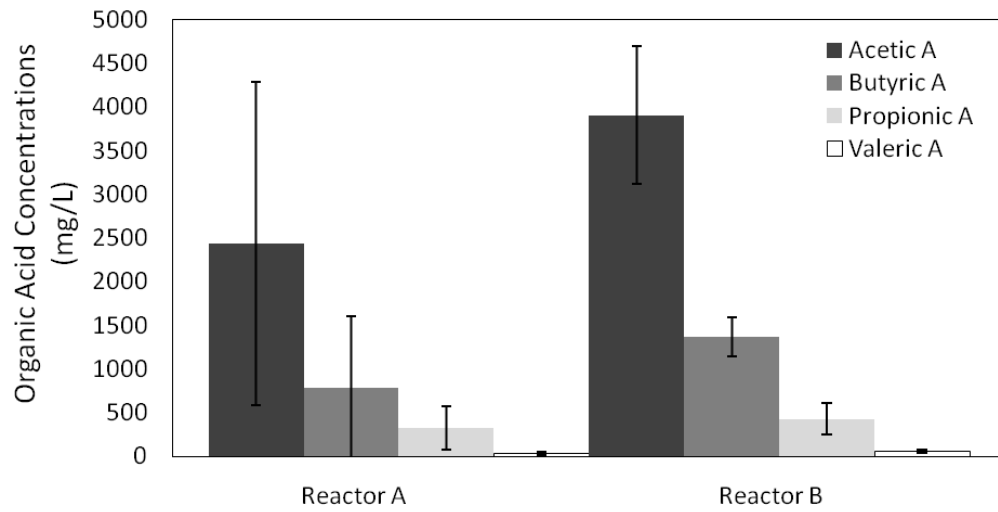
Table C-9 Trial 2 Power Production Summary, Reactor A

	R _{int} (Ω)	R _{ext} at MPP (Ω)	P _{max} (mW/m ³)	V _{max} (V)
Condition 1	NA	NA	NA	NA
Condition 2	141.5	100	87.48	0.577
Condition 3	34.6	50	229.2	0.388

Table C-10 Trial 2 Power Production Summary, Reactor B

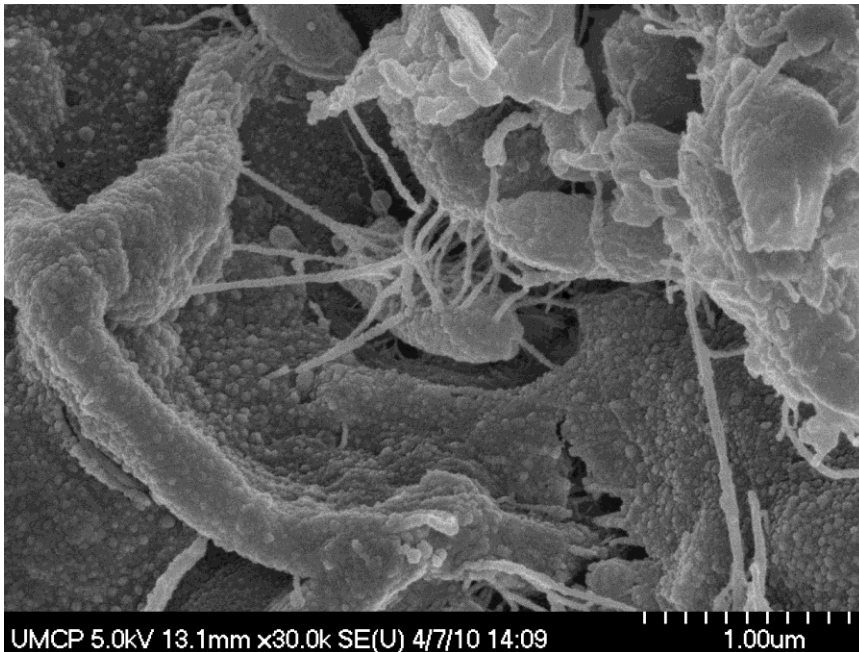
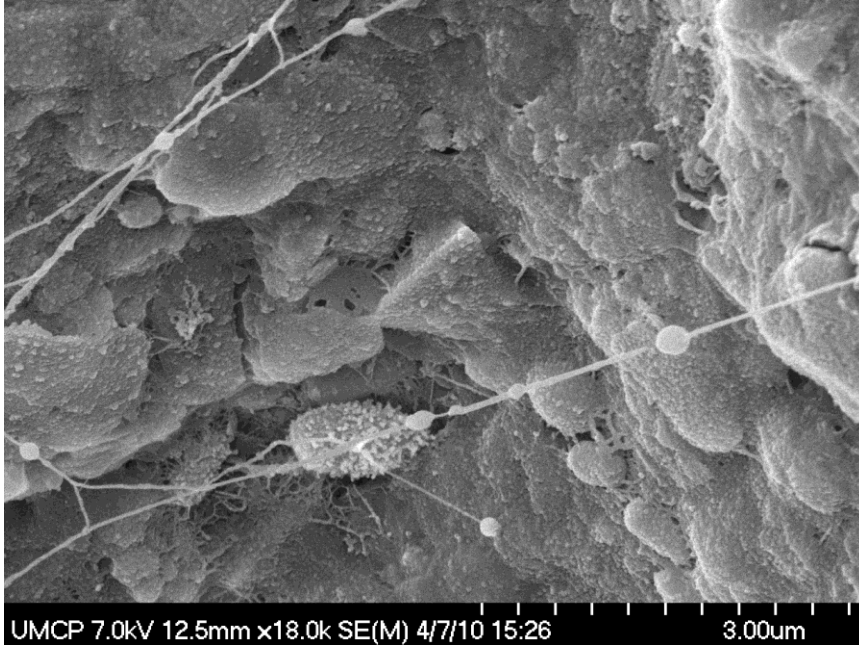
	R _{int} (Ω)	R _{ext} at MPP (Ω)	P _{max} (mW/m ³)	V _{max} (V)
Condition 1	92,751	100,000	0.144	0.471
Condition 2	196.2	100	67.1	0.527
Condition 3	186.9	100	88.8	0.503

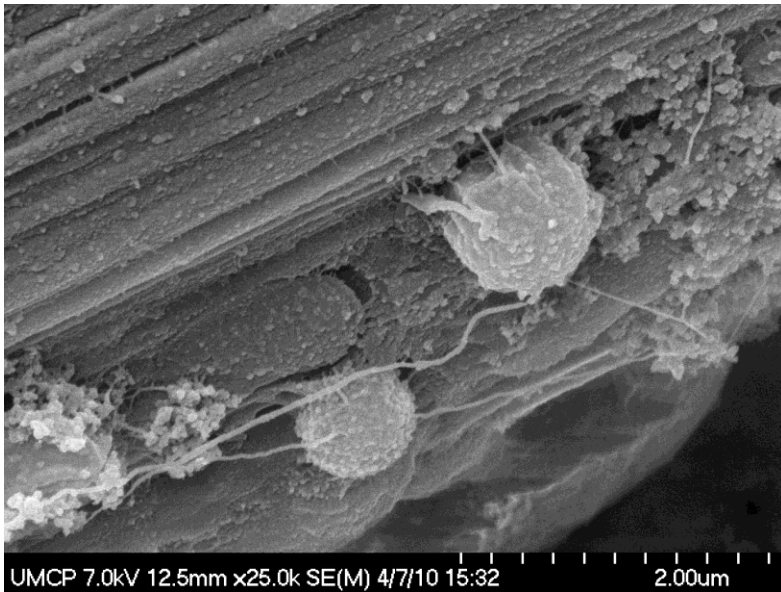
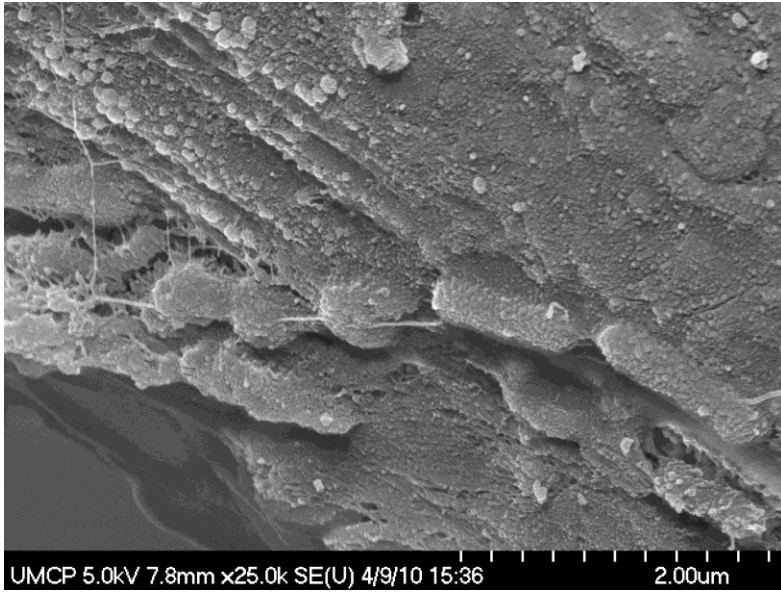
Figure 4-17. Trial 2 average organic acid production in duplicate reactors determined from analysis of liquid samples over the course of the trial.



Appendix D SEM Images

Figures D-1 through D-4. Micrograph from anodic fibers





REFERENCES

- Barbir, F. (2005). PEM Fuel Cells: Theory and Practice. Burlington, MA: Elsevier, Inc.
- Bennetto, H., Stirling, J., Tanaka, K. & Vega, C. (1983). Anodic reactions in microbial fuel cells. *Biotechnology & Bioengineering*, 25: 559-568.
- Biffinger J., Pietron, J., Ray, R., Little, B. & Ringeisen, B. (2007a). A biofilm enhanced miniature microbial fuel cell using *Shewanella oneidensis* DSP10 and oxygen reduction cathodes. *Biosensors & Bioelectronics*, 22(8):1672-1679.
- Bond, D. & Lovley, D. (2003). Electricity production by *Geobacter sulfurreducens* attached to electrodes. *Applied Environmental Microbiology*, 69: 1548-1555.
- Borole, A., Hamilton, C., Vishnivetskaya, T. et al. (2009). Improving power production in acetate-fed microbial fuel cells via enrichment of exoelectrogenic organisms in flow-through systems. *Biochemical Engineering Journal*, 48: 71-80.
- Bratina, B., Stevenson, B., Green, W., & Schmidt, T. (1998). Reduction by microbes from oxic regions of the Lake Vanda (Antarctica) water column. *Applied & Environmental Microbiology*, 64(10): 3791-3797.
- Chang, I., Moon, H., Bretschger, O., Jang, J., Park, H., Nealson, K. & Kim, B. (2006). Electrochemically active bacteria (EAB) and mediator-less microbial fuel cells. *Journal of Microbiology & Biotechnology*, 16(2): 163-177.
- Cheng, S., Liu, H. & Logan, B. (2006). Increased performance of single-chamber microbial fuel cells using an improved cathode structure. *Electrochemistry Communications*, 8: 489-494.
- Cohen, A. (1977). A critical look at critical point drying—theory, practice and artifacts. *SEM/1977/1, IIT Research Institute, Chicago, IL*, 60616, p. 525-536.
- Durand, A. (2003). Bioreactor designs for solid state fermentation. *Biochemical Engineering Journal*, 13: 113-125.
- Fan, Y., Hu, H. & Liu, H. (2007a). Enhanced Coulombic efficiency and power density of air-cathode microbial fuel cells with an improved cell configuration. *Journal of Power Sciences*, 171: 348-354.
- Fan, Y., Hu, H. & Liu, H. (2007b). Sustainable power generation in microbial fuel cells using bicarbonate buffer and proton transfer mechanisms. *Environmental Science & Technology*, 41(23): 8154-8158.
- Feng, Y., Wang, X., Logan, B. & Lee, H. (2008). Brewery wastewater treatment using air-cathode microbial fuel cells. *Appl. Microbiology & Biotechnology*, 78: 8873-880.

- Feng, Y., Yang, Q., Wang, X. & Logan, B. (2010). Treatment of carbon fiber brushes for improving power generation in air-cathode microbial fuel cells. *Journal of Power Sources*, 195: 1841-1844.
- Fischer, C. & Newell, R. (2004). Environmental and technology policies for climate change and renewable energy. *Resources for the Future*. Washington, DC, 20036.
- Gil, G., Chang, I., Kim, B., Kim, M., Jang, J., Park, H. & Kim, H. (2003). Operational parameters affecting the performance of a mediator-less microbial fuel cell. *Biosensors & Bioelectronics*, 18(4):327-334.
- Glassner, D., Hettenhaus, J. & Schechinger, T. (1998). Corn stover collection project—a pilot for establishing infrastructure for agricultural residue and other crop collection for biomass processing to ethanol. *Proc. Bioenergy 1998 Conference*, 4–8 October, 1998, Madison, WI, pp. 1100–1110.
- Gorby, Y., Yanina, S., McLean, J. et al. (2006). Electrically conductive bacterial nanowires produced by *Shewanella oneidensis* strain MR-1 and other microorganisms, *Proceedings of the National Academy of Sciences of the United States of America*, 103: 11358–11363.
- Haydar, M. & Khire, M. (2007). Leachate recirculation using permeable blankets in engineered landfills. *ASCE Journal of Geotechnical and Geoenvironmental Engineering*, April 2007: 360-371.
- He, Z., Minteer, S. & Angenent, L. (2005). Electricity generation from artificial wastewater using an upflow microbial fuel cell. *Environmental Science & Technology*, 39(14): 5262-5267.
- He, Z. (2007). Microbial fuel cells: their application and microbiology, PhD Dissertation. Department of Energy, Environmental, and Chemical Engineering, Washington University. 150 pages.
- Hoogers, G. (2003). *Fuel Cell Technology Handbook*. Boca Raton, FL: CRC Press.
- Hu, Z. & Yu, H. (2005). Application of rumen microorganisms for enhanced anaerobic fermentation of corn stover. *Process Biochemistry*, 40:2371-2377.
- Ishii, S., Hotta, Y. & Watanabe, K. (2008). Methanogenesis versus electrogenesis: morphological and phylogenetic comparisons of microbial communities. *Bioscience, Biotechnology & Biochemistry*, 72(2): 286-294.
- Kadam, K. & McMillan, J. (2003). Availability of corn stover as a sustainable feedstock for bioethanol production. *Bioresource Technology*, 88: 17-25.
- Kaspar, H. & Wuhrmann, K. (1978). Product inhibition in sludge digestion. *Microbial Ecology*, 4: 241–248.

- Kim, J., Min, B. & Logan, B. (2005). Evaluation of procedures to acclimate a microbial fuel cell for electricity production. *Applied Microbiology & Biotechnology*, 68: 23-30.
- Klotz, D. & Moser, H. (1974). Hydrodynamic dispersion as aquifer characteristic: Model experiments with radioactive tracers. *Isotope techniques in ground-water hydrology Vol. II, IAEA, Wien*, pp. 341–354.
- Liu, H. & Logan, B. (2004). Electricity generation using an air-cathode single chamber microbial fuel cell in the presence and absence of a proton exchange membrane. *Environmental Science & Technology*, 38(14): 4040-4046.
- Liu, H., Cheng, S. & Logan, B. (2005a). Production of electricity from acetate or butyrate using a single-chamber microbial fuel cell. *Environmental Science & Technology*, 39(2): 658-662.
- Liu, H., Grot, S. & Logan, B. (2005b). Electrochemically assisted microbial production of hydrogen from acetate. *Environmental Science & Technology*, 39(11): 4317-4320.
- Löffler, F. and Sanford, R. (2005). Analysis of trace hydrogen metabolism. *Methods in Enzymology*, 397: 222-237.
- Logan, B., Oh, S., Kim, I., & Ginkel, S. (2002). Biological hydrogen production measured in batch anaerobic respirometers. *Environmental Science & Technology*, 36: 2530-2535.
- Logan, B., Hamelers, B., Rozendal, R. et al. (2006). Microbial fuel cells: methodology & technology. *Environmental Science & Technology*, 40(17): 5181-5192.
- Logan, B. & Regan, J. (2006). Microbial Fuel Cells: applications and challenges. *Environmental Science & Technology*, 40: 5172-5180.
- Logan, B. (2008). *Microbial Fuel Cells*. Hoboken, NJ: John Wiley & Sons.
- Lovely, D. (2006). Bug juice: harvesting electricity with microorganisms. *Nature Reviews, Microbiology*, 4: 497-508
- Kim, J., Min, B. & Logan, B. (2005). Evaluation of procedures to acclimate a microbial fuel cell for electricity production. *Biotechnological Products and Process Engineering*, 68: 23-30.
- Madigan, M. & Martinko, J., eds. (2005). *Brock Biology of Microorganisms*, 11th ed. Upper Saddle River, NJ: Pearson Prentice Hall.
- Maier, M., Pepper, I. & Gerba, C. (2000). *Environmental Microbiology*, 2nd ed. Burlington, MA: Elsevier.

- Makkar, C. & McSweeney, C., eds. (2005). *Methods in Gut Microbial Ecology for Ruminants*. The Netherlands: Springer.
- Manohar, A., Bretschger, O., Nealson, K. & Mansfeld, F. (2008). The polarization behavior of the anode in a microbial fuel cell. *Electrochimica Acta*, 53: 3508-3513.
- Manohar, A. & Mansfeld, F. (2009). The internal resistance of a microbial fuel cell and its dependence on cell design and operating conditions. *Electrochimica Acta*, 54(6): 1664-1670.
- Mes, T. D.; Stams, A.J.M.; Reith, J. H.; and Zeeman, G. (2003). Methane production by anaerobic digestion of wastewater and solid wastes. *Bio-methane and Bio-hydrogen: status and perspective of biological methane and hydrogen production*- Petten: Dutch Biological Hydrogen Foundation, p. 58-102.
- Mitchell, D., Krieger, N. & Berovic, M. (2004). *Solid-State Fermentation Bioreactors*. Heidelberg, Germany: Springer.
- Montross, M. & Crofcheck, C. (2004). Effect of stover fraction and storage method on glucose production during enzymatic hydrolysis. *Bioresource Technology*, 92: 269-274.
- Niessen, J., Hamisch, F., Rosenbaum, M. et al. (2006). Heat treated soil as convenient and versatile source of bacterial communities for microbial electricity generation. *Electrochemical Communications*, 8: 869-873.
- Oh, S.E., Kim, J., Joo, J., & Logan, B. (2009). Effects of applied voltages and dissolved oxygen on sustained power generation by microbial fuel cells. *Water Science & Technology*, 60: 1311-1317.
- O'Sullivan, C., Burrell, P., Clarke, W. & Blackall, L. (2006). Comparison of cellulose solubilisation rates in rumen and landfill leachate inoculated reactors. *Bioresource Technology*, 97: 2356-2363.
- Pang, Y., Liu, Y., Li, X., Wang, K. & Yuan, H. (2008). Improving Biodegradability and Biogas Production of Corn Stover through Sodium Hydroxide Solid State Pretreatment. *Energy Fuels*, 22(4): 2761-2766.
- Parameswaran, P., Torres, C., Lee, H. et al. (2009). Syntrophic interactions among anode respiring bacteria (ARB) and non-ARB in a biofilm anode: electron balances. *Biotechnology & Bioengineering*, 103(3): 513-523.
- Park, H., Kim, B., Kim, H. et al. (2001). A novel electrochemically active and Fe(III)-reducing bacterium phylogenetically related to *Clostridium butyricum* isolated from a microbial fuel cell. *Anaerobe*, 7: 297-306.
- Parker, D. & Douglas, M. (1984). Effect of plastic media configuration on trickling filter performance. *Journal of the Water Environment Federation*, 56(8): 955-961.

- Perlack, R., Wright, L., Turhollow, A., Graham, R. et al. (2005). Biomass as feedstock for a bioenergy and bioproducts industry: The technical feasibility of a billion-ton annual supply. (Tech. Rep. ORNL/TM-2006/66, Oak Ridge National Laboratory, Oak Ridge, TN, 2005).
- Piwkhow, S. (2007). *Theoretical and experimental evaluation of acetate thresholds as a monitoring tool for in situ bioremediation*. M.S. Thesis. Department of Civil and Environmental Engineering, University of Maryland. 74 pages.
- Rabaey, K., Boon, N., Siciliano, S. et al. (2004). Biofuel cells select for microbial consortia that mediate electron transfer. *Applied & Environmental Microbiology*, 70(9): 5373-5382.
- Reguera, G., McCarthy, K., Mehta, T., Nicoll, J., Tuominen, M. & Lovely, D. (2005). Extracellular electron transfer via microbial nanowires. *Nature*, 435(23): 1098-1101.
- Reguera, G., Pollina, R., Nicoll, J. & Lovely, D. (2007). Possible non-conductive role of *Geobacter sulfurreducens* pilus nanowires in biofilm formation. *Journal of Bacteriology*, 189(2): 2125-2127.
- Reimers, C., Gircuis, P., Stecher, A., Tender, L., Ryckelynck, N. & Whaling, P. (2006). Microbial fuel cell energy from an ocean cold seep. *Geobiology*, 4: 123-136.
- Reinhart, D. & Townsend, T. (1998). *Landfill bioreactor design and operation*, Lewis, Boca Raton, Florida.
- Ren, Z., Ward, T. & Regan, J. (2007). Electricity production from cellulose in a microbial fuel cell using a defined binary culture. *Environmental Science & Technology*, 41(13):4781-4786.
- Richard, T., Veeken, A., Wilde, V. & Hamelers, H. (2004). Air-filled porosity and permeability relationships during solid-state fermentation. *Biotechnology Progress*, 20(5): 1372-1381.
- Rismani-Yazdi, H. (2008). *Bioconversion of cellulose into electrical energy in microbial fuel cells*, PhD Dissertation. Department of Agricultural and Biological Engineering, Ohio State University. 167 pages.
- Rittmann, B. E. (2008). Opportunities for renewable bioenergy using microorganisms. *Biotechnology & Bioengineering*, 100: 203–212.
- Rosenbaum, M. (2007). *Biofuels: Hot Topics*. St. Louis: Washington University. Retrieved from: www.umsl.edu/~biofuels/microbialfuelcellMiriam.html.
- Rovers, F. & Farquhar, G. (1973). Infiltration and landfill behavior. *ASCE Journal of Environmental Engineering*, October 1973: 671-690.

- Searchinger, T., Heimlich, R., Houghton, R. et al. (2008). Use of U.S. croplands for biofuels increases greenhouse gases through emissions from land-use change. *Science*, 319: 1238-1240.
- Shinners, K. & Binversie, B. (2007). Fractional yield and moisture of corn stover biomass produced in the northern US corn belt. *Biomass and Bioenergy*, 31:576-584.
- Sokhansanj, S., Turhollow, A., Cushman, J., & Cundiff, J. (2002). Engineering aspects of collecting corn stover for bioenergy. *Biomass and Bioenergy*, 23: 247-355.
- Tanner, R. S. 2007. Cultivation of bacteria and fungi, p. 69-78. In C. J. Hurst, R. L. Crawford, J. L. Garland, D. A. Lipson, A. L. Mills, and L. D. Stetzenbach (ed.), *Manual of Environmental Microbiology*, 3rd ed. ASM Press, Washington, DC.
- Tengerdy, R. & Szakacs, G. (2003). Bioconversion of lignocellulose in solid state fermentation. *Biochemical Engineering Journal*, 13: 169-179.
- Torres, C. Marcus, A., Lee, H. et al. (2010). A kinetic perspective on extracellular electron transfer by anode-respiring bacteria. *FEMS Microbiology Review*, 34: 3-17.
- USDA/NASS. (2001). Crop production: 2001 summary (Cr Pr 2-1 (02)). US Department of Agriculture, National Agricultural Statistics Service. Washington, DC, 20001.
- USDOE and EG&G Technical Services. (2004). Fuel Cell Handbook, 7th ed. (Doc #?). US Department of Energy, Office of Fossil Energy. Morgantown, WV, 26507.
- Wang, X., Feng, Y. Wang, H. et al. (2009). Bioaugmentation for electricity generation from corn stover biomass using microbial fuel cells. *Environmental Science & Technology*, 43(15): 6088-6093.
- Watanabe, K. (2008). Recent developments in microbial fuel cell technologies for sustainable bioenergy. *Journal of Bioscience & Bioengineering*, 106(6): 528-536.
- Weber, S., Stubner, S., & Conrad, R. (2001). Bacterial populations colonizing and degrading rice straw in anoxic paddy soil. *Applied & Environmental Microbiology*, 67(3): 1318-1327.
- Williams, X. (1966). Fuel Cell book.
- Wool, R. & Sun, X. (2005). *Bio-based polymers and composites*. Burlington, MA: Elsevier Academic Press.
- Zielke, E. (2005). *Design of a single chamber microbial fuel cell*. None. 2005, 12.
- Zuo, Y. (2006). *Novel electrochemical material applications and exoelectrogenic bacteria isolation from microbial fuel cells*. PhD Dissertation. Department of Civil & Environmental Engineering, Pennsylvania State University. 192 pages.